ASSESSMENT OF STONE CRUSHING CHARACTERISTICS AND OPTIMUM DYNAMICAL AND STRUCTURAL DESIGN PARAMETERS OF A STONE CRUSHER FOR SMALL AND MEDIUM SCALE ENTREPRENEURS

BY

DAVID MASINDE MUNYA0SI

A THESIS SUBMITTED IN FULFILMENT FOR THE DEGREE OF DOCTOR OF PHILOSOPHY OF THE UNIVERSITY OF NAIROBI

MARCH 2019

DECLARATION

This thesis is my original work and has not been presented for a degree in any other university.

Signature: ……. …….

David Masinde Munyasi **Date:**

F80/51592/2017

This thesis has been submitted for examination with our approval as university supervisors.

Signature: ……. …….

Prof. Stephen M. Mutuli **Date:**

Signature: ……. …….

Prof. Gideon K. Misoi **Date:**

ACKNOWLEDGEMENT

I express my heartfelt gratitude to my Supervisors Prof. Stephen M. Mutuli and Prof. Gideon K.Misoi for their invaluable guidance, constant encouragement, numerous progressive suggestions and keen interest throughout the research period.

I would like to make a posthumous acknowledgement to my mentor the late Prof. Moses F. Oduori hitherto to my Lead Supervisor who passed away untimely in May 2018.

Prof. Oduori a reputable scholar had a deep accurate understanding of the theory behind this research work. I learnt a lot from him and enjoyed working with him in the course of study. His experience and wisdom added significantly to this research work hence this thesis is dedicated to him. May his soul rest in eternal peace.

I am very much grateful lo my wife Violet, children and grandchildren Deti Munyasi, Aaron Omanga and David Masinde for providing me with moral encouragement.

I am thankful to National Council for Science Innovation and Technology (NACOSTI) and the Deans Committee Research Grant, University of Nairobi for their financial support.

I would like to provide my friendly thanks to all my colleagues and the people who directly or indirectly helped me in my work. *God bless the work of my hands; Deuteronomy; 28;8*

TABLE OF CONTENTS

LIST OF TABLES

LIST OF FIGURES

LIST OF ABBREVIATIONS AND SYMBOLS

$\bar{r}_i$	Vector notation for members
$\emptyset_i$	Angular position of a point on the swing jaw, relative to the vertical
F_{80}	The size at which 80% of the feed passes
F_i	Force experienced in each number
F_y	The force resolved in the vertical direction
F_z	The force resolved in the horizontal direction
G_i	Normalized angular velocity
O_i	Position of a point in the jaw crusher
P_{80}	The size at which 80% of the product passes
T_i	Torque on the members
Y_P	Location of a point P relative to the vertical axis direction
Z_P	Location of a point P relative to the horizontal axis direction
r_i	Length of each member in the mechanism
$\bar{x}$	Mean
α_i	Angular acceleration of a member
α_{ij}	Normalized acceleration
α_{pv}	Angular acceleration of a point in the horizontal axis direction
α_{pv}	Angular acceleration of a point in the vertical axis direction

θ_i	Angle of each member relative to the vertical
σ_x	Normal stress in the x-direction
σ_y	Normal stress in the y-direction
σ_z	Normal stress in the z-direction
τ_{xy}	Shear stress in the *x* face and in the *y* direction
τ_{xz}	Shear stress in the *x* face and in the *z* direction
τ_{yz}	Shear stress in the *y* face and in the *z* direction
υ_{PH}	The velocity of a point in the horizontal direction
υ_{pv}	The velocity of a point in the vertical direction
ω_i	Angular velocity of a member
CEVIS	Comparative Evaluations of Innovative Solutions
CSS	Closed Side Set
GDP	Gross Domestic Product
GoK	Government of Kenya
ILO	International Labour Organization
KNBS	Kenya National Bureau of Statistics
LDVT	Linear Variable Differential Transformer
NEMA	National Environmental Management Authority
OSS	Open Side Sets

TPH	Tonnes Per Hour
UCS	Ultimate Compressive Stress
w	Displacement in the z-direction
E	Young's Modulus of Elasticity
$ASTM$	American Standard for Testing Materials
D	Diameter of specimen
G	Energy release rate or Shear Modulus of Rigidity
H	Input power
$ISRM$	International Standards for Rock Mechanics
K	Crack intensity factor
L	Length of specimen
MA	Mechanical Advantage
P	Random location of a point in the swing jaw
R	Crack resistance
SD	Standard deviation
UTM	Universal testing Machine
Y	Vertical axis direction
Z	Horizontal axis direction
a	Crack length

i	1, 2, 3, ……
j	1, 2, 3, …….
u	Displacement in x-direction
v	Displacement in y- direction

ABSTRACT

In Kenya and other developing countries, crushing of stones into aggregates using manual means is common. The activity is carried out by men, women and children along riverbeds, roadsides, homesteads and near towns. Manual stone breakers do heavy work, expose themselves to health problems like body, ear, skin and eye injuries. The aggregates produced is of low quality and the business is hardly profitable. Manual stone crushing has been necessitated by poverty and unemployment.

Stones are predominantly crushed by compressive forces and the equipment used in the crushing process are Gyratory Crushers, Jaw Crushers, Cone Crushers and Vertical Impact Crushers. Jaw Crushers are the most appropriate for Small and Medium Scale Entrepreneurs because of their simplicity in its structure and mechanism, reliable performance, ease of manufacture and maintenance and affordable. This study therefore assesses the stone crushing characteristics of stones and present design parameters for the design of a more efficient and user-friendly mechanized stone crusher for Small and Medium Scale Entrepreneurs.

This thesis reports the compressive strength of rocks used in construction industry. Laboratory tests were carried out on Schist, Gneiss, Tuff, Quartzite, Granite, Phonolite, Granodiorite and Grey Wecke taken from quarry sites in Bungoma, Uasin Gishu, Siaya, Nairobi, Meru, Thika, Nyeri and Machakos Counties. The results confirm that strength of rocks differ quite a lot, ranging from as low as $23MN/m^2$ for Tuff to as high as $127MN/m^2$ for Gneiss. Using the Vector Loop Closure method, the study presents equations from first principles of displacement, velocity and acceleration. Further analysis is carried out for both static force and mechanical advantage of the crusher mechanisms.

The study shows that in the Single Toggle Jaw Crusher mechanism, the minimum angle of inclination of the swing jaw to the vertical is 159.7º while the maximum value is 161.6º. Thus, the range of variation of the inclination of the coupler (swing jaw) to the vertical for one complete cycle of rotation of the crank is less than 2º, hence the angular orientation of the swing jaw, during the cycle motion is insignificant. In the same cycle of rotation of the crank, the minimum value of the velocity of the swing jaw is found to be-0.476 radians per second while the maximum value is found to be 0.461 radians per second, showing clearly that the angular velocity of the swing jaw is generally small. For one complete cycle of motion of the swing jaw, the minimum value of its angular acceleration which occurs at a crank angle of 123.9° is found to be -13.208 radians per square second whereas the maximum value of angular acceleration which occurs at a crank angle of 291.8° is found to be 13.873 radians per square second. At the crank angle of 26.32º and 207.92º to the vertical, the angular acceleration of the swing jaw, for both vertical and horizontal components become zero. At these instances, the acceleration of the swing jaw becomes purely translational.

In this thesis, the maximum value of the force transmission ratio is found to be about 3268 at the active crushing stroke, the minimum value is found to be 0. 61 and the mean value of 10.6. The force transmission ratio is very high at the beginning of the active crushing stroke, which is of advantage in communition process as it enables the crushing of brittle materials which fracture without undergoing appreciable deformation.

In the Double Toggle Jaw Crusher Analysis, the result shows that the greatest amplitude of the crushing force occurs at the toggle action, which corresponds to the angle of 180º in the first phase and at 360º in the second phase. The Mechanical Advantage suddenly becomes high at 0º to the vertical in the first phase and at 180º in the second phase. This is evidence of the toggle phase which coincides with the commencement of the active crushing stroke, hence advantageous in the stone crushing action. The equations derived in this thesis can be used to investigate the effects of any alterations in the design of the Crusher Mechanisms, upon its kinematics and the

characteristic Mechanical Advantage can be used as a criterion for selecting such mechanisms. The recommendations presented at the end of this thesis are for the development of a more efficient Jaw Crusher which optimizes the Design Parameters. The Vector Loop Closure method used in this thesis is not itself new, but has not been applied before in the study of Jaw crusher Mechanisms.

CHAPTER ONE

INTRODUCTION AND SCOPE FOR STUDY

1.1 Introduction

Long Before Christ (BC), people worldwide have used stones to build structures and superstructures. For example, stones have been used to build homes, townships, roads, railway lines, airports and bridges. Other uses of stones are making of weapons for hunting and warfare, ornaments, and dams to irrigate fields of crops and generate electricity to name but a few. It is one of the greatest gifts God has given in abundance to Mankind.

A stone is a hard, non-metallic mineral matter of which rock is made. In Civil Engineering and Construction Industry, crushed stones are known as aggregates, used as components in the formation of concrete and reinforced concrete structures. Although modern methods of crushing stones to make aggregates involves high level of technology, they are the same old rocks that were used during the Stone Age that remain the major material used in buildings of homes, roads, airport exedra in the present times.

Despite the low value of stones, the stone crushing industry is a major contributor to and an indicator of the well-being of a nation. In the US for example, 1260 companies operating in 3300 active quarries and distribution yards produced 1.5billion tones of crushed stones valued at US 8.6billion and employing more than 20,000 people, and during the last 25 years, production of crushed stones had increased at an average rate of about 3.3% (Guimaraes *et al.*,2007; Satyen Moray *et al.*,2005).

In Kenya, the Real Estate and Construction Sectors continue to be the key drivers of economic growth, as they contribute 7% of GDP (GoK: KNBS, 2017). Data from Kenya Bureau of Standards (GoK, 2017) show that the Construction Industry grew up by 9.2% from an expansion of 13.9% registered in 2015. Increased activity in the construction of Roads, Bridges, Buildings, Canals and other infrastructures translated to an increase in employment in the Sector from 148.6 thousand jobs in 2015 to 163.0 thousand jobs in 2016 (GoK, 2017). This is expected to grow further keeping in view of the Government Vision

2030 agenda for the development of infrastructure that are required for overall development of the country. In Kenya, there are a few licensed stone crushing companies operating commercially as shown in Table 1.1 (GoK, 2017).

Table 1.1: Licensed Stone Crushing Companies in Kenya (GoK: NEMA, 2017).

Region	**Number of Licensed Companies**
Coast	10
Central	31
Eastern	16
North Eastern	1
Western	1
Nyanza	5
Rift Valley	24

In Kenya and other developing countries, the stone crushing industry is managed by international foreign entrepreneurs who build structures and superstructures or run very large capacity mining industry. These highly mechanized stone crushing plants are well beyond the reach of small-scale entrepreneurs (Machine Roll, 2008). These plants are often operated far away from the point of construction, leading to high cost of transportation of the aggregates. In South Africa, for example, the cost of transporting the aggregates to the construction site is by far more than the price of the aggregate itself (Zuma *et al.,* 1989).

However, "hammer-anvil" manual stone crushing activities is common in the rural areas and around towns in sub-Sahara Africa and other developing countries as reported by Zuma *et al.,* (1989)., Ugbogu *et al.,* (2000); Jambiya *et al.,* (1997), Elisante (2003), Munyasi *et*

al., (2013) and Mbandi (2017). Figure 1.1 and Figure 1.2 show the disparity between large scale and manual stone crushing activities respectively.

Figure 1.1: Large Scale Aggregate Production (Courtesy of Zenith Mining and Construction Company Ltd, Kenya)

Figure 1.2: A Manually Crushing Stone Activity at Milo Village near Webuye town, Kenya (Photo: *Munyasi)*

Manual stone breakers do heavy work and expose themselves to hand and eye injury as well as inhalation of dust, leading to opportunistic diseases. Ugbogu *et al., (*2000) reported that over 80% of stone quarry workers are aware of the dangers of stone crushing but could not quit because of rampant poverty and unemployment. A study in India showed consistent generational exposure of quarry workers to health problems (Durvsula, 1990). Study by Fatusa *et al.,* (1996) and Bakke *et al.,* (2001) reported the same prevalent health hazards to quarry workers. Munyasi *et al.,* (2013) and Mbandi (2017) reported adverse

environmental effects of quarrying on the health of quarrying workers in Kenya. Though stone crushing activities are carried out mostly by men and women, studies in Uganda, South Africa, Nigeria, Kenya, Uganda and Tanzania have reported extensive use of child labour in quarries (ILO-IPEC, 2001; 2006; Ugbogu *et al.,* 2000, Ottilino, 2012; Elisante, 2003; Zuma, 1989; Munyasi *et al.,* 2013 and Mbandi, 2017).

Manual stone crushing industry is characterized by low productivity as it takes about 3 weeks for a man and 4 weeks for a woman to produce ten tonnes of aggregate worthy U$80 (Zuma, 1989; Jambiya *et al.,* 1997). Furthermore, the quality of aggregate produced is poor as it is not measured to any known standard.

1.2. Problem Statement

There has been tremendous infrastructural development in Kenya in the past 15 years (GoK, 2017) and the Real Estate and Construction Industry remain the major contributor to the wellbeing of the nation as for example in Kenya, they contribute 7% GDP (GoK; KNBS, 2017). The core material used in these sectors is aggregates and the demand for it is bound to increase in view of the Governments Agenda 4 and Vision 2030 Strategies for National Development.

The stone crushing industry in Kenya and other developing countries is managed by international foreign entrepreneurs who built structures and superstructures using highly mechanized plants that Small-Scale Entrepreneurs can hardly afford. However, "hammer-anvil" manual stone crushing activities are common (Ugbiogu, 2000; Durvasula, 1990; Fatusa *et al.,* 1996; Bakke *et al.,* 2001, Jambiya *et al.,* 1997; Elisante, 2003; Zuma, 1989, Munyasi *et al.,* (2013); Mbadi, 2017).

These manual stone crushing artisans do heavy work subjecting themselves to drudgery and hardships. At times, they work in extreme weather conditions either very hot and sunny or very extreme cold. All these constitute to health hazard. Moreover, the quality of aggregates produced is poor and the business is hardly profitable.

1.3. The Main Objective of the Study

The main objective of the present study is;

To assess the crushing characteristics of various stones used in the Construction Industry and come up with an Optimum Dynamical and Structural Design Parameters of a Stone Crusher that is suitable for Small and Medium Scale Entrepreneurs.

1.4. The Specific Objectives

The specific objectives of the study are:

i) To identify and determine the Compressive Strength of selected Rocks.
ii) To carry out Kinematic Analysis, Static and Force Transmission Analysis and Mechanical Advantage Analysis of the Single Toggle Jaw Crusher and the Double Toggle Jaw Crusher mechanisms.
iii) To validate the Kinematical, Static and Force Transmission equations using the dimensional data of the existing Jaw Crusher.
iv) To compare the functionality of the two types of crusher mechanisms and selecting one where parameters are suitable for the design of a Stone Crusher for Small and Medium Scale Entrepreneurs.

1.5. Scope of study

The present study looks at the challenges the Small-Scale Entrepreneurs encounter in the production of aggregates. The study focuses on the production method with an aim of mechanizing it. This will result in the production of a high efficiency and improved performance stone crusher so that the entrepreneurs can get;

i) High quality aggregates
ii) Increased quality of the aggregates
iii) Improved safe and healthy working conditions

CHAPTER TWO

LITERATURE REVIEW

2.1 THE MECHANICS OF STONE CRUSHING

2.1.1 Introduction

The stones used in construction work are often in the form of aggregates. However, the stone occurs naturally in the form of sand or gravel deposits, or as bed rock. The main types of rocks found in Kenya can be subdivided into various categories as shown in Table 2.1. (GoK; Ministry of Mining and Natural Resources, Annual Report, 2013).

Table 2.1: Types of Rocks found in Kenya

Origin of rock	Name of rock	Characteristics and uses	Predominant Location
Sedimentary	Sandstone	Sandstone is cemented or compacted sediment composed predominantly of quartz grains of sand grade. It is one of the commonly used ornamental stones	Coast North Eastern
	Coral Limestone	Limestone is a rock containing over 50% calcium carbonate. The hardest rock in this family is referred to as Coquina and is difficult to shape manually. Limestone is widely used as ornamental stones.	Coast
	Shale	Shale is made up of laminated sediments. Shale is formed as a result of increasing degree of centimentation from clay to mudstone/shale. Used as ornamental stones.	Coast
Igneous	Tuff	Tuff originated from volcanic ash. When ashes are compacted, they yield tuff. It is usually fine grained and	Nairobi, Thika, Londiani

		compact. Tuff is used as a building material.	
	Trachyte, Hornblende Boinite, Gneiss	These are extrusive rocks dominated by alkali felspars. They occur as lava. The ground mass is microcrystalline. They are used as construction materials.	Central and Rift Valley
	Phonolite	Is a fine grained extensive igneous rock consisting of alkali feldspar, feldspathoids and ferro-magnesium. It is hard and not easily shaped. It is used for Bridge construction work	Nyanza and Rift Valley, Western
Metamorphic	Granitoid	These are high grade metamorphic rock of the Mozambican belt system. These rocks are extremely hard. Shaping of these rocks is only possible using machinery. These stones are used for building construction.	Western, Eastern, Rift Valley and Nairobi
	Quartzite	This is a granulose metamorphic rock consisting essentially of quartz. It is closely associated with granitoid rocks. It is brittle and hard and is commonly used as an ornamental stone for outside finishes.	Eastern and Nyanza
	Granite	Granite is very similar in composition to granitoid except that unlike the latter, it is a result of ingenious activity. It is hard and can only be shaped using machinery. Granite is used as building material.	Western, Rift Valley and Central, Nairobi
	Marble	Marble is a metamorphosed limestone also referred to as crystalline	Rift valley South Nyanza

		limestone. It is used as an ornamental stone for outside use in buildings.	
Mixed	Laterite/ Murram	Laterite is a weathering residue comprising of hydroxides of aluminum and iron that is left in a highly insoluble state. These occur near the surface and gradually accumulate to reddish-brown deposits. Laterite can be shaped into brick. They set hard on exposure to the sun. It is used for building construction.	Western, Nyanza, Central and Rift Valley

The aggregate used in the construction industry occurs naturally in the form of rock, therefore, it is necessary to reduce these large masses of rocks to the size required for particular construction work specification. This brings up the technology of stone crushing.

The process of reducing a large masses of stones (boulders) into aggregates of smaller sizes is known as Stone Crushing. Crushing reduces the size of stones to 12mm, 25mm, 50mm, 75mm or 100mm depending on the requirements of the user.

2.1.2 The Stone Crushing Characteristics

Stone crushing into aggregates starts with breaking large boulders of rocks commonly referred to as run-of-mine (ROM) ore by blasting and is followed by a series of crushing starting with primary crushing (250-100mm), followed by secondary crushing (50-100mm) and tertiary crushing (12-50mm).

The technology of stone crushing has been in existence for over 70 years (Coulson and Richardson, 1999). Stone crushing or size reduction is achieved by four principal methods: Compression, Impact, Attrition or Shear.

2.1.2.1 Compression

Compression is the application of a slow large force to cause the rock held between two surfaces to fracture. It is a process employed when the material is hard, tough and abrasive.

2.1.2.2 Impact

It is a sharp, instantaneous collision of one moving object against another. It is used for hard and abrasive material.

2.1.2.3 Attrition

Attrition is a process of reducing of material to desired size by rubbing or scrubbing them between two hard surfaces. It is used for crushing the less abrasive materials. However, it is a process that uses high power and causes wear on the equipment. It is mostly applied to materials which is friable and less abrasive.

2.1.2.4 Shear

Shear involves cleaving action. It is mostly used for materials with relatively low silica content.

2.1.3 Rock Fracture Mechanics

Generally, rock masses contain cracks and discontinuities, hence the extension of fracture mechanics to stone crushing technology (Whittaker *et al.*, 1992). Fracture Mechanics basically deals with the fracture toughness of the material and the geometry of the flaws or cracks. In the communition process, the individual particles are subjected to forces and the fracture toughness invariably constitute to the breakage control (Bearman, 1998).

Griffith (1921) in his classic fracture theory applied the first law of thermodynamics to the formation of a crack. He defined the critical condition for fracture as the point where crack growth occurs under equilibrium conditions without change in the total energy.

Irwin (1957) showed that, the Energy Approach is equivalent to a Stress Intensity Factor K approach. According to Irwin, fracture occurs when a critical stress distribution ahead of a crack tip is reached. In the Griffith's energy balance approach

$$\sigma \sqrt{a} = \left(\frac{2E\gamma_e}{\pi}\right)^{½} \quad \text{..... (2.1)}$$

where σ is the uniform tensile stress applied at infinity on an infinite plate of unit thickness that contains a through thickness crack of length $2a$, γ_e is the elastic surface energy of the material. Equation (2.1) can be written as;

$$\frac{\pi\sigma^2 a}{E} = 2\gamma_e \quad \text{.....(2.2)}$$

Equation (2.1) is the Irwin modification of the Griffith's theory. In equation (2.2), the right-hand side and left hand are respectively.

$$\left.\begin{aligned} R &= 2\gamma_e \\ G &= \frac{\pi\sigma^2 a}{E} \end{aligned}\right\} \quad \text{.....} \quad (2.3)$$

G is designated Energy Release Rate which represent the elastic energy per unit crack surface area that exists for infinitesimal crack extension.

R is the surface energy increase that would occur owing to infinitesimal crack extension referred to as Crack Resistance.

Dowling (1999) explains that G is the fundamental physical property controlling the crack growth.

The stress concentration factor is given as:

$$K = \sigma\sqrt{\pi a} \quad \text{.....} \quad (2.4)$$

The stress σ_y acting normal to the crack plane is given by;

$$\sigma_y = \frac{K}{\sqrt{2\pi r}} \quad \text{.....} \quad (2.5)$$

where r is the distance from the crack tip as shown in Figure 2.1 (Tada *et al.*, 2000)

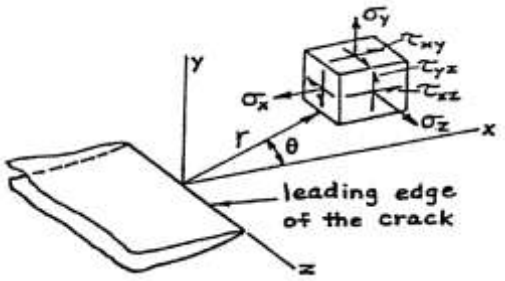

$$\left.\begin{aligned}\tau_{xy} &= \tau_{yx}\\ \tau_{xz} &= \tau_{zx}\\ \tau_{yz} &= \tau_{zy}\end{aligned}\right\} \quad \text{..... (2.6)}$$

Figure 2.1: A Crack Tip Cartesian Coordinate System

2.1.4 Linear Elastic Facture Mechanics (LEFM)

The Linear Elastic Fracture Mechanics is a based on the analytical procedure that related the stress field and stress distribution in the vicinity of a crack tip to the normal stress σ_y applied to the structure; to the size, shape and orientation of the crack or crack like discontinuity and to the material properties, *K* and *G* (Dowling, 1999). Figure 2.2 shows the possible deformation modes at the crack tip (Irwin, 1957).

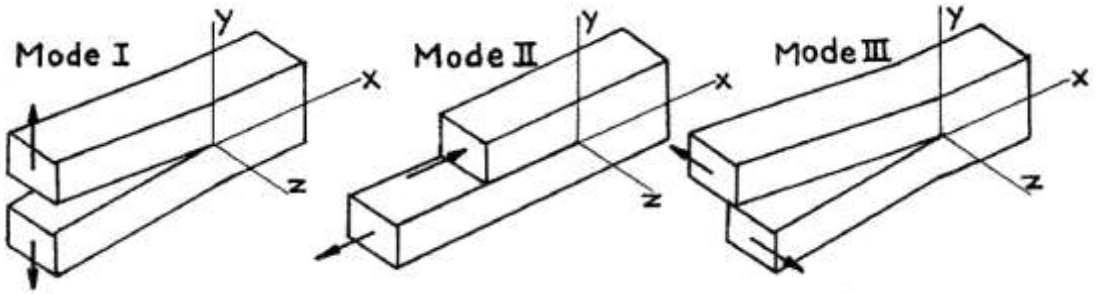

Figure 2.2: The Crack Surface Displacement Modes

The tensile stress applied in the y-direction normal to the face of the crack gives rise to Mode I fracture. The shear stress applied normal to the leading edge of the crack but in the plane of the crack gives rise to Mode II fracture while the shearing stresses applied parallel to the leading edge gives rise to Mode III fracture. Mode I is invariably the mode for

fracture toughness tests and the Critical Stress Intensity Factor determined by this mode is K_{IC}, The fracture toughness of the material given by:

$$K_{IC} = \sigma = \sqrt{\pi a} \quad \ldots\ldots\ldots\ldots\ldots\ldots\ldots\ldots \quad (2.7)$$

The parameter K_{IC} is independent of crack length geometry or loading mode. It is material property in the same sense as yield strength is a material property (Schinidt and Rossmattihm, 1983). Muskhelishvilli (1963) determined K for steel by applying the theory of elasticity and using the coordinate system shown in Figure 2.1 and derived the following field equations for Mode I stress field.

$$\left.\begin{array}{c} \sigma_x = \frac{K_I}{\sqrt{2\pi r}} \cos\frac{\theta}{2}\left[1 - \sin\frac{\theta}{2}\sin\frac{3\theta}{2}\right] \\ \sigma_y = \frac{K_I}{\sqrt{2\pi r}} \cos\frac{\theta}{2}\left[1 + \sin\frac{\theta}{2}\sin\frac{3\theta}{2}\right] \\ \tau_{xy} = \frac{K_I}{\sqrt{2\pi r}} \cos\theta\left[\sin\frac{\theta}{2}\cos\frac{3\theta}{2}\right] \\ \sigma_{\text{ʒ}} = v\left(\sigma_x + \sigma_y\right) for\ plane\ strain \\ \sigma_{\text{ʒ}} = 0, or\ plane\ stress \\ t_{x\text{ʒ}} = t_{y\text{ʒ}} = 0 \end{array}\right\} \quad \ldots\ldots\ldots\ldots\ldots\ldots\ldots\ldots\ldots\ldots \quad (2.8)$$

Moreover, having u, v and w as displacement in the x, y and ʒ direction and substituting Equation (2.7) into Hooke's constitutive law gives:

$$\left.\begin{array}{c} u = \frac{K_I}{G}\sqrt{\frac{r}{2\pi}}\cos\frac{\theta}{2}\left[1 - 2v + \sin^2\frac{\theta}{2}\right] \\ v = \frac{K_I}{G}\sqrt{\frac{r}{2\pi}}\sin\theta\left[2 - 2v - \cos^2\frac{\theta}{2}\right] \\ w = 0 \end{array}\right\} \quad \ldots\ldots\ldots\ldots\ldots\ldots\ldots\ldots\ldots\ldots \quad (2.9)$$

Where G is the Shear Modulus and v the Poison's ratio of the material and K_I is the Stress Intensity Factor of Model I.

From equation (2.8) as the radius r tends to zero, the stresses approach infinity (Inglis, 1913). It is also evident that stresses in equation (2.8) are directly proportional to K_{IC} (Dowling, 1999; Pook, 1972; Murakami, 1987; Rooke and Cartwright, 1976).

2.1.5 Single Particle Breakage (SPB)

The hardness of the stones to be crushed is of importance in the design of the Stone Crusher. Determination of the hardness of material is done via compressive test. Compressive strength is a common strength property associated with comminution equipment and investigative schemes. The work of King (2001) contributed to the understanding of the mechanism responsible for particle fracture process. He concluded that although the rock particle is exclusively loaded in compression, there are multiple loading conditions that cause the set-up of tensile stresses that contribute to catastrophic splitting that are

responsible for the particle breakage. Two modes contribute to fracture mechanism, the catastrophic Splitting and Crushing that cause fructure (Briggs *et al.,* 1996). Berryl *et al.,* (1984) studied the laws of mechanism concerning rock breakage characteristics. George Muir (2007) proved that cracks and the particle behavior becomes weaker as load increases and the macroscopic cracks spread in a tortuous manner until the major crack appears that cause fracture.

Laboratory experiments to determine the uniaxial compressive strength of rocks is due to Al Chalaby *et al.,* (1974), the biaxial compressive tests due to Brown (1974), uniaxial tensile test by Crech (1974), the Brazilian tests by Andrew (1995) and triaxial tests by Peng (1971).

2.1.6 Compression and Tensile Testing

Laboratory experiments to determine the compressive strengths of rocks are due to Al-Chalaby *et al.,* (1974), the biaxial compressive tests due to Brown (1974), uniaxial tensile tests by Crech (1974), the Brazilian tests by Andrew (1995) triaxial tests by Peng (1971). The commonly used standards for comprehensive tests are the International Standards for Rock Mechanics (Carmichael 1989) and the American Standards for Testing Materials (ASTM-D2938).

2.2 THE UNIAXIAL COMPRESSIVE TESTS OF KENYAN ROCKS

2.2.1 Introduction

In engineering, strength of materials is extremely important because the sizing of machine elements depend on the ultimate strength of load bearing components. Therefore, in the design of a stone crusher, it is important to know the compressive strength of the rocks to be crushed. The Uniaxial Compression Test is the most popular test and values in rock mechanics for rock classification and in the design of stone crushing equipment.

2.2.2 Mechanical Properties of Rocks

In communition process, one works with natural material, that is, a stone of which a rock is made, hence it is imperative to understand the properties and behavior of such material at the loading stage, such as in crushing. The laboratory experiments to determine the compressive strength of rocks are due to Al Charby *et al.*, (1974), the biaxial compression test due to Brown (1974), the Brazilian tests by Andrew (1995) and triaxial tests by Peng (1971). Of all these tests, the unconfined Uniaxial Compression Test is the simplest.

2.2.2.1 Uniaxial Compression Test

Uniaxial compression is measured by loading the right circular cylinder along its axis. The Compressive Tests are done according to the American Society for Testing Materials (ASTM-D2938) or the International Standards for Rock Mechanics (Carmichael *et al.*, 1989) reproduced at Appendix I. The ratio of the height of the sample to its diameter lies between two and half to three while the specimen diameter falls in the range of 50mm to 54mm. The Ultimate Compressive Strength (UCS) is then the maximum compressive load to fracture (in Newtons) divided by the original cross-sectional area of the sample (in metrer-squared).

2.2.2.2 Indirect Tensile Test

The Ultimate Tensile Strength (UTS) of a material is defined as the maximum stress to which the material will withstand under a tensile load. However, direct measurement of UTS of a geomaterial such as a rock is difficult because of the challenges in gripping the specimen hence an indirect method is applied where the tensile stress generated by compressive loading. It has been proved that the magnitude of Ultimate Tensile Strength of a rock compared to the magnitude of the Ultimate Compressive Strength is low (Vutukuri et al, 1974).

2.2.2.3 The Brazilian Test

The Brazilian Test (Andrew, 1995) is carried out by loading a cylindrical specimen between two loading plates in compression. The specimen has length to radius ration of 0.9-1.1. and the compression strength at fracture is calculated as;

$$\sigma_f = \frac{2P}{\pi D t} \qquad \ldots\ldots\ldots\ldots\ldots\ldots\ldots\ldots \qquad (2.10)$$

Where σ_f is the fracture stress in MPa

P is the load in kN

D is the diameter of the specimen, in metres

t is the thickness of the specimen, in metres

It is found that the ultimate compressive strength is 0.8 times the Brazilian strength (ISRM, 1988).

2.2.3 Failure Mechanism of Rocks

Rock masses in their natural environment are not uniform, but contains randomly located cracks of various sizes. Hudson and Harrison (1997) investigated the fracture mechanism on rocks and concluded that under compressive loading, cracks develop and increase as the

specimen intensity of these cracks increase and the specimen loses ability to sustain further loads hence fracture.

2.2.4 Factors Affecting the Measurement

In carrying out the uniaxial compressive tests, there are factors that have to be taken into account such as;

i) Shape
ii) Size
iii) Loading rate
iv) Environment
v) Anisotropy and inhomogeneity

2.2.4.1 Effect due to Shape

It has been established that as the ratio of the diameter to height increases, the Ultimate Compressive stresses increased (Hudson *et al.*, 1997).

2.2.4.2 Effect of Size

Vutukuri *et al.,* (1974) found out that specimens with high dimensional ratios tend to be elastically stable. However, Brady et al (2004) in their work concluded that the size effect has not be universally accepted.

2.2.4.3 Loading Rate

The International Standard for Rock Mechanics (ISRM) have recommended the loading rate between 0.5MPa per second to1.0 MPa per second. According to Brady (2004), and referring to ISRM Commission (1979) while testing rock samples for uniaxial compressive strength recommended the strain rates between 10^{-5} per second and 10^{-4} per second.

2.2.4.4 Effect of Environment

Environmental effect needs to be taken into account. Among them the most significant in moisture. Vutukuri *et al.,* (1974) reported that moisture causes significant reduction in compressive strength of rocks.

2.2.4.5 Anisotropy and Inhomogeneity

The rocks in the earth crusts are anisotropic in nature mainly because of their differences in the crystal orientation (bedding and cleavage planes). It has been established (Brady and Brown, 1985) and Jaeger, (1972) that each plane in the rock structure withstand different levels of shear stress and slip occurs when shear stress is equal to shear strength. A rock is not a continuum due to the amount of cracks in them. In addition, the rock material is inhomogeneous as it consists of various mineral grains (Hudson *et al.,* 1997).

2.3. STONE CRUSHER DESIGN CONCEPT

2.3.1. Introduction

Stone crushing is generally done in two or three stage process depending on the end use of the product (aggregates). It is done in either an open circuit, or closed-circuit arrangement as shown in Figure 2.3 and Figure 2.4 respectively (Gansuli and Anderson, 2006).

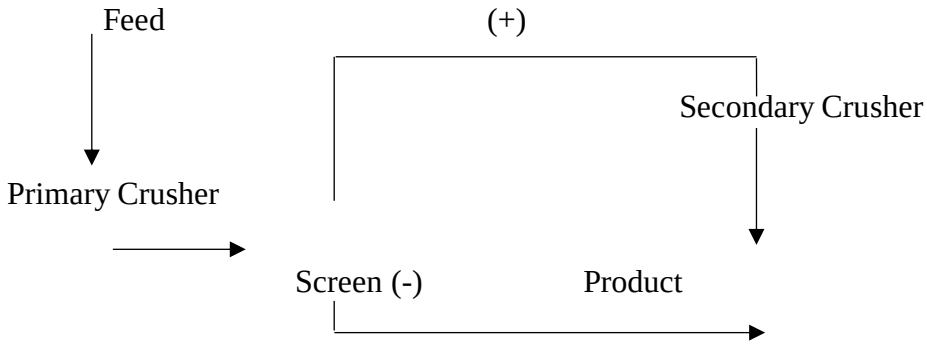

Figure 2.3: Open Circuit in Communition Process

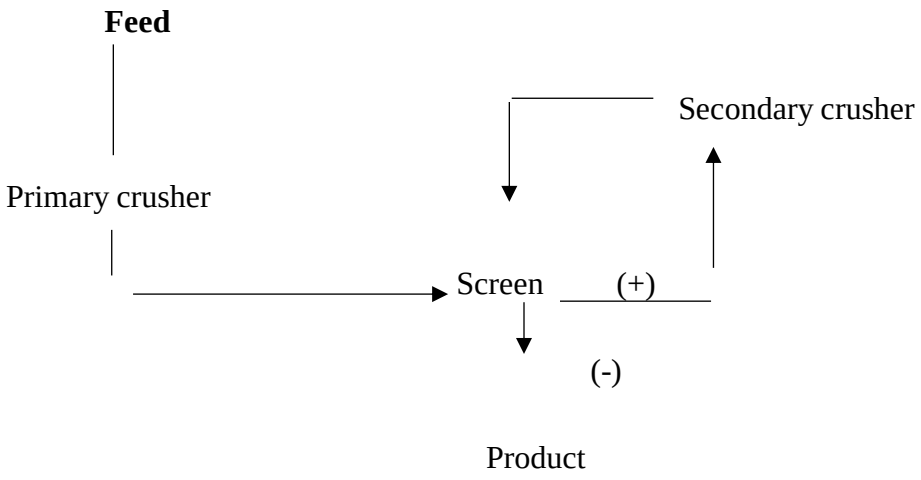

Figure 2.4: Closed circuit in Communition Process

The screen in both cases allows for the sieving of the product before the next stage.

2.3.2. Types of Stone Crushers

There exist four types of crushers, the Jaw Crusher the Gyratory Crusher, the Cone and the Vertical Shaft Impactors (Mular, *et al.*, 2002). Table 2.2 shows the main characteristics of the types of crushers and Figures 2.5 to 2.8 show the types of crushers in the market (Pennsylvania Crusher Corporation, 2003).

Table 2. 2: Types, Characteristics and Application of Stone Crushers

Type of Crusher	Hardness of Crusher Material	Abrasion Limit	Moisture Content of Crushed Material	Size Reduction Ratio	Main uses
Jaw	Soft to very hard	No limit	Dry to slightly wet. Not sticky	3:1 to 5:1	Quarried Material, Sand and Gravel
Gyratory	Soft to very hard	Abrasive	Dry to slightly wet. Not sticky	4:1 to 7:1	Quarried Material
Cone	Medium hard to very hard	Abrasive	Dry or wet. Not sticky	3:1 to 5:1	Sand and Gravel
Vertical Shaft Impactors (Shoe and Anvil)	Medium hard and very hard	Slightly abrasive	Dry or wet. Not sticky	6:1 to 8:1	Sand and Gravel

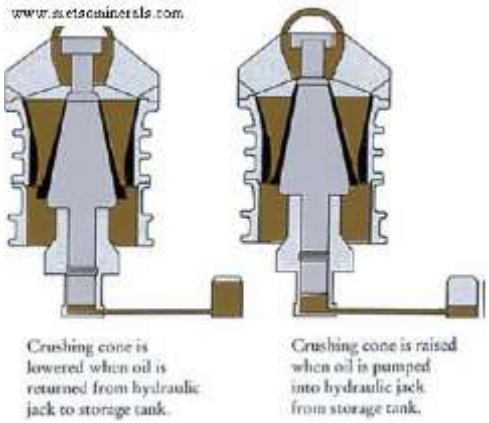

Figure 2.5: Gyratory crusher

Figure 2.6: Jaw crusher

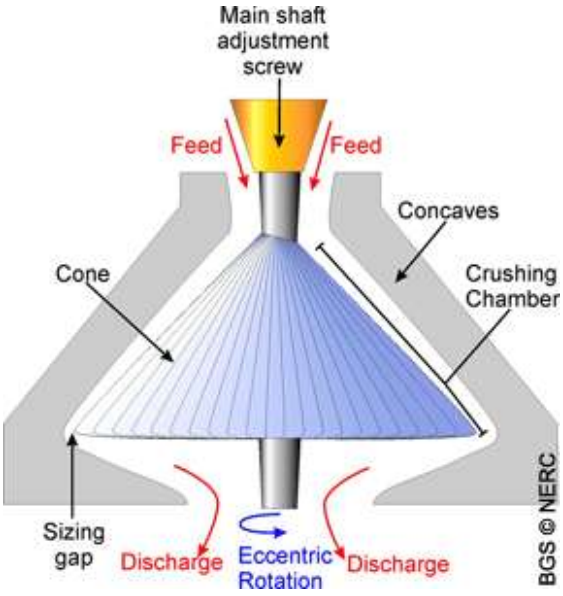

Figure 2.7: Cone crusher

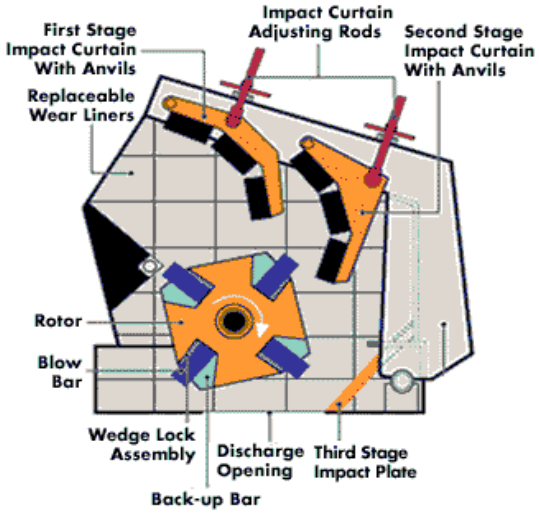

Figure 2.8: Impact crusher

2.3.2.1 Gyratory Crushers

These were invented by Charles Brown in 1877, developed by Gates around 1881 and are at times referred to as Gates Crushers (Weiss, 1985). Gyratory crushers are suitable for a very high capacity crushing plants that are designed to receive run-on-mine (ROM) direct from the mines. Figure 2.5 shows the Gyratory Crusher.

2.3.2.2 Cone Crushers

Cone Crushers were designed and developed by Symons around 1920 and therefore often called the Symons Cone Crushers (Weiss, 1985). The crushing mechanism is similar to that of the gyratory crashers, but in the case of cone crushers, the spindle is supported at the bottom of the gyratory cone instead of being suspended. Figure 2.7 shows a Cone Crusher.

2.3.2.3 Vertical Shaft Impact (VSI) Crushers

In the Vertical Shaft Impact Crushers, the material is fed through a hopper and the tube and drops on a very high velocity rotating table. The attached impellers eject the material at high velocities on to stationary anvils wherein the material is crushed. VSI crushers have higher wear rate compared to jaw or gyratory crushers. Figure 2.8 shows the VSI crusher.

2.3.2.4 Jaw Crushers

In most of the quarries that operate on large or small stone crushing activities, the most easily recognized type of crusher is the Jaw Crusher. The Jaw Crushers have been in operation as early as 1600 (Weiss, 1985). Eli Whitney Blake invented the Blake Jaw Crusher in 1857 (Weiss, 1985).

A Jaw Crusher is versatile, and can be used to crush rocks, whose hardness may range from medium-hard to extremely hard, as well as different kinds of ore, building rubble and glass, among other hard materials. It is widely used in a variety of demolitions, extractions, reclamation and recycling industries, but especially in mining and construction industry (AUBEMA Jaw Crusher, 2013; SBM Mining and Construction Machinery, 2013; Pennsylvania Crusher Corporation, 2006).

The heart of the crushing mechanism of a Jaw Crusher consists of two metallic jaw plates that are slightly and oppositely inclined away from the vertical to form a V- shaped crushing zone with a wide upper opening and narrow lower opening. One of the jaw plates is fixed, whereas the other is movable and referred to as the swinging jaw. When in operation, the charge of the material to be crushed is fed into the crushing zone through the upper opening. The swing jaw is driven to execute a cyclic reversing motion and to apply cyclic intermittent compressive forces that crush the charge of material against the fixed jaw. As the larger lump of material are crushed into smaller lumps, they fall, under gravity, into the narrower lower section of the crushing zone, where they are crushed again into even smaller lumps. This process is repeated until the charge of material is crushed into aggregates that are small enough to fall out of the crusher, through the opening at the lower

end of the crushing zone (Gupta and Yan, 2006). The crushing mechanism is enclosed in a box-like metallic frame.

A Jaw Crusher can be crawler track-mounted to realize a mobile unit that can be repositioned, when the need arises or even as the work advances. In many cases, the Crusher can be easily disassembled for relocation or access to confined places (Carter, 1999). This enables the Jaw Crusher to be used in both surface and underground mining.

Other advantages of the Jaw Crusher include its simplicity in structure and mechanism, reliability, ease of maintenance and high capacity compared to other types of crushers, such as the Cone Crusher, the Gyratory Crusher and the various designs of Impact Crushers (Zhong and Chen, 2010).

The Single Toggle and the Double Toggle Jaw Crushers are presently the most common in the stone crushing and mining industries. They are reliable, affordable and transportable (Carter, 1999).

2.3.2.4.1 The Double Toggle Jaw Crusher

The original Double Toggle Jaw Crusher was designed by El Whitney Blake in the USA in 1857 (Mular *et al.*, 2002). Figure 2.9 shows that Blake Double Toggle Jaw Crusher Mechanism. The movement (motion) of the moving jaw (swing jaw) makes it apply a direct compressive force on the stones being crushed. This kind of loading minimizes the wear of the stone crushing surfaces. This makes the Double Toggle Jaw Crusher to be used in crushing very hard and abrasive material. The role of the toggle, other than to cause a forward and backward movement also acts as overload protection device so that they fail in the event the crusher in overloaded. The Double Toggle Crushers are commercially available (Pensylvania Crusher Cooperation, 2003).

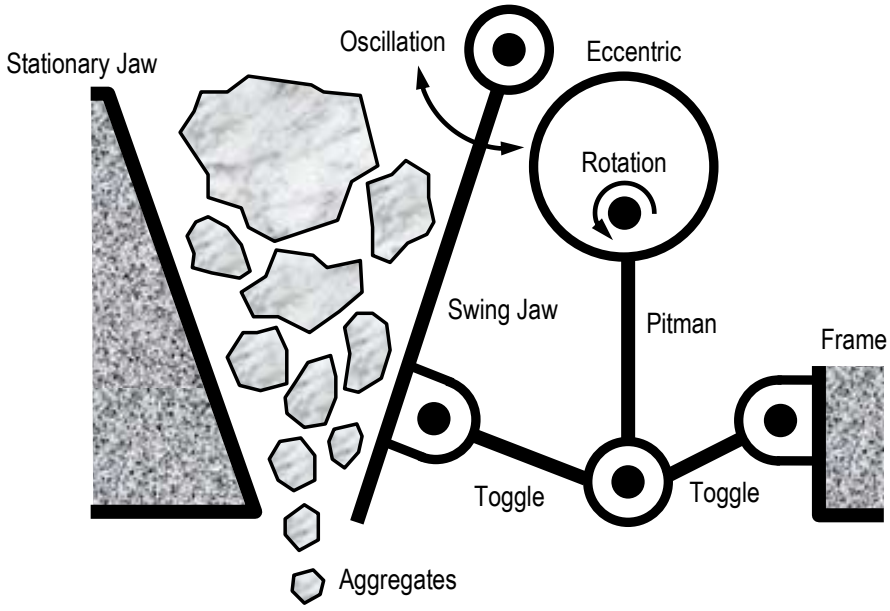

Figure 2.9: The Blake Double Toggle Jaw Crusher Design Concept

2.3.2.4.2 The Single Toggle Jaw Crusher

The Single Toggle Jaw Crusher design, which was developed between 1920 and the 1950 is a simpler and lighter crusher (Mular *et al.*, 2002). Figure 2.10 shows the design of a Single Toggle Jaw Crusher.

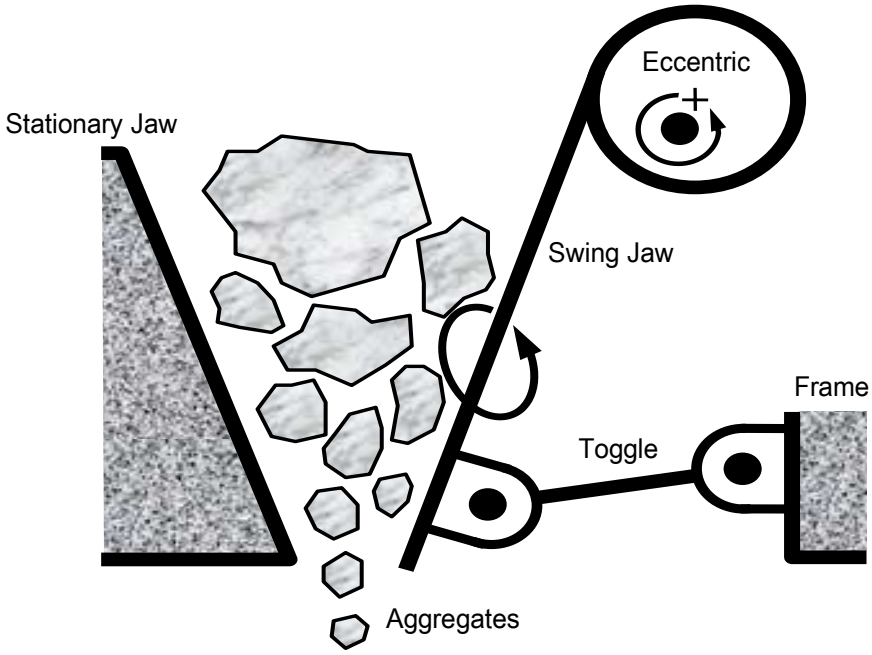

Figure 2.10: Concept of the Single Toggle Jaw Crusher

The swing jaw of the Single Toggle Jaw Crusher has an elliptical rolling motion of the stroke as opposed to the direct reciprocating action of the Double Toggle Jaw Crusher. The motion of the swing jaw is cyclic in nature hence applies both compressive and a rubbing force on the stones being crushed. This action causes heavy wear on the plates of the swing jaw. Improvements in design have made the Single Toggle Jaw Crusher popular in quarrying operations (The Institute of Quarrying, Australia, 2013). Single Toggle Jaw Crushers are easily available (Pennsylvania Crusher Corporation, 2003). Single Toggle Jaw Crushers are easily available (Pennsylvania Crusher Cooperation Ltd, 2003).

The Single Toggle and Double Toggle Jaw Crushers seem to overlap in their application as primary crushers. However, each type has its specific advantage. Table 2.3 shows Single Toggle versus Double Toggle Jaw Crushers (Mular *et al.*, 2002).

Table 2.3: Single Toggle versus Double Toggle Jaw Crushers

	Typical Ore		**Very Hard Ore**
	Single Toggle	Double Toggle	Double Toggle
At top of jaws	30°	25°	20°
1/3 of the way down the jaw	26°	25°	20°

It is observed that;

a) The Single Toggle Jaw Crusher has a longer angle of nip than the Double Toggle Jaw Crusher.
b) With the same feed opening, the Single Toggle Jaw Crusher has a higher capacity than the Double Toggle Jaw Crusher.
c) The life of the Single Toggle Jaw Crusher is shorter than that of jaw of a Double Toggle Jaw Crusher of the same capacity due to the rubbing action of the Single Toggle Jaw Crusher.
d) The Single-Toggle Jaw Crushers is simple in construction, low weight and occupies a smaller space compared to the Double Toggle Jaw Crusher.

Table 2.4 shows a generic crusher selection guide as well as unloaded power drawn (Satyen Moray *et al.*, 2005) for various stone crushers.

Table 2.4: Selection of Crusher Technologies (Satyen Moray *et al.*, 2005)

Type	Hardness	Abrasively	Capacity Range	Reduction Ratio	Use	Unloaded Power Range
Jaw	Medium hard to very hard	Abrasive	Below 600-700tph	8/1 to 10/1	Mostly as primary	40-50% of full load power (FLP)
Gyratory	Medium hard to very hard	Abrasive	Over 1000tph	6/1 to 8/1	Secondary and tertiary	40-50% of FLP
Cone	Medium hard to very hard	Abrasive	Flexible	6/1 to 8/1	Secondary and tertiary	4-0-50% of FLP
VSI	Soft to medium hard	Slightly abrasive	Flexible	15/1 to 25/1	Primary Secondary and tertiary	12-40% of FLP

At the primary crushing stage, the rock is reduced from 1000mm to 230mm rock size, while the secondary and tertiary crushers reduce the rock from 230mm to less than 50mm (Satyen Moray *et al.*, 2005).

The crushers are designed for a certain rock size output, the information for which can be easily found from the stone crusher manufacturers like Pennsylvania Crusher Co. Ltd (2003). Selecting a crusher with the desired rock size output and throughput is critical since it impacts greatly on selection and operation of equipment by the users. Satyen Moray *et al.*, (2003) have given typical gradation curves for a cone from manufactures' perspective (Satyen Moray *et al.*, 2005). Table 2.5 shows the comparison of the crushers. Small Crushes are rated as 3kW to 15kW, medium Crushers are rated 20kW-30kW; high capacity crushers are rated 40kW to as high as 250kW (Pennsylvania Crusher Corporation Ltd, 2003).

Table 2.5: The Advantages and Disadvantages of Various Types of Stone Crushers

Types of Crusher	Advantages	Disadvantages
Jaw crusher	○ Little wearing parts ○ You can make the sizing gap adjustable ○ Easily movable ○ Simple technique ○ The machine has low manufacturing costs ○ Desired output size can be controlled ○ Less force needed	○ The production expires slowly
Gyratory crusher	○ Fast production processes ○ Big capacity	○ Requires too much maintenance ○ Size of the stones is very small ○ Has a lot of wear ○ Uses a lot of power
Cone crusher	○ Low wear ○ Easy to sort out the size of the stones ○ Handles a great capacity of stones ○ Little wearing parts	○ Its heavy machine ○ Much force needed to keep it operating ○ It cannot be operated manually
VSI crusher	○ High capacity	○ Heavy ○ The machine needs a lot of maintenance ○ The size of the crushed stone can't be adjusted

2.4. JAW CRUSHER MODELS

2.4.1 Introduction

The main objective of the stone crushing is to produce good quality aggregates to the customer satisfaction. This has to be accompanied by high productivity in the most efficient manner.

The crusher selection criteria (Section 3.2) and brochures of crusher manufactures can be used to select the ideal crusher in terms of capacities and product size. This will guide in predicting the crusher performance. In the event that these parameters are not known, laboratory test using small scale jaw crushers are used. The laboratory test results are compared to other materials in use to estimate overall performance (Pennsylvania Crusher Corporation, 2003).

Crusher design and evaluation can also be done using mathematical modelling techniques. The advantage of mathematical modelling is that they are simple (Napier- Munn *et al.,* 1999). The major performance parameters to put into consideration include crusher Capacity, Power Drawn and Product Size.

2.4.2 Modeling of Jaw Crusher Capacity

The size of the Jaw crusher is usually described by the gape and the width expressed as GAPE X WIDTH. For instance, 800 x 1000 Jaw crusher has opening of 800mm x 1000mm; a 1600 x 1600 Jaw crusher has opening of 1600mm x 1600mm square (Mular *et al.,* 2002). The man crusher dimensions are defined by:

i. The volume of the particles that go through the crusher, F_{80}
ii. The volume of the particles that can be crushed
iii. The volume of the particles that drops between the jaws at any given time
iv. The volume of the particles that drops down the chamber when the jaws are open as wide as possible, P_{80}

Figure 2.11 shows the main dimensions of the jaw crusher as defined by the volume or the mass of the stone.

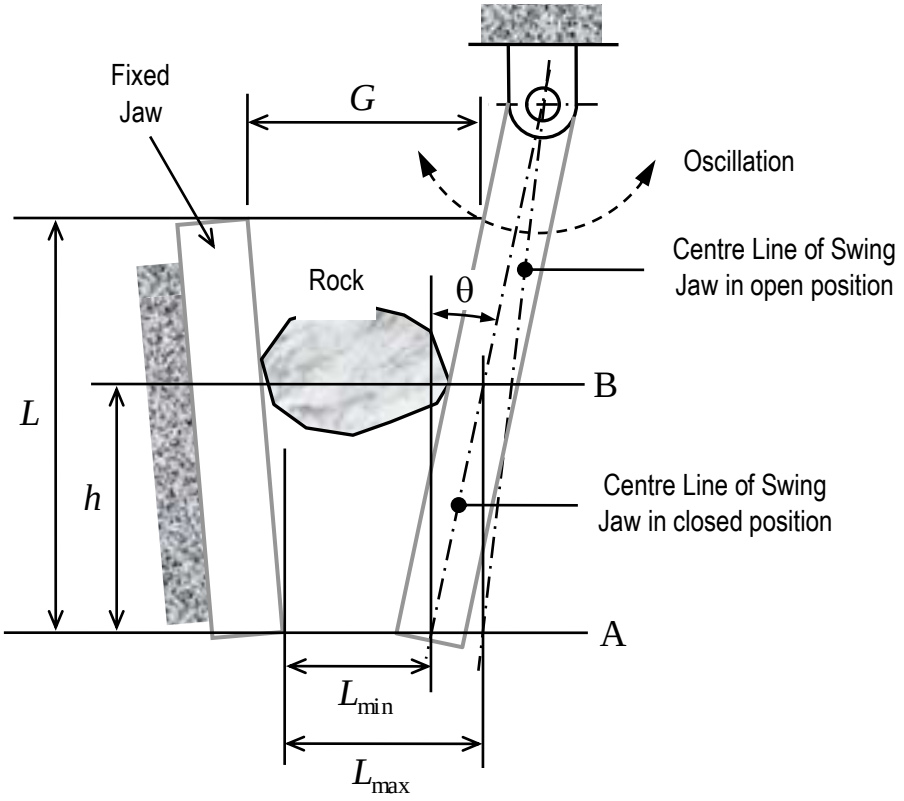

Figure 2.11: Geometrical Model of Material Flow in a Jaw Crusher

i. G = The gape is the distance between the jaws and the feed opening
ii. L = height of the Jaw Plate
iii. L_{min} =The Closed Side Set (CSS) is the Opening between the jaws during the crushing cycle (minimum opening aperture)
iv. L_{max} =The Opening Side Set (OSS) in the maximum opening aperture
v. $L_T = L_{max} - L_{min} = Throw$
vi. The throw is the stroke of the opening jaw. It is the difference between OSS and CSS.

The rule of the thumb (de la Vergne, 2003) applicable for the operation of a jaw crusher with respect to its design characteristics can be summarized as follows;

Vertical height of the Jaw Plate L_x 2 x G……. (2.11)

Nialt of Jaw Plate W > 30 x G…….. (2.12)

Feed size = $(0.8\ to\ 0.9)x\ G$ ……..…… (2.13)

Reduction Ratio: R; 1: 4 to 1: 7……(2.14)

Throw L_T= $0.0502\ x\ G^{0.85}$ ……..(2.15)

Frequency of Stroke = 100 to 300 cycles per minute ……..(2.16)

Mathematically, the jaw crusher capacity can be expressed by the following general relationship.

$$Q = f\ (w, L, L_{min}, L_{max}, L_T, n, \theta, K)\ \text{……..(2.17)}$$

where L_{max} , L_{min} , L_T as defined earlier and

Q is the capacity in tonnes/hour

W is the width of the jaw in, metres

L is the depth of jaws in metres

n is the frequency of strokes (cycles of stroke per minute, rpm).

K is the constant related to machine characteristics

θ is the jaw angle in degrees

The mechanism of movement of the rock down the chamber determines the capacity of the jaw crusher. The movement can be visualized as a succession of wedges that reduce the size of rocks progressively by compressing, until the smallest aggregates pass through the

crusher in a continuous manner. The output of the crusher per minute will therefore depend on the time taken for a rock that is fed to the crusher to the crushed and pass through the successive wedges until it is discharged through the bottom (CSS). The frequency of oscillation of the swing jaw has a significant effect as the output of the crusher.

From Figure 2.11, a stone would fall through the distance *h* during half a revolution of the eccentric, provided that the duration of the half- revolution is long enough to allow the stone to fall through this distance under the action of gravity. If *n*/s the number of revolutions per minute (*rpm*) of the eccentric shaft, then the duration of half a revolution would be

$$t = \frac{60}{2n} = \frac{30}{n}\ seconds \quad \text{.....(2.18)}$$

Thus, by considering the uniform acceleration of the freely failing stone under the action of gravity, the distance for which the particle moves is;

$$h = \frac{1}{2}gt^2 \quad \text{..... (2.19)}$$

$$= \frac{1}{2}\ x\ 9.81x\ \left(\frac{30}{n}\right)^2 = \frac{4414.5}{n^2}\ meters$$

$$\therefore n = 66.44\ \sqrt{h}\ \ rpm \quad \text{..... (2.20)}$$

For a fragmented stone to fall through the distance *h*, the rate of revolution of the eccentric shaft must be less than the value determined by equation (5.9). The distance h can be expressed in terms of L_{min} and L_{max} provided that the angle θ is known. From Figure 4.10

$$\tan\theta = \frac{L_{max} - L_{min}}{h}$$

$$\therefore h = \frac{L_{max} - L_{min}}{\tan\theta} \quad \text{..... (2.21)}$$

In this model, the fixed jaw is assumed to be vertical while the centerlines of the swing jaw in the closed position and in the open position are assumed to be parallel.

Rose and English (1967) observed that as the frequency of oscillation of the swing jaw increased, the rate of production of aggregates first increased upto a maximum value and then decreased with further increase in frequency. This may be explained by the fact that an increase in frequency of oscillation of the swing jaw reduces the time allowed for a stone fragment to free- fall through a distance *h*. Thus, beyond a certain frequency, the distance *h* through which a stone free- fall is so small as to be counter- productive.

For relatively low frequencies of oscillation of the swing jaw, Rose and English (1967) derived the following expression for the productivity of the crusher:

$$Q_s = 60 L_T n W\ (2L_{min} + L_T)\left(\frac{R}{R-1}\right) \qquad (2.22)$$

where

$Q_s =$ is the machine's productivity in terms of volume of materials produced per hour

Equation (2.22) reveals that the productivity Q_s is directly proportional to the frequency of oscillation of the swing jaw, *n*.

With faster oscillation of the swing jaw where the rock fragments cannot complete their free fall, the productivity was found to be inversely proportional to frequency as could be expressed as follows (Rose and English, 1967):

$$Q_s = 132435 W\ (2L_{min} + L_T\left(\frac{1}{n}\right) \qquad (2.23)$$

2.4.3. Modeling of the Power Drawn

Based on Bond's Third Theory of Communition (Bond, 1952), the power requirements in kilowatts was expressed in terms of the Bond's Work Index as follows:

$$H = 10 W_i Q \left[\frac{1}{\sqrt{P_{80}}} - \frac{1}{\sqrt{F_{80}}}\right] \qquad (2.24)$$

where H is the power requirement in kilowatts

Q is the crusher's productivity in metric tones per hour (t/h)

W_i is the Bond's Work Index

P_{80} is the size at which 80% of the product passes measured in tonnes

F_{80} is the size at which 80% of the feed passes measured in tonnes

The Bond's Work Index is a measure of Grindability or Crushability of minerals as is a metre is a measure of linear dimensions, in metres as Young's Modulus, E, is a measure of strength of materials in GPa; while the Critical Stress Intensity factor, K_{IC} is a measure of Material Toughness in MPa $m^{3/2}$. Table 2.6 shows Bond's Work Index for some rocks.

Table 2.6: Bond's Work Index for some Mineral (Weiss, 1985)

Minerals	**Work Index (kWh/t)**
Andesite	20.12
Basalt	18.85
Bauxite	9.68
Gabbro	20.34
Glass	13.57
Gneiss	22.19
Granite	16.59
Quartzite	10.59
Diorite	23

2.4.4 Modeling of Product Size

The particle breakage process inside the crushing chamber operates simultaneously with classification process. The feed material entering the crusher is first classified, with

particles smaller than the CSS of the crusher avoiding breaking and moving on as product. Particles larger than OSS of the crusher "report" to breakage and will undoubtedly be broken, while particles in between CSS and OSS report to breakage but with a probability of broken that decreases with size. The process continues with each cycle of the swing jaw and is illustrated in the flow chart of Figure 2.12.

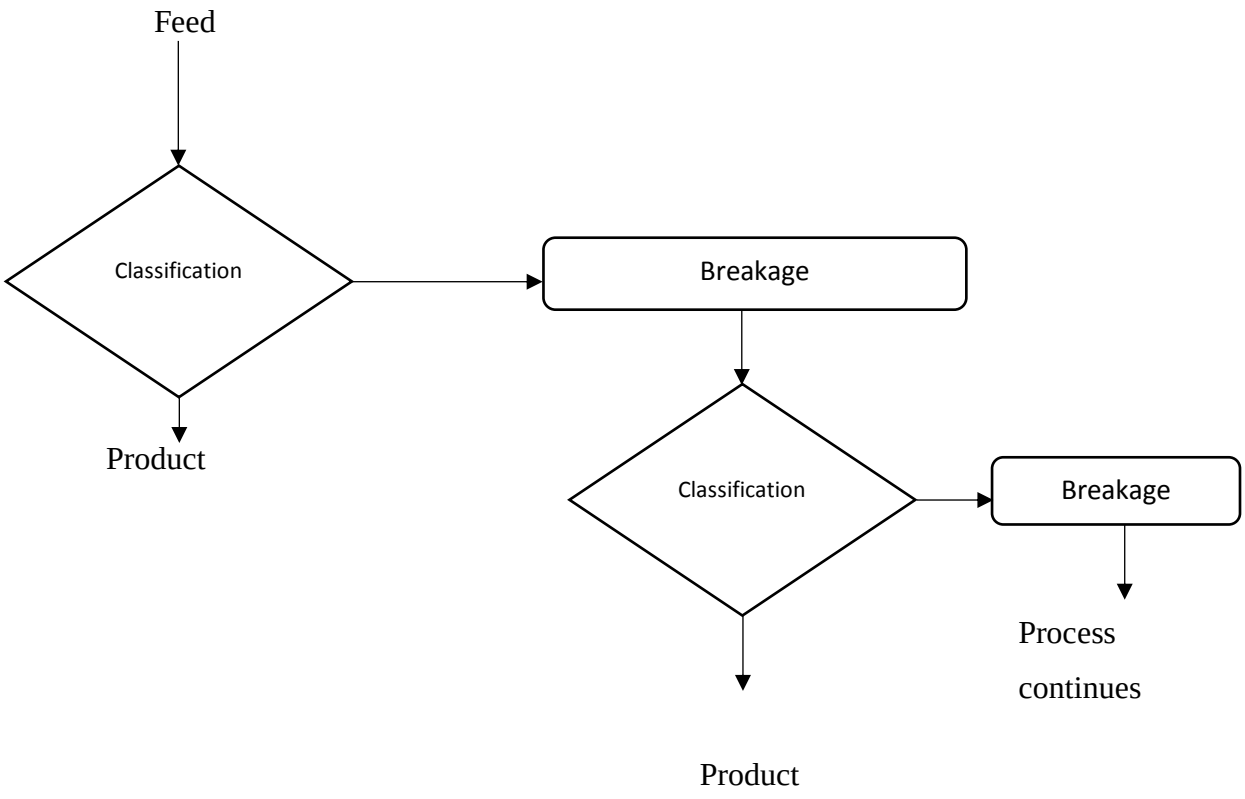

Figure 2.12: Flow chart of Classification – Breakage Process (After Napier – Munn et al; 1999)

Considering the classification and breakage of particles in a jaw crusher as a closed circle process, reduces Figure 2.12 to a flow path shown in Figure 2.13 after (Whitten (1972).

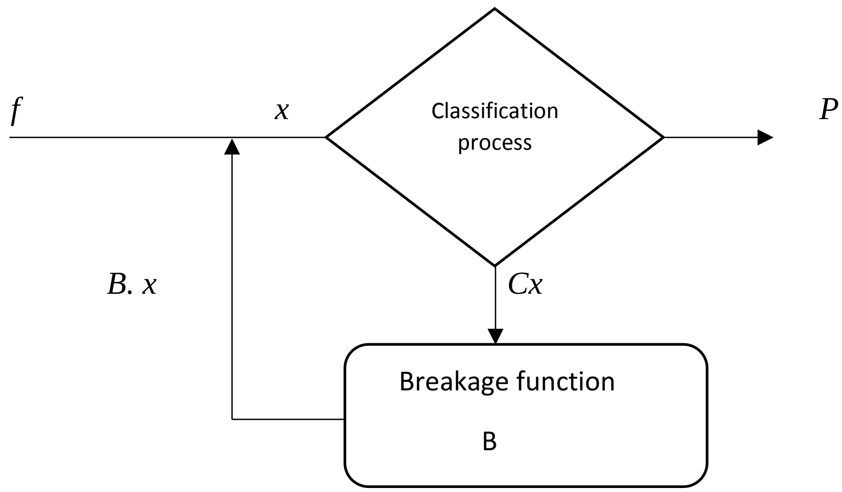

Figure 2.13: Whitten Crusher Model

The mass balance equation written at each node of Figure 2.13 describes the repetitive process of classification and breakage and can be expressed as (Kajovic *et al.,* 1997).

$$\bar{x} = \bar{f} + B\bar{x} \quad \text{..} \ (2.25)$$

$$\bar{x} = \bar{p} + C\bar{x} \quad \text{..} (2.26)$$

where $\bar{x}$ = a vector representing the amount in each fraction entering the chamber

$\bar{f}$ = the feed size distribution vector

$\bar{p}$ = the product distribution vector

B = the breakage function

C = the classification diagonal matrix

The classification matrix C describes the propagation of particles entering the crushing zone. The breakage distribution matrix gives the relative distribution of each size fraction after a breakage event. Combining equations (2.24) and (2.26), result in the Whitten Crusher Model equation (Whitten, 1972).

$$P = (\bar{I} - \bar{C}).(I.BC)^{-1}\bar{f} \quad \text{.....(2.27)}$$

where I the unit matrix

Equation (2.27) can be used to determine the product size of a jaw crusher given the feed size classification function and the breakage function.

The classification function is the probability of a particle being selected for breakage and which is dependent upon particle size. For example, a particle smaller than the CSS of the crusher probably will not be broken or has only a small probability of being selected for breakage. Whitten (1972) used the following set of functions to describe the classification function.

$$\left.\begin{array}{ll} C(x) = 0 & for\ x < K_1 \\ C(x) = 1 - \left(\frac{K_2 - x}{K_2 - K_1}\right)^{K_3} & for\ K_1 < x < K_2 \\ C(x) = 1 & for\ x < K_2 \end{array}\right\} \quad \text{.....(2.28)}$$

Where K_1 is the particle size below which all particles will "by-pass" breakage and go directly to the product.

$K_2 =$ the size below which all the particles will be broken. These two parameters are expected to be functions of the crusher sets, K_1 being dependent upon CSS and K_2 upon OSS. As an exponent, K_3 describes the shape of the classification function for particles between the K_1 and K_2 sizes as shown in Figure 2.14.

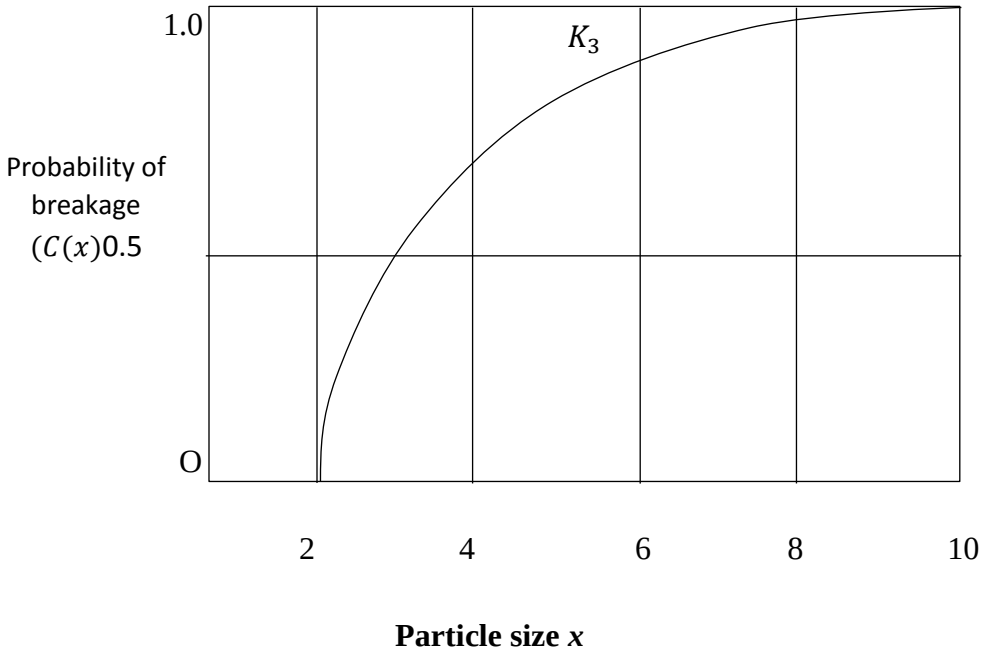

Figure 2.14: Whitten Classification Function

Research has shown that K_1 and K_2 are, in addition to closed and open side set, functions of feed size, throughout, crusher throw, and plate linear characteristics with exact relationships being found empirically using usual operating conditions/parameters (Napier-Munn et al, 1999; Whiten, 1984; Karra, 1982; Anderse, 1988; Anderson and Napier-Munn, 1990).The same work has shown that K_3 remains fairly constant in most instances with a value around 2.3.

2.5. THE SINGLE TOGGLE JAW CRUSHER KINEMATICS

2.5.1. Introduction

The Single Toggle Jaw Crusher has advantages over the Double Toggle Jaw Crusher, such as simplicity in its structure and mechanism, reliable performance, ease of manufacture and maintenance. It is widely used in the mining and construction industries.

The crushing action is brought about by the motion of the swing jaw and the forces that it exerts on the material being crusher. Therefore, in the study and design of the Single Toggle Jaw Crusher, it is important to understand the kinematics of the swing jaw in order to obtain equations that can be used to describe the motion of any given point in the swing jaw of the crusher.

2.5.2. Analysis of the Single Toggle Jaw Crusher Kinematics

Analysis of the Jaw Crushers has been done by several researchers (Ham *et al.,* 1958; Martin George, 1982; Erdman and Sandor, 1991). Until Cao *et al.,* (2006), Deepak (2010), the literature on the kinematical analysis of jaw crushers of any kind, in general and Single Toggle Jaw Crushers, in particular, has not been common to find. Cao *et al.,* (2006) presented the kinematical equations for Single Toggle Jaw Crusher without giving details of their derivations. The paper deals with the mechanism of fracture of the material being crushed, the wear of the crushing jaw surfaces, and it endeavors to explain these phenomena with regard to the kinematics of the swing jaw.

Deepak (2010) derived, in details, the same kinematical equations that had been presented by Cao *et al.,* (2006). Garnaik (2010) used the equations that had been presented by Cao *et al.,* (2006) and wrote MATLAB programmes that were used to plot graphs of the kinematical quantities that described the motion of the Single Toggle Jaw Crusher.

2.6. THE SINGLE TOGGLE JAW CRUSHER FORCE TRANSMISSION CHARACTERISTICS

2.6.1. Introduction

The linkage mechanisms like those in jaw crushers have three main functions:

i. Function Generation
ii. Motion Generation
iii. Path Generation

Several researchers (Erdman and Sandor, 1991; Norton, 1992; Shigley and Vicker, 1980) have written extensively on the Single Toggle Jaw Crusher Force Transmission Characteristics. For Functional Generation, Fraudestien (1955) introduced analytical method for the design of four Bar Planer Mechanisms. For Motion Generation, which is also known as Rigid Body Guidance, Wang et al (2002) made a study on planar linkage mechanism. Path Generation Mechanism was reported by Soong and Wu (2009).

In general, linkage mechanism like those in Jaw Crushers are used for;

i. Transformation of Motion and Force
ii. Transmission of Motion and Force

The primary work of a Single Toggle Jaw Crusher is not only to transmit and transform motion but has also to transmit and transform the large forces that are required to crush the stones by compression. It is therefore important to understand the characteristics of Motion and Force Transmission while in the crushing process. This will enable the design engineer to use this information for proper design of the crusher. Figure 2.15 shows a cross-section of the Single Toggle Jaw Crusher.

In this section;

i. A static Force Analysis is carried out
ii. A Characteristic Force Transmission Ratio (FTR) commonly referred to as mechanical Advantage (MA) is accomplished.

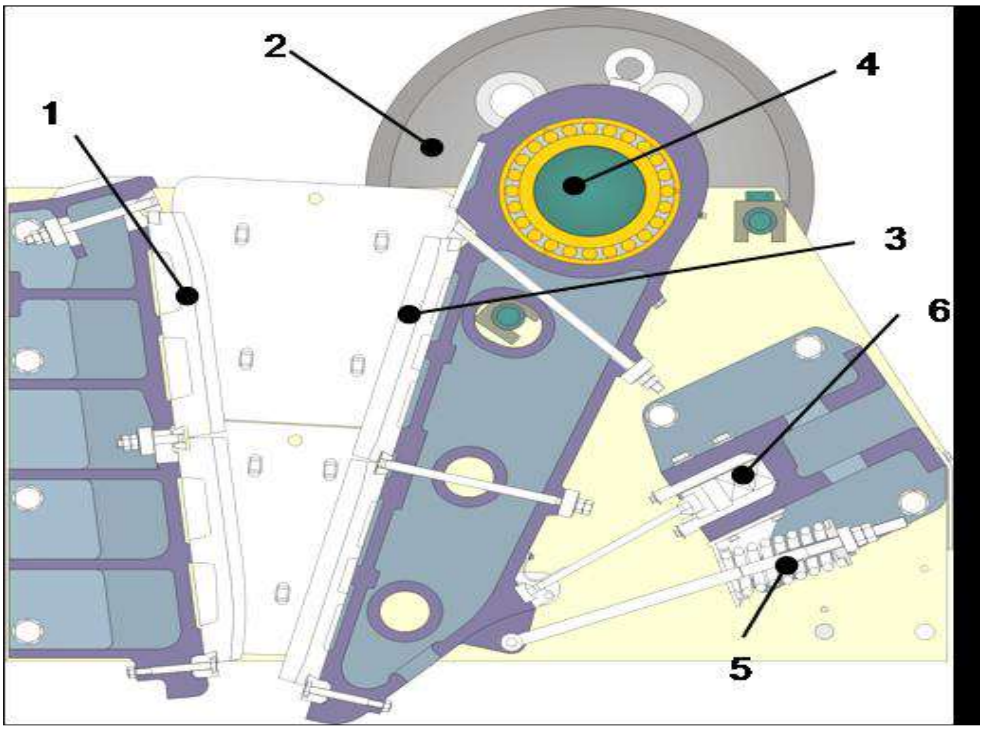

Figure 2.15: Jaw Crusher Cross Section (1. Fixed jaw, 2. Flywheel, 3. Moving jaw, 4. Eccentric Shaft, 5. Tension Spring, 6. Toggle Plate) (Metso Minerals, 2008)

2.6.2. Analysis of the Single Toggle Jaw Crusher Force Transmission Characteristics

Several researchers have done work on Force Transmission Characteristics of Single Toggle Jaw Crushers. Lin and Chang (2002) worked on the Force Transmissivity in planar linkage mechanisms. They derived equations that related input and output power flow in the linkages. From their research work, they came up with what they referred to as Force Transmission Index (FTI). Lin and Chang (2002) further derived the Effective Force Ratio (EFR) as the ratio of the sum of the actual maximum possible power transmitted in the power flow to the sum of the maximum possible power that could be transmitted along the same power path. They compared their results with those of Danvit *et al*., (1965) who used the Jocobian Matrix Method. Holte and Chase (1994) derived the Joint Force Index (JFI) and found that the Force Transmissions Index was more superior and accurate. The main difference in these methods is that the Jacohian Method does not consider the external loads while the Joint Force Index Method does not consider the power flow in the system.

2.7. THE DOUBLE TOGGLE JAW CRUSHER KINEMATICS AND MECHANICAL ADVANTAGE

2.7.1 Introduction

Eli Whitney Blake invented the Double Toggle Jaw Crusher in the USA in 1857 (Mular, et al, 2002). Figure 2.16 shows a typical cross section of a Double Toggle Jaw Crusher. In the Double Toggle Jaw Crusher, the moving jaw (Swing Jaw) applies a direct reciprocating compressive force on the stones being crushed. This implies that the wear on the crushing surfaces in minimal. This makes the Double Toggle Jaw Crusher ideal for crushing very hard and abrasive materials.

In order to analyze the force transmission characteristics and the dynamics of the mechanism of the Double Toggle Jaw Crusher, it is important to first analyze the kinematics of the Double Toggle Jaw Crusher.

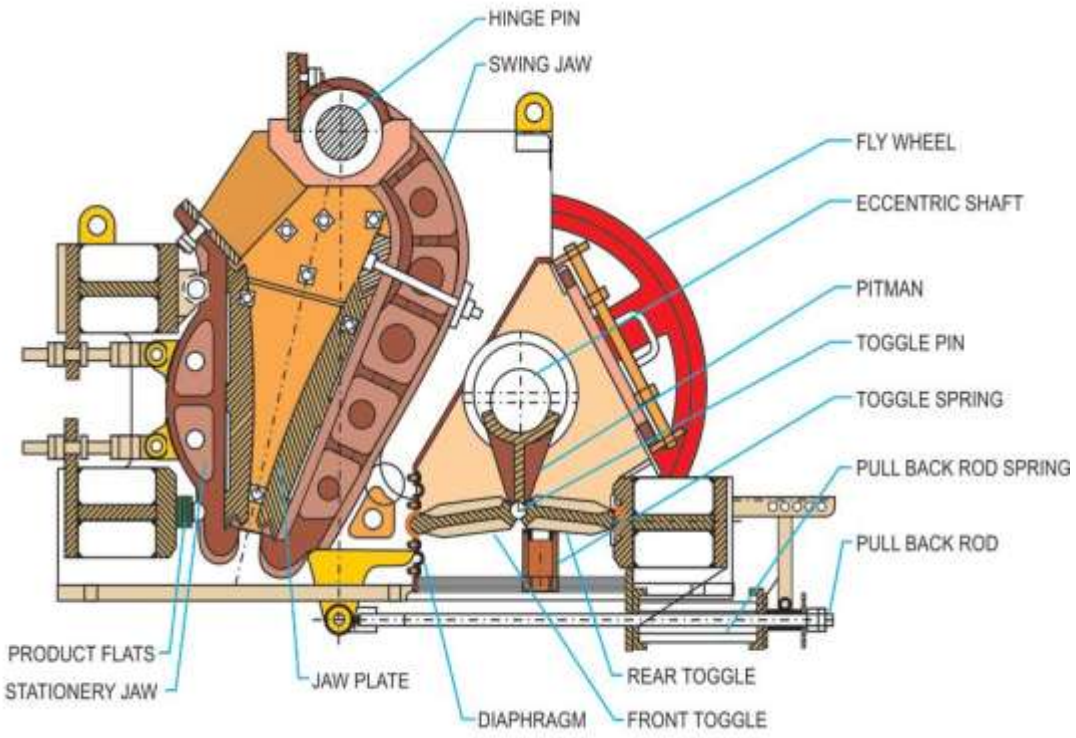

Figure 2.16: Typical Cross Section of a Double Toggle Jaw Crusher

2.7.2. Kinematics and Mechanical Advantage of the Double Toggle Jaw Crusher

For a long time, the attention of various researchers has been drawn to the mechanics of the Jaws Crusher (Ham *et al.,* 1958, Martin, 1982; Erdman and Sader, 1991). Yet until recently (Cao *et al.,* 2006; Deepak, 2010; Luo, 2012; Oduori *et al.,* 2015; Zhandfeng *et al.,* 2015), it has not been common to find the treatises on the kinematics of the Jaw Crushers in general, and a Double Toggle Jaw Crusher, in particular. Oduori *et al.,* (2015 reviewed publications, by Ham *et al.,* (1958) as well as Martin (1982) presented the crusher as an example of a toggle mechanism. Oduori *et al.,* (2015) also reviewed publications, by Erdman and Sandor (1991) that presented the Double Toggle Jaw Crusher as a typical example of a toggle linkage mechanism in the determination of mechanical advantage using the method of complex numbers but did not present a kinematical analysis of the mechanism. Further, Oduori *et al.,* (2015) reviewed publications by Cao *et al.,* (2006), Deepak (2013) and Garnak (2013) each of which performed kinematical analysis of the Single Toggle Jaw Crusher. None of these presentations deals with the kinematics of the Double Toggle Jaw Crusher.

Luo and Shehuan (2012) presented a design optimization of the Double Toggle Jaw Crusher that includes a kinematical analysis. Likewise, Zhangfeng *et al.,* (2015) presented what they called a Biaxial Compound Pendulum Jaw Crusher, which commenced with a kinematical analysis. This crusher may be regarded as a cross between the Single Toggle and the Double Toggle Jaw Crusher. It has two driven eccentric mechanism and was modelled by Zhangfeng *et al.,* (2015) as a seven-bar planar linkage mechanism. Though the mechanism of this crusher in more complex and likely to be more costly, its performance was reported to be superior to the Single and the Double Toggle types.

Ham, Crane and Rogers (1958) discussed the Double Toggle Jaw Crusher as an example of a machine that utilizes the toggle effect to exert the large forces that are necessary for crushing the hard rocks. They performed a static force analysis of the mechanism but they did not perform a kinematical analysis. Martin (1982) who presented the Double Toggle Jaw Crusher as a typical example of a toggle mechanism but did not carry out a kinematical or statical force analyses of the system. Oduori *et al.,* (2015) used a convenient Cartesian

coordinate reference frame in setting up a kinematical model of the Single Toggle Jaw Crusher. They applied the Vector Loop Closure Method (Erdman and Sandor, 1991; Norton, 1992; Kimbrell, 1991; Shigley and Vicker, 1980) and managed to derive the required kinematical expressions in logical and efficious manner. Subsequently, Oduori *et al.*, (2015) went further and performed an analysis of the force transmission characteristics of the Single Toggle Jaw Crusher Mechanism. The power and versatility of the Vector Closure Loop Method is used here to carry out a kinematical analysis of the Double Toggle Crusher Linkage Mechanism.

CHAPTER THREE

METHODOLOGY

3.1 THE UNIAXIAL COMPRESSIVE STRENGTH TEST OF KENYAN ROCKS

3.1.1. Introduction

The primary objective of laboratory tests is to determine the Mechanical and Physical Properties of Materials, from Concrete, Steel, Composites, Hair to Ceramics. The construction of structures and superstructures like Roads, Buildings, Railways, Machinery and so forth would have been impossible without the knowledge and experimental work in research laboratories.

In this work, the results of the Ultimate Compressive Tests carried out at the Laboratory of Strength of materials at the University of Nairobi, are analyzed. The results of these tests will not only be useful in designing a stone crusher machine element but also useful in the future research work. The result of these tests will not only be useful in designing a Stone Crusher machine element but also useful in future research work.

3.1.2. Research Plan

The research plan consists of;

i) The test data by rock identification and classification
ii) Analyze the compressive strength of different types of rocks
iii) Statistical Analysis of the results of the tests (average, variance, standard deviation)
iv) Compare the results with other researchers' findings

3.1.3. Experimental Procedure

The rock samples were collected from quarry sites in Bungoma, Siaya, Vihiga, Meru, Nyeri, Nairobi, Uasin Gishu and Machakos Counties of Kenya. They were identified by the Geology Department at the University of Nairobi, and classified according to the

mineral composition, texture and color. Twelve test specimens were prepared from various rock types by cutting into flat ends using a diamond wheel saw and turned on a lathe machine into a cylindrical shape as per ISRM (1988). This was done at the Ministry of Mining and Natural Resources Workshop, Nairobi.

The samples were designated as shown in Table3.1 for identification purposes.

Table 3.1: Designation of Rock Samples

Name of rock	Designation
Schist	K1
Gneiss	K2
Tuff	K3
Granodiorite	K4
Quartzite	K5
Granite	K6
Phonolite	K7
Grey Wacke	K8

In the Strength of Materials Laboratory at the University of Nairobi; experiments were carried out. Twelve specimens per rock type were tested.

The test equipment is Universal Testing Machine (UTM), Senstar. The loading equipment consists of a servo-hydraulic system incorporating a load cell as shown in Figure 3.1. A digital acquisition system accompanied the UTM system (upper right-hand corner of Figure 3.1) displays and records the raw data during each test. The raw data is the total displacement measure by the LVDT and the load is measured by the load cell.

Each sample is placed on the platen in the stone loading (crushing) chamber then loaded to fracture.

Figure 3.1: Experimental Set Up for Compressive Strength Test (Photo: Institute of Computing and Informatics, University of Nairobi).

3.1.4 Statistical Analysis Method

The method adapted in this research work is that due to Holman (1994) in which the main parameters adopted include the average (mean), the variance and the standard deviation of the samples. Therefore;

$$Mean, \qquad \bar{x} = \frac{1}{n}\sum_{i=1}^{n} x_i \quad \ldots\ldots\ldots\ldots\ldots\ldots \quad (3.1)$$

$$Variance, \qquad S^2 = \frac{1}{n-1}\sum_{i=1}^{n}(x_i - \bar{x})^2 \quad \ldots\ldots\ldots\ldots\ldots\ldots\ldots \quad (3.2)$$

$$Standard\ Deviation, \qquad SD = \left[\frac{1}{n-1}\sum_{i=1}^{n}(x_i - \bar{x})^2\right]^{1/2} \quad \ldots\ldots\ldots\ldots\ldots\ldots\ldots \quad (3.3)$$

3.1.5 Laboratory Test Results

Each rock type was analyzed separately. In total 12 rock samples for each rock type were tested for uniaxial compressive strength. The results are presented in Tables 3.2 to 3.9

Table 3.2: Experimental Results for Schist

Specimen number	**1**	**2**	**3**	**4**	**5**	**6**	**7**	**8**	**9**	**10**	**11**	**12**
Diameter x 10^{-2}m	5.1	5.2	5.05	5.0	5.2	5.2	5.0	5.0	5.05	5.1	5.1	5.2
Cross sectional area x $10^{-3}m^2$	2.043	2.124	2.003	1.963	2.124	2.124	1.963	1.963	2.003	2.043	2.043	2.124
Compressive crushing load (kN)	100	170	120	160	140	170	180	200	190	171	160	156
Compressive stress (MN/m^2)	50.93	80.04	59.91	81.5	65.91	80.03	91.7	101.88	94.86	83.7	78.32	73.45

Table 3.3: Experimental Results for Hornblende Boilite Gneiss

Specimen number	**1**	**2**	**3**	**4**	**5**	**6**	**7**	**8**	**9**	**10**	**11**	**12**
Diameter x 10^{-2} m^2	5.0	5.1	5.2	5.1	5.0	5.3	5.2	5.1	5.0	5.2	5.1	5.2
Area $10^{-3}m^2$	1.963	2.043	2.124	2.043	1.963	2.206	2.124	2.043	1.963	2.124	2.043	2.124
Compressive Crushingload (kN)	225	220	180	120	90	170	240	140	200	270	195	210
Compressive stress (MN/m^2)	114.6	107.68	84.75	58.74	45.85	77.06	112.99	68.53	101.88	127.12	95.45	98.87

Table 3.4: Experimental Results for Tuff

Specimen number	1	2	3	4	5	6	7	8	9	10	11	12
Diameter x 10^{-2}m	5.0	5.0	5.1	5.0	5.05	5.1	5.2	5.1	5.0	5.2	5.1	5.0
Cross sectional area x $10^{-3}m^2$	1.963	1.963	2.043	1.963	2.003	2.043	2.124	2.043	1.963	2.124	2.043	1.963
Compressive crushing load (kN)	260	160	90	90	210	70	50	110	112	200	180	105
Compressive stress (MN/m^2)	132.45	81.51	44.53	45.85	104.54	34.63	23.54	53.84	57.06	94.16	88.11	53.49

Table 3.5: Experimental Results Granodiorite

Specimen number	1	2	3	4	5	6	7	8	9	10	11	12
Diameter x 10^{-2}m	5.0	5.2	5.1	5.05	5.0	5.1	5.2	5.3	5.0	5.1	5.2	
Cross sectional area x $10^{-3}m^2$	1.963	2.124	2.043	2.003	1.963	2.043	2.124	2.206	2.124	1.963	2.043	2.124
Compressive crushing load (kN)	130	150	90	70	160	200	250	170	220	215	105	150
Compressive stress (MN/m^2)	66.23	70.62	44.05	34.95	81.51	97.90	117.70	77.10	103.58	109.53	51.40	70.62

Table 3.6: Experimental Results for Quartzite

Specimen number	1	2	3	4	5	6	7	8	9	10	11	12
Diameter x 10^{-2}m	5.0	5.05	5.1	5.0	5.2	5.1	5.0	5.1	5.2	5.1	5.1	5.1
Cross sectional area x $10^{-3}m^2$	1.963	2.003	2.043	1.963	2.124	2.043	1.963	2.043	2.124	2.043	1.963	2.043
Compressive crushing load (kN)	190	150	180	220	190	100	150	160	70	60	75	120
Compressive stress (MN/m^2)	91.79	76.41	88.11	112.07	89.45	48.95	76.41	78.32	32.96	29.37	38.21	58.74

Table 3.7: Experimental Results for Granite

Specimen number	1	2	3	4	5	6	7	8	9	10	11	12
Diameter x 10^{-2}m	5.0	5.1	5.2	5.2	5.1	5.0	5.0	5.2	5.1	5.0	5.2	5.0
Cross sectional area x $10^{-3}m^2$	1.963	2.043	2.124	2.124	2.043	1.963	1.963	2.124	2.043	1.963	2.124	1.963
Compressive crushing load (kN)	220	150	250	150	250	180	1250	230	160	190	150	175
Compressive stress (MN/m^2)	113.19	73.42	117.70	70.62	112.37	91.70	76.41	108.29	78.32	96.79	70.62	89.15

Table 3.8: Experimental Results for Phonolite

Specimen number	1	2	3	4	5	6	7	8	9	10	11	12
Diameter x 10^{-2}m	5.2	5.1	5.3	5.0	5.1	5.3	5.0	5.1	5.2	5.0	5.2	5.1
Cross sectional area x $10^{-3}m^2$	2.124	2.043	2.206	1.963	2.043	2.026	1.963	2.043	2.124	1.963	2.124	2.043
Compressive crushing load (kN)	70	150	110	150	220	110	80	230	160	200	120	180
Compressive stress (MN/m^2)	32.96	73.42	49.86	76.41	107.68	53.40	40.75	112.58	75.33	101.88	56.5	88.11

Table 3.9: Experimental Results for Gray Wacke

Specimen number	1	2	3	4	5	6	7	8	9	10	11	12
Diameter x 10^{-2}m	5.0	5.1	5.1	5.2	5.3	5.2	5.0	5.1	5.3	5.2	5.1	5.0
Cross sectional area x $10^{-3}m^2$	1.963	2.043	2.124	2.043	2.206	2.124	1.963	2.043	2.206	2.124	2.042	1.963
Compressive crushing load (kN)	240	80	140	60	200	190	220	90	160	230	150	170
Compressive stress (MN/m^2)	122.26	39.16	65.91	29.37	90.66	89.45	112.01	44.05	72.53	108.29	73.42	86.60

3.2. STONE CRUSHER DESIGN CONCEPT

3.2.1. Introduction

The objective of the present work is to come up with design parameters of a Crusher that is suitable for Small and Medium Scale Entrepreneurs. The main crusher design concepts proposed are:-

i. Jaw Crushers -Concept 1
ii. Gyratory Crushers —Concept 2
iii. Cone Crushers -Concept 3

3.2.2. Decision Making Matrix

The three design concepts are evaluated in terms of performance criteria formulated as follows:

Criteria A Technical Performance

Criteria B Reliability

Criteria C Maintainability

Criteria D Life Cycle Cost

Criteria E Development Risk

Criteria F Production Rate

Criteria G Schedules

Criteria H Safety

These eight criteria are rated on a scale of 0-3 in order of importance as shown in Table 3.10.

Table 3.10: Evaluation Criteria

Performance Criteria	Rating (R)
Critical difference of importance	3
Major difference of importance	2
Minor difference of importance	1
No difference of importance	0

The decision matrix shown in Table 3.11 shows the pairing of criteria according to importance.

Table 3.11:Pairing of Criteria According to Importance

A	B	C	D	E	F	G	H		CRITERIA	WEIGHT, W
	B1	A0	DI	A3	A1	A2	A0	A	Technical performance	6
		B3	B2	B2	B1	B2	B0	B	Reliability	11
			C0	C3	C2	C2	H1	C	Maintainability	7
				D3	D2	D3	H3	D	Life cycle cost	9
					F2	G2	H3	E	Development risk	0
						F1	H1	F	Production rate	3
						H1	G	G	Schedule	2
								H	Safety	9

The influence of each performance criteria on each concept is now determined. This is done by rating each criteria of each concept according to the rating priority based on a scale of 7 to 1 whereby;

7- Complete satisfaction

6 -Extensive satisfaction

5-Cornsiderable satisfaction

4 -Moderate satisfaction

3 -Minor satisfaction

2 -Minimal satisfaction

1 -Marginal satisfaction

The rating R for each criterion and for each design concept is now multiplied by the weighing factor W obtained in Table 3.11 to obtain a final value of weight as shown in Table 3.12

Table 3.12: Weighing Criteria Concept

		Concept 1		**Concept 2**		**Concept 3**	
Criteria	**W**	**R**	**WR**	**R**	**WR**	**R**	**WR**
Technical Performance	6	5	30	4	24	3	18
Reliability	11	4	44	4	44	4	44
Maintainability	7	4	28	1	7	1	7
Life Cycle cost	9	5	45	3	27	2	18
Development Risk	0	4	0	1	0	1	0
Production rate	3	3	9	6	18	4	12
Schedule	2	4	8	3	6	2	4
Safety	9	5	45	4	36	4	36
Total			**209**		**162**		**139**

From Table 3.12 the Jaw Crusher concept 1 has the highest weighing, therefore the most suitable design concept for small scale stone crusher. The merits of this crusher type are:

i. Suitable for crushing hard and abrasive material since there is limited rubbing or grinding action
ii. Has high mechanical efficiency and low power cost

iii. Easy to operate and maintain

iv. Produces cubical products with minimum fines

However, this crusher is limited in production capacity compared to Gyratory or Cone Crushers particularly for large scale production.

Figure 3.2 shows a Cutaway Section of a Jaw Crusher (Metso Minerals, 2008)

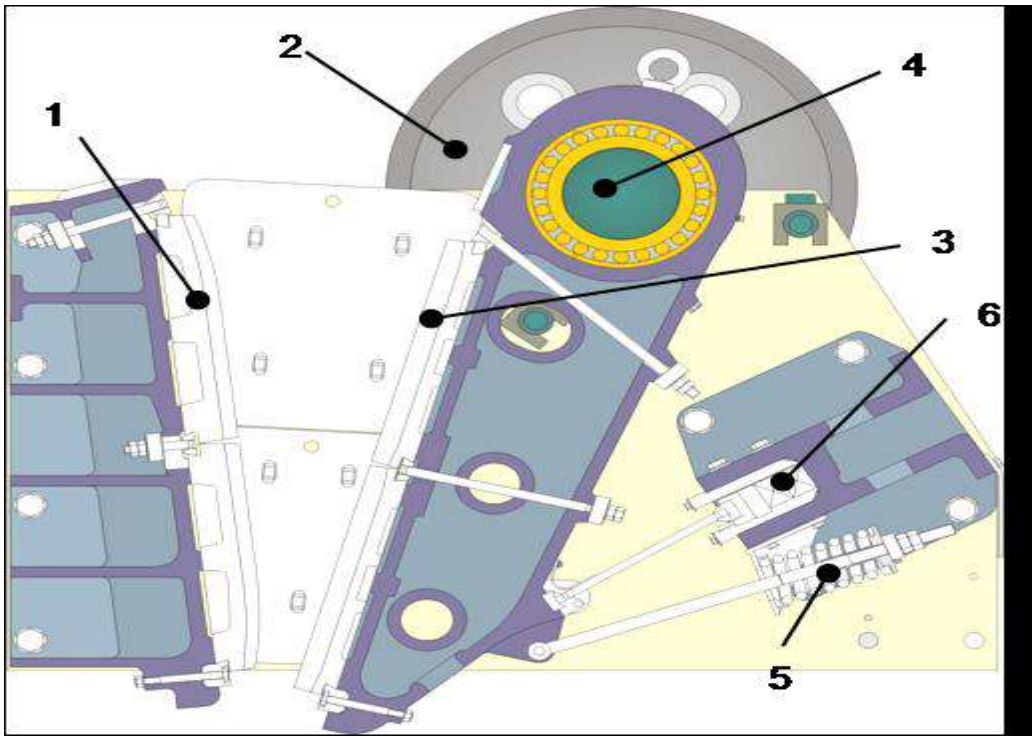

Figure 3.2: Jaw Crusher. (1. Fixed jaw, 2. Flywheel, 3. Moving jaw, 4. Eccentric Shaft, 5. Tension Spring, 6. Toggle Plate)

3.2.3. Working Principle of the Toggle Jaw Crusher

The motor or internal combustion engine transmits power through a belt drive, drives the moving Jaws, through the eccentric shaft, to execute periodic motion towards and away from the fixed jaw. The jaw crusher squeezes the rock between two surfaces, one moving which opens and closes like a jaw while the other one is stationary.

The opening between the fixed and moving jaw tapers vertically from the wide gap at the top to narrow at the bottom, thus, gradually reducing the size of the rock as it moves through the crushing chamber. The opening and crushing action of the movable jaw against a fixed jaw continues to reduce the size of the lodged pieces of rock until the pieces are small enough to fall through the opening at the bottom of the jaw. Rock size reduction is generally carried out in several stages since the ratio of size reduction through a single stage has practical limitations.

The moving plate applies the force of compression on the particles held against the stationary plate. Both plates are bolted onto a heavy block. The moving plate is pivoted at the top or at the bottom end and connected to an eccentric shaft. The function of the toggle, apart from being a safety device, is to move the pivoted jaw. The retrieving action of the jaw from the furthest end of travel is by springs for small crushers or by a Pitman for large crushers.

As the reciprocating action moves the moving jaw away from the fixed (stationary) jaw, the broken rock particles slip down, but are again caught at the next movement of the swinging jaw and crushed. This process is repeated until the particle sizes are smaller than the smallest opening between the crusher plates at the bottom of the crusher. For a smooth reciprocating action of the moving jaw, heavy flywheels are used.

3.3 ANALYSIS OF THE SINGLE TOGGLE JAW CRUSHER KINEMATICS

3.3.1 Introduction

Generally speaking, the aim of any kinematical analysis of a mechanism is to determine the output motions, given the input motion and the kinematical parameters of the mechanism. In the Single Toggle Jaw Crusher mechanism, the input motion is the rotation of the eccentric shaft; the kinematical parameters of the mechanism are the effective lengths of the links that comprise the mechanism, and the output motion is the resulting motion of the swing jaw.

The methods of kinematical analysis can be classified into three categories, namely: Graphical, Analytical and Computer Aided Methods. Graphical methods can be likened to still photography because they can deal with only one phase of motion at a time hence separate graphical constructions must be done for each of the displacements, velocity and acceleration analyses. Thus, a very large number of graphical constructions would be required to obtain anything close to a complete kinematical description of the mechanism. However, availability of graphical software has made it easier to use graphical methods.

Analytical Methods usually result in a small number of equations that contain all the information that is required to completely describe the kinematics of the mechanisms. With these equations, the effects of design alteration can be investigated. Therefore, Analytical Methods are inherently more effective and powerful, as compared to Graphical Methods. Moreover, Analytical Methods are more accurate than Graphical Methods.

Computer Aided Methods use software packages that are specially designed for the purpose. Today, there are many, commercially available, interactive and user-friendly software packages that can be used, not only to simulate the motion of the mechanisms but also to determine such quantities as displacements, velocities, accelerations, forces and moment among others. However, the required software and hardware are expensive and the user requires a good knowledge of the mechanical principles that govern the behaviour of the mechanisms, as well as the skill required to use the software (Monkova *et al*, 2001). In the design of complex mechanisms, Computer Aided Design (CAD) methods may be the best choice, but in this study the mechanism to be analyzed is relatively simple, and therefore the Analytical Method will suffice.

In this thesis, all points in the crushing mechanism of the Single Toggle Jaw Crusher are constrained to move in parallel planes. The mechanism consists of four links, namely, the Eccentric, the Swing Jaw, the Toggle Link and the Frame, in the form of a closed kinematic chain. Thus, the mechanism can be modelled as four-bar mechanism with four revolute joints all in one plane. Further, the analysis of the mechanism recognizes the following two constraints:

i) All the links in the mechanism are assumed to be completely rigid. Therefore, the effective lengths of the links remain invariant through one complete cycle of motion of the linkages

ii) The kinematic chain that lies the linkages remains closed throughout the cycle of motion of the mechanism.

As a result of the above-mentioned constraints, for any phase of motion of the mechanism, the effective lengths of the links can be taken to be vectors of known magnitudes, that form a closed loop. In this thesis, the Vector Closure Method (Erdman and Sandor, 1991; Kimbrell, 1991; Shigley and Vicker, 1980) is used to obtain the kinematical equations. The application of the results of the kinematical analysis in validated using the dimensional data of a practical Single Toggle Jaw Crusher used by Cao *et al.,* (2006) in his analysis.

3.3.2 Kinematical Model of the Single Toggle Jaw Crusher

The concept of the Single Toggle Jaw Crusher is illustrated in Figure 3.3. When considering the kinematics of this type of crusher, the crushing jaw and the toggle link, can be modelled as a common planar four bar mechanisms that is known as Crank and Rocker Mechanism (Erdman and Sendor, 1991; Kimbrell, 1991). The Single Toggle Jaw Crusher Kinematical model set up in this analysis is based on the Vector Loop Closure Method (Erdman and Sandor, 1991; Kimbrell, 1991; Shigley and Vicker, 1980).

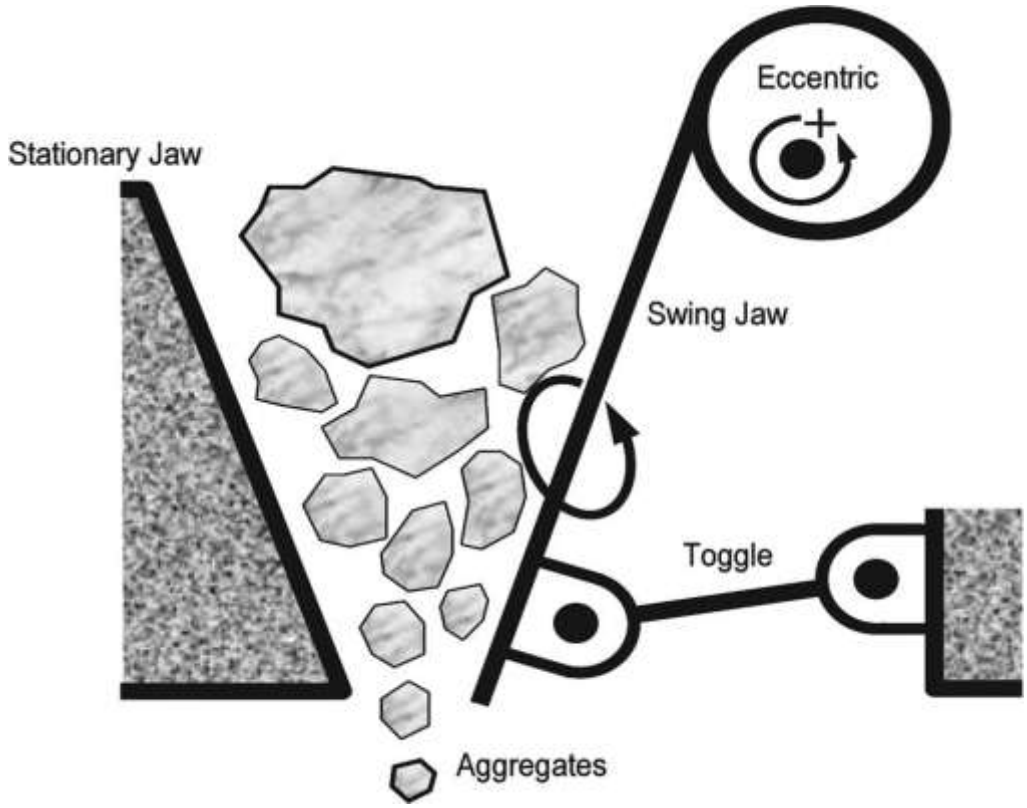

Figure 3.3: Concept of the Single Toggle Jaw Crusher

In the kinematical model, which is illustrated in Figure 3.4, the eccentric shaft is modelled as a short crank, O_2O_3 of length r_2, that continuously rotates about a fixed axis, at O_2. The swing jaw is modelled as the coupler link O_3O_4, of length r_3, which moves with a complex planar motion that consists of both rotational and translational components. The toggle link is modelled as the rocker O_4O_1, which oscillates about the fixed axis at O_1. The fixed jaw may be considered to be an integral part of the frame of the machine.

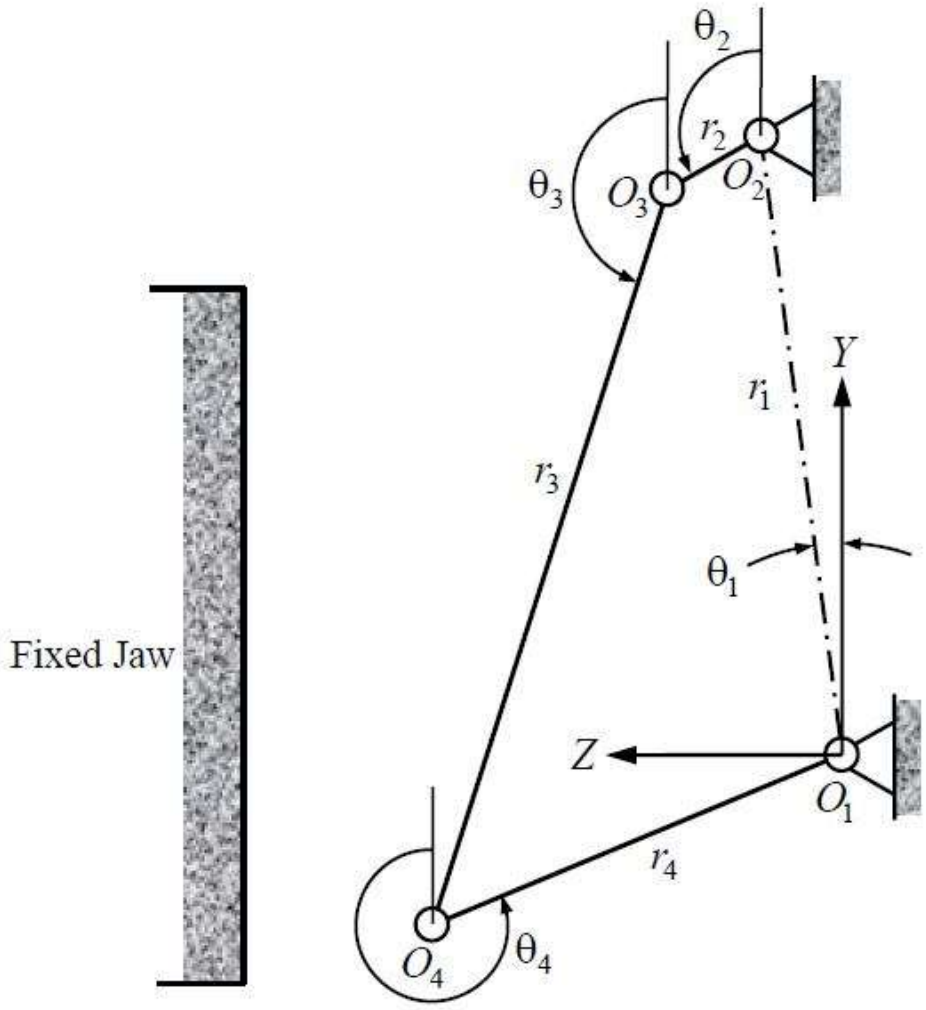

Figure 3.4: Kinematical Model of the Single Toggle Jaw Crusher

In analyzing the kinematics of the Single Toggle Jaw Crusher, it is particularly important to understand the motion of the coupler link O_3O_4, relative to the fixed jaw, as the crank rotates through a complete cycle. Therefore, a right-handed Cartesian reference frame that is convenient for analyzing this motion will be used, as shown in Figure 3.4. All angular displacements are taken counter clockwise relative to the positive *Y* direction. This reference frame may be compared with the one that was used by Cao *et al.*, (2006).

3.3.3. Kinematical Analysis- Vector Loop Closure

3.3.3.1 Position and Displacement Analysis

The analysis of position and displacement can be accomplished through the use of the well-known Vector Loop Closure Method (Erdman and Sandor, 1991; Kimbrell, 1991; Shigley and Vicker, 1980), which is illustrated in Figure 3.5.

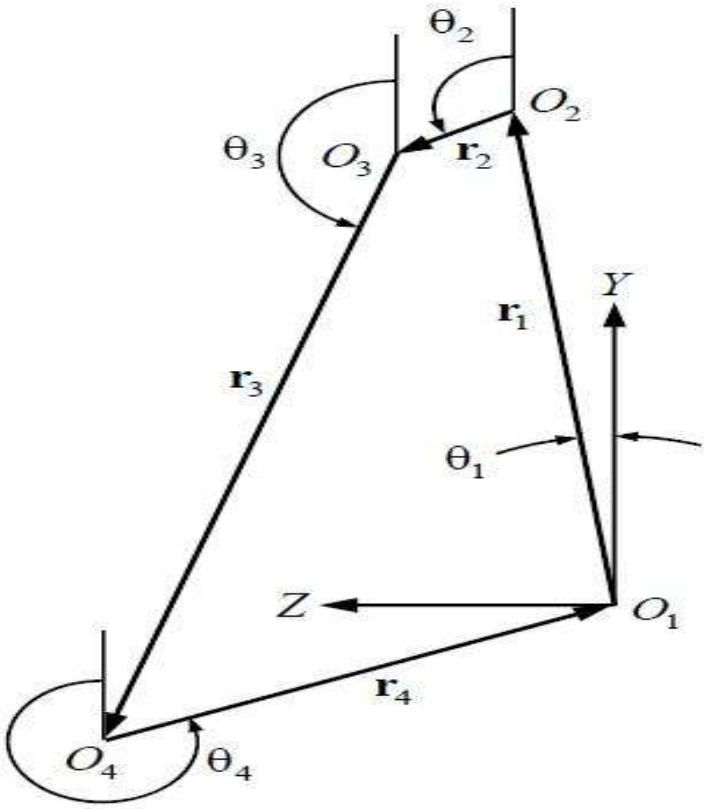

Figure 3.5: Vector Loop Closure diagram

In Figure 3.5, the vector loop closure equation can be written as follows:

$$\bar{r}_1 + \bar{r}_2 + \bar{r}_3 + \bar{r}_4 = 0 \qquad \text{.....(3.4)}$$

Equation (3.4) can be re-written in the complex vector notation as follows:

$$r_1 e^{j\theta 1} + r_2 e^{j\theta 2} + r_3 e^{j\theta 3} + r_4 e^{j\theta 4} = 0 \qquad \text{.....} \quad (3.5)$$

The Euler identities state as follows:

$$\left.\begin{aligned} e^{j\theta} &= \cos\theta + j\sin\theta \\ e^{-j\theta} &= \cos\theta - j\sin\theta \end{aligned}\right\} \quad \text{(3.6)}$$

At this stage, for conciseness, let us introduce the following notation:

$$\left.\begin{aligned} \cos\theta_i &= c_i \\ \sin\theta_i &= s_i \end{aligned}\right\} \quad \text{(3.7)}$$

By using equations (3.6) and (3.7), equation (3.5) may be re-written as follows:

$$r_1(c_1 + js_1) + r_2(c_2 + js_2) + r_3(c_3 + js_3) + r_4(c_4 + js_4) = 0 \quad \text{(3.8)}$$

In equation (3.8) if the real terms and the imaginary terms are considered separately, the following two equations are readily obtained:

$$\left.\begin{aligned} r_1c_1 + r_2c_2 &= -(r_3c_3 + r_4c_4) \\ r_1s_1 + r_2s_2 &= -(r_3s_3 + r_4s_4) \end{aligned}\right\} \quad \text{(3.9)}$$

By squaring each of equations (3.9), the following is obtained:

$$\left.\begin{aligned} r_1^2\,c_1^2 + 2r_1r_2c_1c_2 + r_2^2\,c_2^2 &= r_3\,c_3^2 + 2r_3r_4c_3c_4 + r_4^2\,c_4^2 \\ r_1^2\,s_1^2 + 2r_1r_2s_1s_2 + r_2^2\,s_2^2 &= r_3\,s_3^2 + 2r_3r_4s_3s_4 + r_4^2\,s_4^2 \end{aligned}\right\} \quad \text{(3.10)}$$

By adding corresponding terms in equations (3.10), and noting that $c_i^2 + s_i^2 = 1$, the following is obtained:

$$r_1^2 + 2r_1r_2c_1c_2 + 2r_1r_2s_1s_2 + r_2^2 = r_3^2 + 2r_4c_4(r_3c_3) + 2r_4s_4(r_3s_3) + r_4^2 \quad \text{(3.11)}$$

Now, equations (3.9) can be rearranged into the following:

$$\left.\begin{aligned} r_3c_3 &= -(r_1c_1 + r_2c_2 + r_4c_4) \\ r_3s_3 &= -(r_1s_1 + r_2s_2 + r_4s_4) \end{aligned}\right\} \quad \text{(3.12)}$$

It is known from trigonometry that (Carmichael and Smith, 1962)

$$\cos\theta_i\cos\theta_k + \sin\theta_i\sin\theta_k = \cos(\theta_i - \theta_k) \quad \text{(3.13)}$$

By substituting equations (3.12) into equation (3.11), and using the identity in equation (3.13), the following is obtained:

$$\left.\begin{aligned} 2r_1r_2\cos(\theta_2-\theta_1)+2r_1r_4\cos(\theta_4-\theta_1)+2r_2r_4\cos(\theta_4-\theta_2) \\ = \ r_3^2-\ r_1^2-\ r_2^2-\ r_4^2 \end{aligned}\right\} \qquad (3.14)$$

From Figure 3.4, θ_1, is a fixed quantity and, for given values of r_1, r_2, r_3 and r_4, the value of θ_1 will be known. The motion of the crank O_2O_3. is the input motion and may be considered to be a rotation at uniform angular velocity ω_2. Thus, at an instant in time, t after commencement of the motion, the value of θ_2 , in radians, will be determined as follows:

$$\theta_2(t) = \ \omega_2 t \quad \text{.....(3.15)}$$

For given lengths of the four links in the mechanism, equation (3.14) can be used to determine the values of θ_4 that correspond to any given values θ_2. In that case, equation (3.14) will therefore describe all the possible spatial configurations of the mechanism, for given lengths of the four links.

In the special case where $\theta_1 = 0$, equation (3.14) reduces to the following:

$$2r_1r_2\cos\theta_2+2r_1r_4\cos\theta_4+2r_2r_4\cos(\theta_4-\theta_2)=r_3^2-\ r_1^2-\ r_2^2-\ r_4^2 \text{.....(3.16)}$$

Each of the terms in equation (3.16) can he divided by $2r_2r_4$ and the resulting equation can be re-arranged to obtain the following;

$$\frac{r_1}{r_4}\cos\theta_2+\frac{r_1}{r_2}\cos\theta_4+\frac{r_1^2+r_2^2+r_4^2-r_3^2}{2r_2r_4}=\ \cos(\theta_4-\theta_2) \text{..... (3.17)}$$

Equation (3.17) can be re-written as follows:

$$\left.\begin{aligned} K_1\cos\theta_2+K_2\cos\theta_4+K_3=\cos(\theta_4-\theta_2) \\ K_1=\frac{r_1}{r_4} \\ K_2=\frac{r_1}{r_2} \\ K_3=\frac{r_1^2+r_2^2+r_3^2-r_4^2}{2r_2r_4} \end{aligned}\right\} \text{..... (3.18)}$$

Equation (3.18) is the well-known Freudenstein's equation that has been commonly used in the synthesis of four bar mechanisms (Erdman and Sandor, 1991; Kimbrell, 1991; Shigley and Vicker, 1980).

3.3.3.2 Angular Displacement of the Swing Jaw

In the study and design of the Single Toggle Jaw Crusher, the motion of the coupler (swing jaw), relative to that of the crank (eccentric shaft), is of greater interest than that of the rocker (toggle link). Therefore, in finding the angular displacement of the Swing Jaw, re-arrange equations in (3.9) into the following:

$$\left.\begin{aligned} r_1c_1 + r_2c_2 + r_3c_3 &= -r_4c_4 \\ r_1s_1 + r_2s_2 + r_3s_3 &= -r_4s_4 \end{aligned}\right\} \quad \text{.....(3.19)}$$

By substituting equations (3.19) into equation (3.11), and using equation (3.13), the following equation is obtained:

$$\left.\begin{aligned} 2r_1r_2\cos(\theta_2-\theta_1) + 2r_2r_3\cos(\theta_3-\theta_2) + 2r_3r_1\cos(\theta_3-\theta_1) \\ = r_4^2 - r_3^2 - r_2^2 - r_1^2 \end{aligned}\right\} \text{.....(3.20)}$$

For given lengths of the four links in the mechanism along with the value of θ_1, equation (3.20) can be used to determine the corresponding values of θ_3, for any given values θ_2. When compared to equation (3.14), equation (3.20) is of greater utility in describing the motion of the Swing Jaw, relative to that of the Crank.

Again, if $\theta_1 = 0$, equation (3.20) reduces to the following:

$$2r_1r_2\cos\theta_2 + 2r_3r_1\cos\theta_3 + r_4^2 - r_3^2 - r_2^2 - r_1^2 = -2r_2r_3\cos(\theta_3-\theta_2) \text{.....(3.21)}$$

Equation (3.21) can be divided through by $2r_2r_3$ to obtain the following:

$$\frac{r_1}{r_3}\cos\theta_2 + \frac{r_1}{r_2}\cos\theta_3 + \frac{r_4^2 - r_3^2 - r_2^2 - r_1^2}{2r_2r_3} = -\cos(\theta_3-\theta_2) \text{.....(3.22)}$$

Equation (3.22) can be re-written as fallows:

$$\left.\begin{aligned} K_1\cos\theta_2 + K_2\cos\theta_3 + K_3 - \ -\cos(\theta_3-\theta_2) \\ K_1 = \frac{r_1}{r_3} \\ K_2 = \frac{r_1}{r_2} \\ K_3 = \frac{r_4^2 - r_3^2 - r_2^2 - r_1^2}{2r_2r_1} \end{aligned}\right\} \quad \text{.....(3.23)}$$

Equation (3.23) may be regarded as another version of Freudenstein's equation. For given values of the lengths of the four links, the equation can be used to determine the values of θ_3 that correspond to any given values of θ_2.

The concept of the Single Toggle Jaw Crusher is illustrated in Figure 3.3. When considering the kinematics of this type of crusher, the swing jaw drive mechanism includes

i) the eccentric shaft, θ_2 θ_3
ii) the swing jaw, $\theta_3\theta_4$
iii) the toggle link, $\theta_1\theta_4$
iv) the frame

The four components of the linkage system is commonly referred to as a planar four-bar mechanism or in mechanisms Palour is known as the Crank and Rocker (Erdman and Sandor, 1991; Kimbrell, 1991).

Cao *et al.,* (2006) used the data for a PE 400 x 600Single Toggle Jaw Crusher, as shown in Table 3.12. This data can still be used to validate the application of the kinematic equations. The PE 400 x 600 can be regarded as a medium size Jaw Crusher.

Table 3.13: Data for a PE 400 by 600 Single Toggle Jaw Crusher

$r_1 \sin\theta_1$ (mm)	r_1 $\cos\theta_1$(mm)	r_2 (mm)	r_3 (mm)	r_4 (mm)
45.3	815.7	12	1085	455

The data in Table 3.13 will be adopted in the validation of the equations.

By using the data in Table 3.13, equation (3.20) can be reduced to the following:

$$\left.\begin{array}{c} K_1\cos\theta_3 + K_2\cos\theta_3 + K_3 = 0 \\ K_1 = \cos\theta_2 + 68 \\ K_2 = \sin\theta_2 + 3.8 \\ K_3 = 62.9 + 0.752\cos\theta_2 + 0.042\sin\theta_2 \end{array}\right\} \quad \ldots\ldots\ldots\ldots\ldots\ldots\ldots\ldots \quad (3.24)$$

In equation (3.24), for any given value of θ_2, K_1, K_2, K_3 will be determined. The first of equations (3.24) may be re-written as follows:

$$K_1\cos\theta_3 = -(K_2\cos\theta_3 + K_3) \qquad \ldots\ldots\ldots\ldots\ldots\ldots\ldots\ldots\ldots\ldots \quad (3.25)$$

By squaring both sides of equation (3.25), using the well-known trigonometric identity, $\cos^2\theta = 1 - \sin^2\theta$, and then re-arranging the result, the following can be obtained:

$$\left.\begin{array}{c} A\sin^2\theta_3 + B\ \sin\theta_3 + C = 0 \\ A = K_2^2 + K_1^2 \\ B = 2K_2K_3 \\ C = K_3^2 - K_1^2 \end{array}\right\} \quad \ldots\ldots\ldots\ldots\ldots\ldots\ldots\ldots\ldots\ldots \quad (3.26)$$

For any given value of θ_2, equation (3.26) is a quadratic in $\sin\theta_3$, and it can therefore, be solved to yield two values of θ_3. Thus, there are two possible configurations of the four-bar mechanism in Figure 3.4 for every possible value of θ_2. However, only one of these configurations will be suitable for the proper functioning of the crusher mechanism. The suitable configuration should have the values of θ_3 falling between 90° and 180°. The unsuitable configuration would have the values of θ_3 that are greater than 180°, as shown in Figure 3.6.

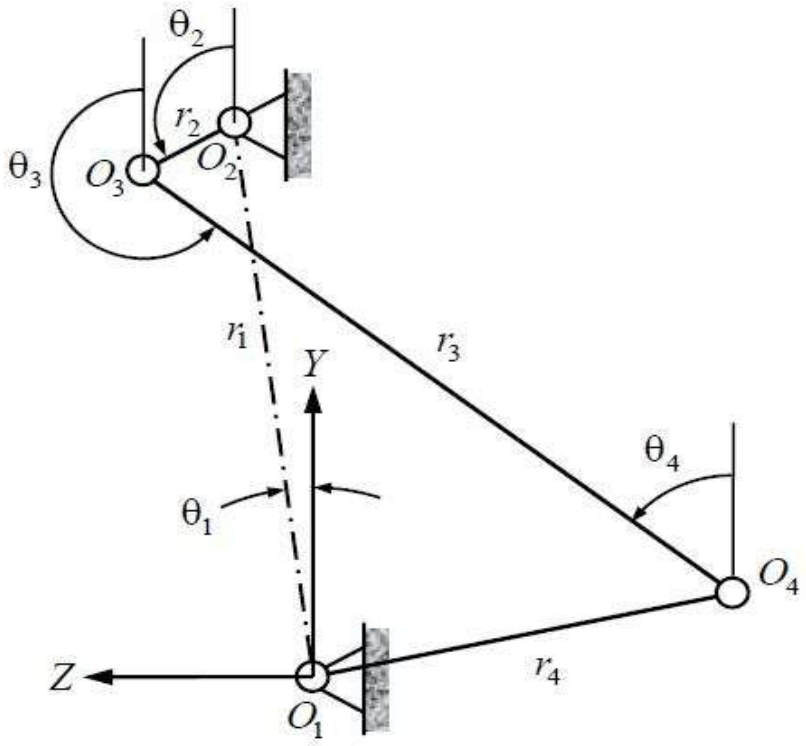

Figure 3.6: Another Possible Configuration of the Mechanism in Figure 3.4

For the suitable configuration of the mechanism, as shown in Figure 3.4, equations (3.24) and (3.26) were used in a Microsoft Excel worksheet, along with the data in Table 3.13, to determine the values of θ_3, as θ_2 varied from 0º to 360°. Some of these calculated values are given in Table 3.14.

Table 3.14: Analytically Determined Values of θ_3 for Given Values of θ_2

θ_2 (degrees)	θ_3 (degrees)	θ_2 (degrees)	θ_3 (degrees)
0	160.2	195	160.8
15	160.5	210	160.6
30	1607	225	160.4
45	160.9	240	160.1
60	161.1	255	160
75	I61.3	270	159.8
90	161.5	285	159.7
105	161.5	300	159.7
120	1616	315	159.5
135	161.5	330	159.9
150	161.4	345	160
165	161.3	360	160.2
180	161.1		

For one full cycle of rotation of the crank, the minimum value of θ_3 was found to be 159.7° while the maximum value of θ_3 was found to be 161.6°. Thus, the range of variation of the inclination of the coupler (swing jaw), to the vertical, for one complete cycle of rotation of the crank, is less than 2º. The change of angular orientation of the swing jaw, during its cycle of motion, appears to be quite small hence insignificant.

In one complete cycle of motion of the mechanism, two particular phases of special interest are identified. These special phases, which are known as toggle positions, occur when the crank O_2O_3 and the coupler O_3O_4 fall on the same straight line. For this to happen, either θ_3 must be equal to $(\theta_2 + 180)$ degrees or θ_3 must be equal to θ_2. When these conditions are used in equation (3.20), along with the data in Table 3.13, it is found that the toggle positions will occur when $\theta_2 = 161.35$ and when θ_2= 340°. Cao *et al.,* (2006) in their study found that the minimum value of θ_3 was 160° while the maximum value of θ_3 was

162°. Therefore, the values obtained in this thesis are in agreement with those calculated by Cao *et al.*, (2006). In determining the toggle positions, due regard must be given to the fact that, for each value of θ_2, there will be two possible configurations of the mechanism, only one of which will be suitable for the proper operation of the crusher.

A graph of the variation of θ_3 with θ_2 is shown in Figure 3.7.

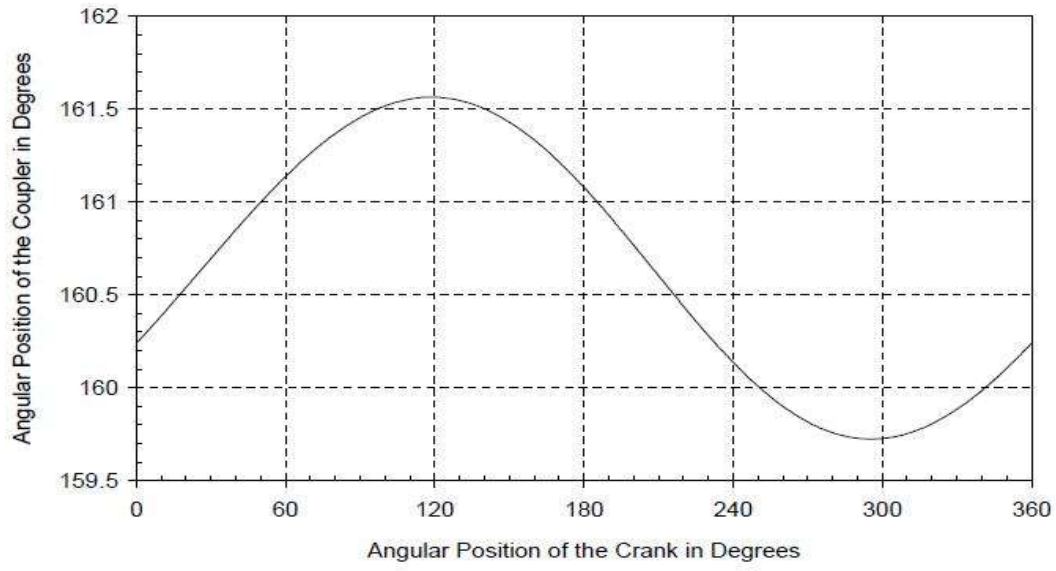

Figure 3.7: Variation of Coupler Angle θ_3 with Crank Angle θ_2

For a given set of the values of θ_1, θ_2 and θ_3 along with the knowledge of the length of the four links in the mechanism, the corresponding value of θ_4 can be readily determined using equation (3.19).

3.3.3.3 Position and Displacement of a Point in the Swing Jaw

It is possible to determine the motion of a point in the swing jaw; particularly on the crushing surface of the swing jaw, as it varies with the motion of the crank. The position of such a point would be fixed relative to that of the coupler link O_3O_4 in Figure 3.8. For the purpose of locating such a point, the coordinate system illustrated in Figure 3.8 will be used.

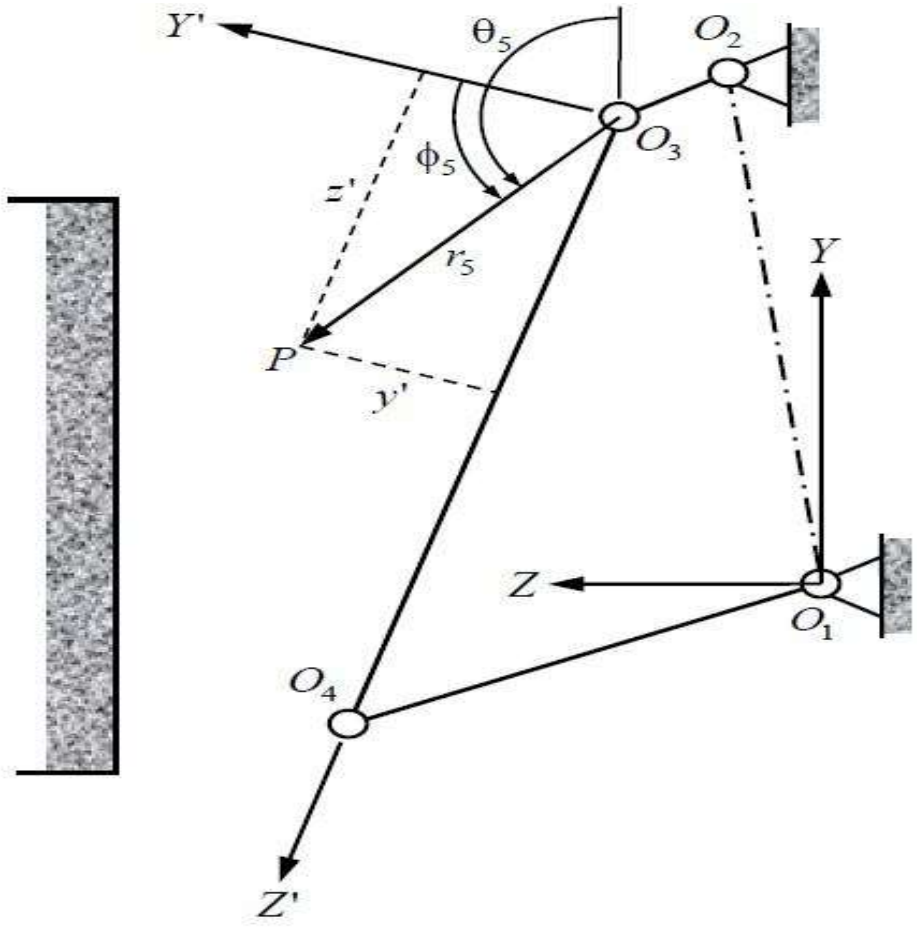

Figure 3. 8: Location of a Point P in the Swing Jaw

In Figure 3.8, the $Y'Z'$ coordinate reference frame has its origin at O_3, and it is fixed in the swing jaw. The point *P* too is fixed in the swing jaw and its position is located by the vector $\bar{\boldsymbol{r}}_{\mathbf{5}}$ of magnitude r_5, whose origin is at O_3 and whose direction is indicated by the angle $\phi_5$relative to the positive Y' direction. Thus:

$$\left.\begin{aligned} y' &= r_5 cos\phi_5 \\ z' &= r_5 sin\,\phi_5 \end{aligned}\right\} \quad \text{..... (3.27)}$$

The direction of the vector $\boldsymbol{r_5}$ taken relative to the Y direction is indicated by the angle θ_5, such that:

$$\theta_5 = (\theta_3 + \phi_5 - 90^{\circ}) \quad \text{(3.28)}$$

Thus:

$$\left.\begin{aligned} \sin\theta_5 &= -\cos(\theta_3 + \phi_5) = \sin\theta_3 \sin\phi_5 - \cos\theta_3 \cos\phi_5 \\ \cos\theta_5 &= \sin(\theta_3 + \phi_5) = \sin\theta_3 \cos\phi_5 + \cos\theta_3 \sin\phi_5 \end{aligned}\right\} \quad \text{(3.29)}$$

In the special case where $\phi_5 = 90°$, θ_5 becomes equal to θ_3 and the point *P* then lies on the line O_3O_4, at a distance of r_5 from O_3.

In Figure 3.8 the location of point *P* relative to the *YZ* coordinate reference frame may now be expressed as follows:

$$\left.\begin{aligned} y_p &= r_1 \cos\theta_1 + r_2 \cos\theta_2 + r_5 \cos\theta_5 \\ z_p &= r_1 \sin\theta_1 + r_2 \sin\theta_2 + r_5 \sin\theta_5 \end{aligned}\right\} \quad \text{(3.30)}$$

By using equations (3.29), equations (3.30) can be re-written as follows:

$$\left.\begin{aligned} y_p &= r_1 \cos\theta_1 + r_2 \cos\theta_2 + r_5(\sin\theta_3 \cos\phi_5 + \cos\theta_3 \sin\phi_5) \\ z_p &= r_1 \sin\theta_1 + r_2 \sin\theta_2 + r_5(\sin\theta_3 \sin\phi_5 - \cos\theta_3 \sin\phi_5) \end{aligned}\right\} \quad \text{(3.31)}$$

In the special case where $\phi_5 = 90°$, equations (3.31) reduce to the following:

$$\left.\begin{aligned} y_p &= r_1 \cos\theta_1 + r_2 \cos\theta_2 + r_5 \cos\theta_3 \\ z_p &= r_1 \sin\theta_1 + r_2 \sin\theta_2 + r_5 \sin\theta_3 \end{aligned}\right\} \quad \text{(3.32)}$$

Given the lengths r_1, r_2, r_3 and r_4 of the links, along with the angle θ_1 equations (3.20) and (3.32) can be used to determine the *locus* of any point on the line O_3O_4, for a complete cycle of rotation of the crank O_2O_3, provided that the distance r_5 of that point from O_3 is known.

Five points were selected along the length of the line O_3O_4, whose distances from O_3 are given in Table 3.15.

Table 3.15: Locations of Selected Points along the Coupler

Point	*P1*	*P2*	*P3*	*P4*	*P5*
$r_5\ (mm)$	0	271.25	542.5	813.75	1085

In Table 3.15. it should be evident that the point *P1* is coincident with O_3 and the point *P5* is coincident with O_4. The rest of the points are uniformly spaced along the length of the line O_3O_4.

Using equations (3.32), along with the data given in Tables 3.13 and 3.15, the positions of the points *P1* to *P5* were determined for one complete cycle of motion of the mechanism. The data in Tables 3.16 and 3.17 are representative of the results.

Table 3.16: Ranges of Displacements in the Y Direction

Point	**P1**	**P2**	**P3**	**P4**	**P5**
$y_{min}\ (mm)$	803.75	547.09	290.32	33.46	- 223.47
$y_{max}\ (mm)$	827.75	572.54	317.45	62.46	-192.44
Range of *y (mm)*	24	25.45	27.13	29	31.03

Table 3.17: Ranges of Displacements in the Z Direction

Point	***P1***	***P2***	**P3**	***P4***	***P5***
$z_{min}\ (mm)$	33.18	126.57	219.02	308.98	396.52
$z_{max}\ (mm)$	57.18	143.67	231.02	320.44	412.44
Range of z(mm)	24	17.10	12.00	11 46	15.92

As can be seen in Table 3.16, the range of displacement in the *Y* direction increases gradually, but at a slightly increasing rate, as we move from point *P1* to *P5.* Motion of the swing jaw in the *Y* direction causes a rubbing action between the material being crushed and the swing jaw, thereby causing the surface of the swing jaw to wear. One would, therefore, expect an increasing wear rate as we move from *P1* to *P5.* On the other hand, during the crushing stroke, the motion of the swing jaw has a downward vertical component that forcefully feeds the material being crushed into the crushing chamber, which is desirable because it increases the throughput of the crusher.

In Table 3.17, the range of displacement in the *Z* direction increases at a decreasing rate, as we move from point *P1* to *P4* but then increases as we move from point *P4* to *P5*. Displacement of the swing jaw in the Z direction should be the greater contributor to the crushing action.

The locus of points *P1* to *P5* for one complete cycle of motion, are shown in Figures 3.9 to 3.13. These loci have been referred to as *coupler curves* (Kimbrell, 1991; Martin George, 1982; Shigley and Vicker, 1980).

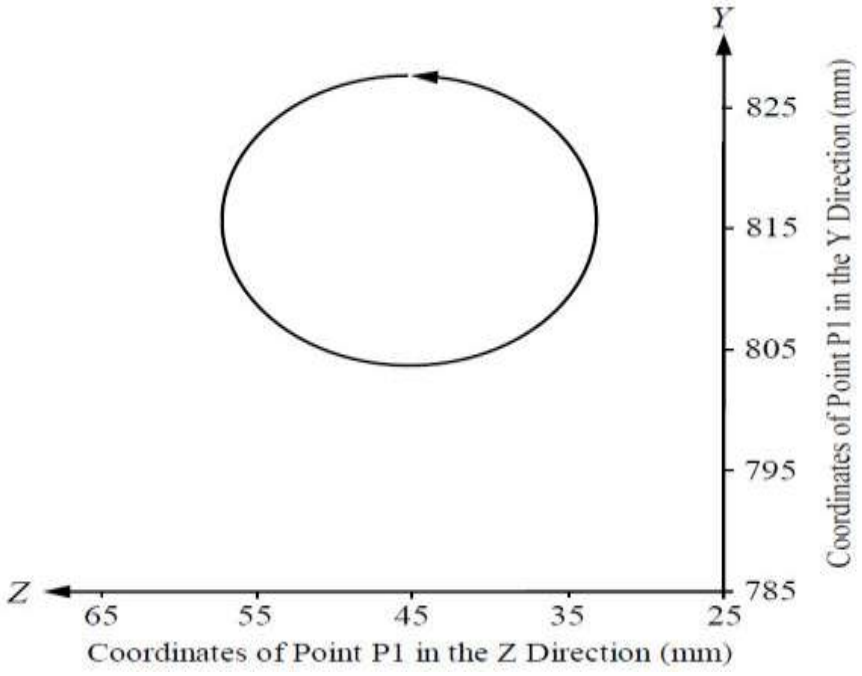

Figure 3. 9: The Locus of Point PI for One Complete Cycle of Motion

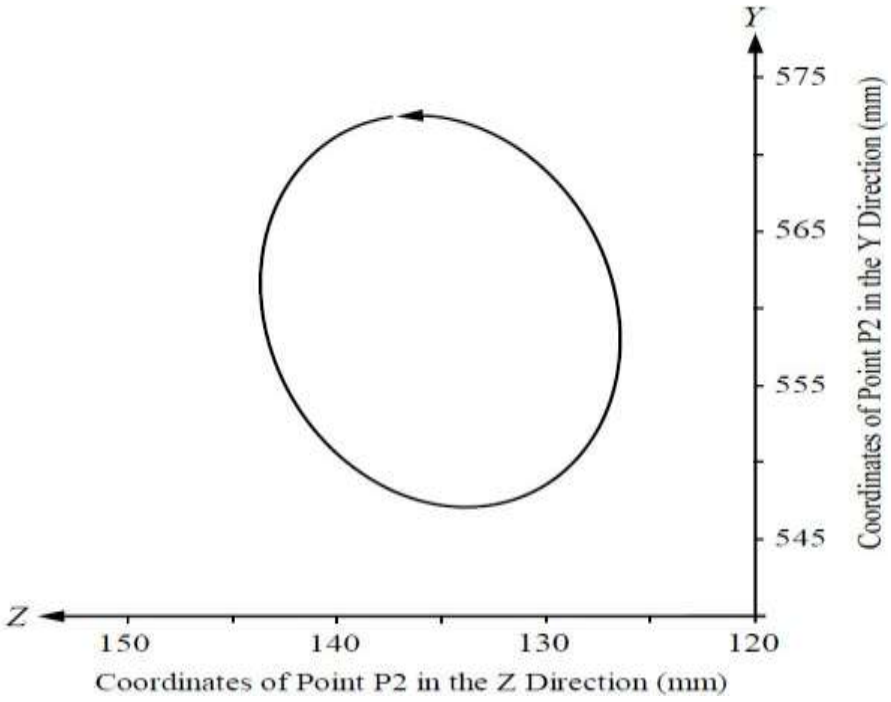

Figure 3. 10: The Locus of Point P2 for One Complete Cycle of Motion

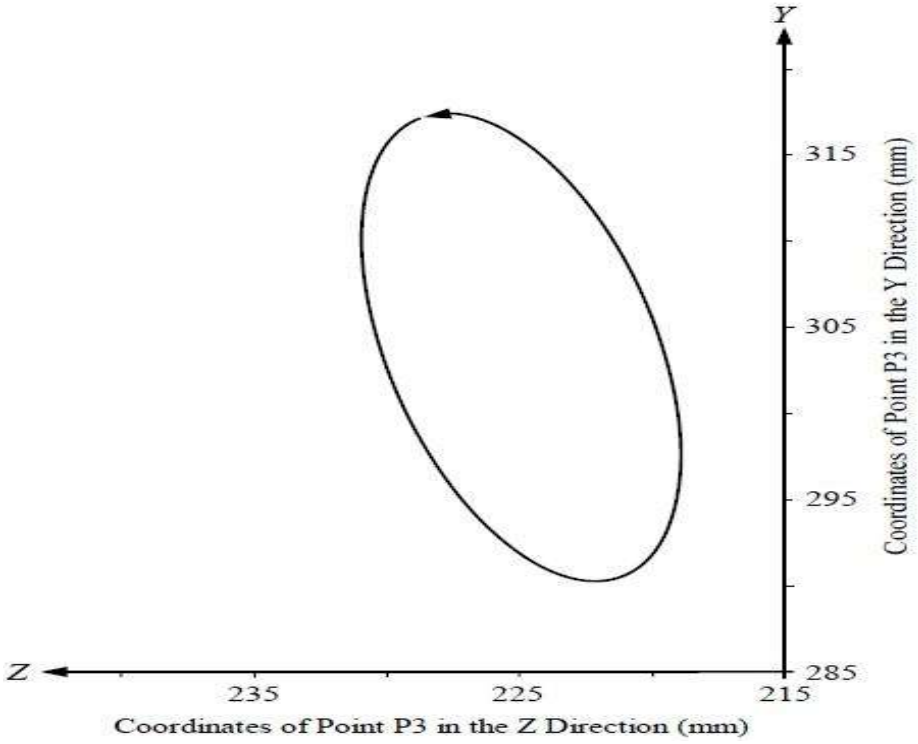

Figure 3. 11: The Locus of Point P3 for One Complete-Cycle of Motion

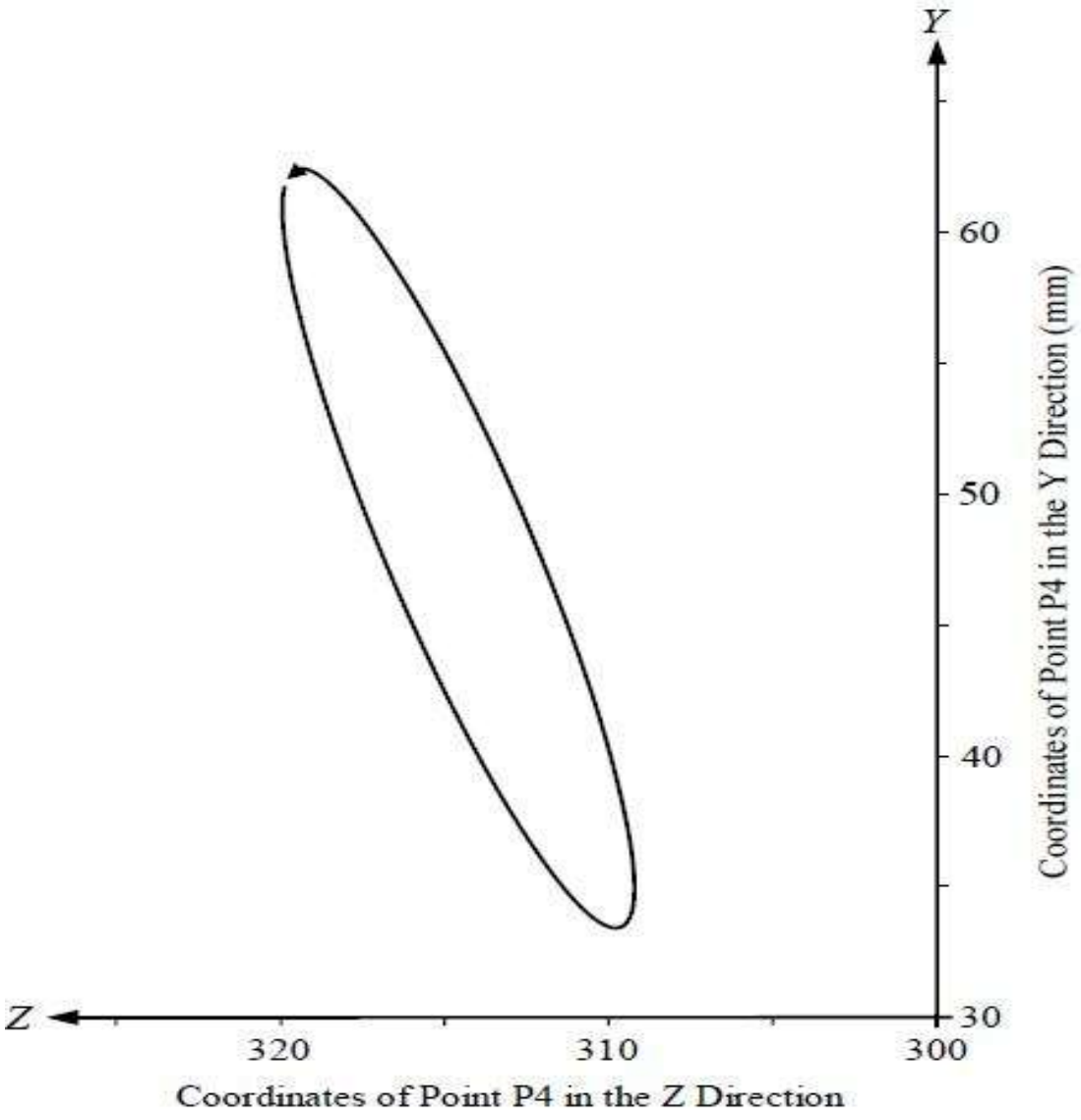

Figure 3. 12: The Locus of Point P4 for One Complete Cycle of Motion

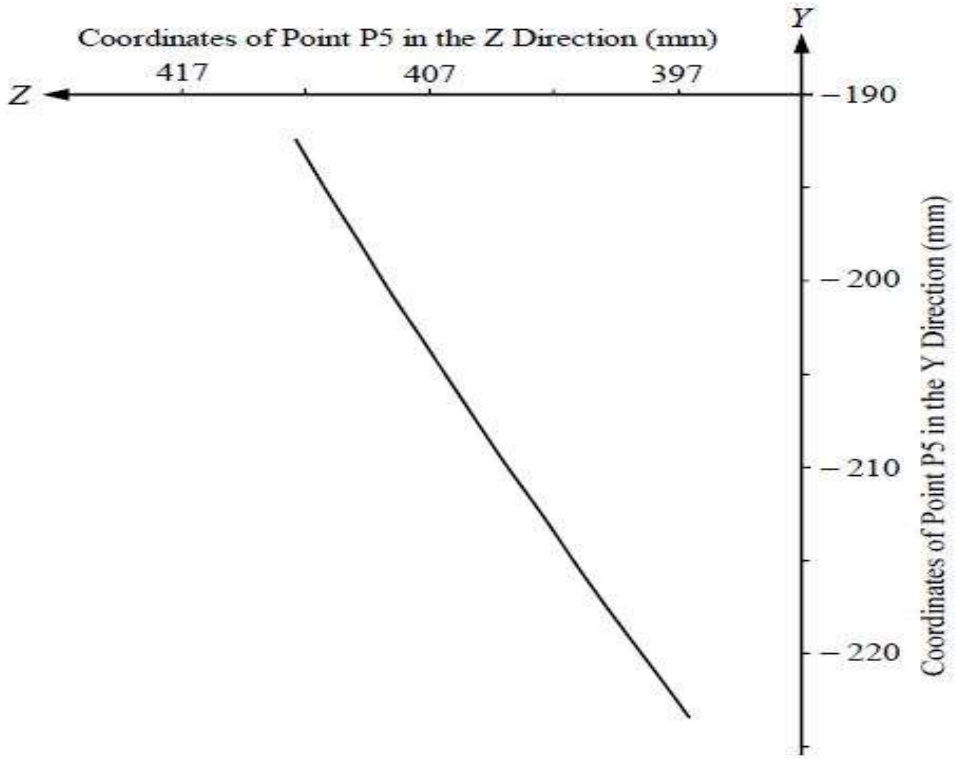

Figure 3. 13: The Locus of Point P5 for One Complete Cycle of Motion

In Figures 3.9 to 3.13, the scales on the *Y* and the *Z* axes should be equal in order for the forms of the loci to be correct. In Figure 3.9, the locus of point *P1* is the circle that is described by the crankpin O_3 and centred at O_2 .With the data that were used to determine these loci, this circle has a radius of 12mm.

As can be seen in Figures 3.10, 3.11 and 3.12, the loci of points *P2, P3* and *P4* are ellipses of varying proportions. As we move from point *P2* to *P3* and on to *P4*, the major axis of the ellipses grows longer while the minor axis grows shorter. Moreover, the major and minor axes of these ellipses are increasingly angled from the *YZ* coordinate reference frame.

In Figure 3.13, the locus of point P5 appears to be a straight line but. in reality, it is a circular arc that is described by the rocker pin $O_4$and centred at O_1.With the data that were used to determine the loci, the rocker has a length of 455 mm and the rocker pin O_4 would describe a circle of circumference 2859mm in one complete rotation. However, for one

complete rotation of the crank, the range of oscillation of the rocker is only 4.39°. Thus, the length of the arc described by the rocker pin O_4 is only about 35mm or 1.2 percent of the circumference of the complete circle. Thus, the arc described by the rocker in O_4 is infinitesimal, compared to the complete circle that it is a part of. This is why it appears to be a straight line as its curvature is hardly noticeable in Figure 3.13.

3.3.4 Angular Velocity of the Swing Jaw

An expression for the angular velocity of the coupler (swing jaw) can be obtained be differentiating equation (3.20) with respect to time. In doing so, it should be borne in mind that r_1, θ_1, r_2, r_3 and r_4 are all constant with respect to time. The result of the differentiation is then as follows:

$$\left.\begin{aligned} r_1 r_2 \sin(\theta_2 - \theta_1)\frac{d\theta_2}{dt} + r_2 r_3 \sin(\theta_3 - \theta_2)\frac{d\theta_3}{dt} + r_3 r_1 \sin(\theta_3 - \theta_1)\frac{d\theta_3}{dt} \\ = r_2 r_3 \sin(\theta_3 - \theta_2)\frac{d\theta_2}{dt} \end{aligned}\right\} \quad \text{.....(3.33)}$$

Equation (3.33) can be divided through by $r_2 r_3$ to obtain the following:

$$\left.\begin{aligned} \frac{r_1}{r_3}\sin(\theta_2 - \theta_1)\frac{d\theta_2}{dt} + \sin(\theta_3 - \theta_2)\frac{d\theta_3}{dt} + \frac{r_1}{r_2}\sin(\theta_3 - \theta_1)\frac{d\theta_3}{dt} \\ = \sin(\theta_3 - \theta_2)\frac{d\theta_2}{dt} \end{aligned}\right\} \text{..... (3.34)}$$

The following additional notation can be introduced:

$$\frac{d\theta_2}{dt} = \omega_2;\ \frac{d\theta_3}{dt} = \omega_3 \quad \text{..... (3.35)}$$

While ω_3 is expected to vary with time, the crank (eccentric shaft) is assumed to rotate at constant rotational velocity and therefore, ω_2 should be constant. According to the manufacturer's specifications (Henan Hongxing Mining Machinery Company Limited, 2013), for a PE 400 x 600 Single Toggle Jaw Crusher, ω_2 may be taken to be 28.8 radians per second. Thus, with the data given in Table 3.13, equation (3.34) may be re-written as follows:

$$\left.\begin{aligned} \omega_3 = \left(\frac{K_2 - K_1}{K_2 - K_3}\right)\omega_2 = 28.8\left(\frac{K_2 - K_1}{K_2 - K_3}\right) \\ K_1 = \frac{r_1}{r_3}\sin(\theta_2 - \theta_1) = 0.753\ \sin(\theta_2 - \theta_1) \\ K_2 = \ \sin(\theta_3 - \theta_2) \\ K_3 = \frac{r_1}{r_2}\sin(\theta_3 - \theta_1) = 68.08\ \sin(\theta_3 - \theta_1) \end{aligned}\right\} \quad \ldots\ldots\ldots\ldots\ldots\ldots\ldots\ldots\ldots\ldots \quad (3.36)$$

In equation (3.36), for any given value of θ_2, with the corresponding value of θ_3 having been determined, K_1, K_2 and K_3can be determined.

Equations (3.36) were used to determine the values of ω_3, as θ_2 varied from 0º to 360º. Some of these calculated values are given in Table 3.18. For one full cycle of rotation of the crank, the minimum value of ω_3 was found to be -0.476 radians per second while the maximum value of ω_3 was found to be 0.451 radians per second. Thus, the angular velocity of the coupler (swing jaw) is generally small.

A graph of the variation of ω_3 with θ_2 is shown in Figure 3.14.

Table 3.18: Analytically Determined Values of ω_3 for Given Values of θ_2

$\boldsymbol{\theta_2}$ (degrees)	ω_3 (rad/s)	$\boldsymbol{\theta_2}$ (degrees)	ω_3 (rad/s)
0	0.407	195	-0.463
15	0.443	210	-0476
30	0.450	225	-0454
45	0.429	240	- 0.397
60	0.381	255	-0.313
75	0.309	270	-0.206
90	0.216	285	- 0.087
105	0.108	300	0.036
120	-0.009	315	0.154
135	-0.129	330	0.259
150	-0242	345	0.345
165	-0.341	360	0.407
180	-0.417		

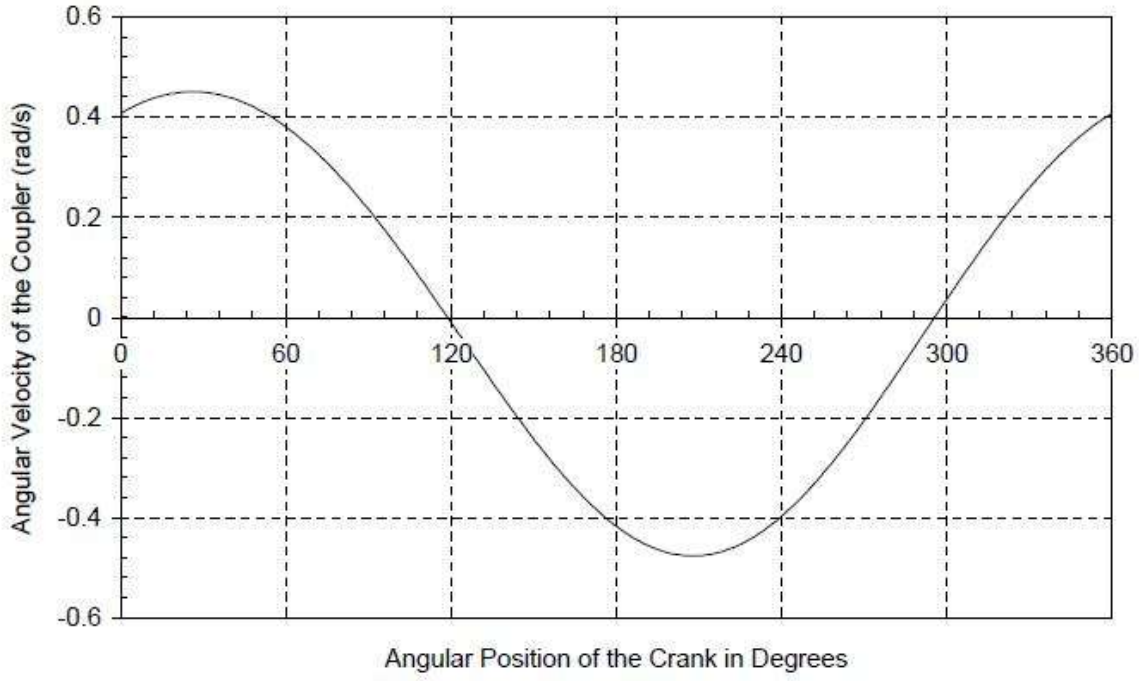

Figure 3.14: Variation of Coupler Angular Velocity ω_3 with Crank Angle θ_2

3.3.4.1 Velocity of a Point in the Swing Jaw

The position of a point in the swing jaw is determined by equations (3.31). In the particular case where the point falls on line O_3O_4, its position is then described by equations (3.32). Thus, the vertical and horizontal components of the velocity of a point on line O_3O_4 can be determined by differentiating equations (3.32) with respect to time, to obtain the fallowing;

$$\left.\begin{aligned} v_{PV} = \acute{y}_p &= -\omega_2 r_2 \sin\theta_2 - \omega_3 r_5 \sin\theta_3 \\ v_{PH} = \acute{z}_P &= \omega_2 r_2 \cos\theta_2 - \omega_3 r_5 \cos\theta_3 \end{aligned}\right\} \quad \ldots\ldots\ldots\ldots\ldots\ldots \quad (3.37)$$

With the data given in Table 3.12 and the value of ω_2 taken to be 28.8 radians per second, equations (3.37) can be re-written as follows;

$$\left.\begin{aligned} v_{PV} = y_p &= -0.3456 \sin\theta_2 - \omega_3 r_5 \sin\theta_3 \\ v_{PH} = z_P &= 0.3456 \cos\theta_2 - \omega_3 r_5 \cos\theta_3 \end{aligned}\right\} \quad \ldots\ldots\ldots\ldots\ldots\ldots\ldots\ldots\ldots\ldots \quad (3.38)$$

In equations (3.38), if r_5 is given, in metres, then, for any given value of θ_2, the corresponding values of θ_3 and ω_3 can be determined, as was earlier done, and therefore the velocity components v_{PV} and v_{PH} can be determined in metres per second.

For the values of r_5 given in Table 3.15, the values of the velocity components v_{PV} and v_{PH} were determined for one complete cycle of motion of the mechanism. The data in Tables 3.19 and 3.20 are representative of the results.

Table 3.19: Velocities in the Y Direction

Point	**P1**	**P2**	**P3**	**P4**	**P5**
$y_{min}\ (m/s)$	-0.346	-0.366	-0.389	-0.414	- 0.442
$y_{max}\ (m/s)$	0.346	0.367	0.393	0.421	0.452

Table 3.20: Velocities in the Z Direction

Point	**P1**	**P2**	**P3**	**P4**	**P5**
$z_{min}\ (m/s)$	-0.346	-0.383	-0.421	-0.46	-0.50
$z_{max}\ (m/s)$	0.346	0.383	0.421	0.46	0.50

In Table 3.19, negative values of velocity indicate a vertically downward direction while positive values indicate a vertically upward direction. From Table 3.19, the magnitude of the maximum value of the component of velocity in the *Y* direction, whether it is directed upward or downward, increases gradually, and at a slightly increasing rate, as we move from point *P1* to *P5*. Once again, this could suggest an increasing rate of wear as we move from P1 to P5. Moreover, as we move from point P2 to P5, slightly greater velocities are

achieved in the vertically upward direction, as compared to the vertically downward direction, though the difference is so small that it can be neglected.

The vertical components of velocity for points *P1* to *P5* are compared graphically in Figure 3.15, for one complete rotation of the crank. It can be seen in Figure 3.14 that the angular oscillation of the swing jaw instantaneously stops when $\theta_2 \cong 118.81^{\circ}$ and when $\theta_2 \cong 295.625^{\circ}$. With no angular oscillation of the swing jaw, its motion becomes a pure translation and all the points in it have the same vertical components of velocity, as can be seen in Figure 3.15.

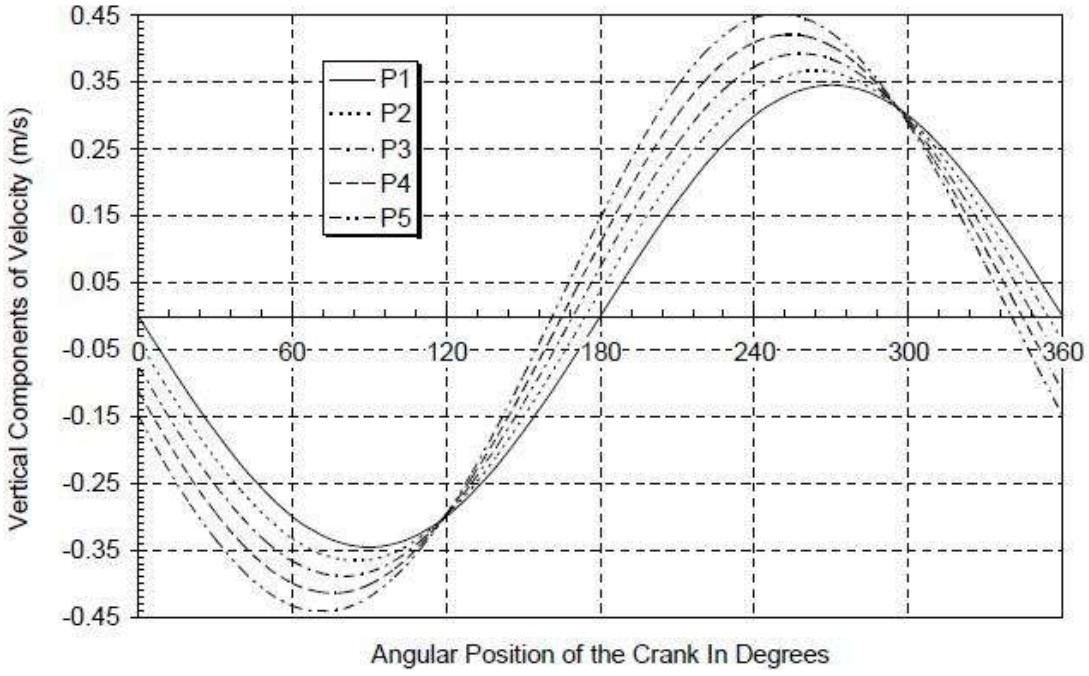

Figure 3.15: Vertical Components of Velocity of Points in the Swing Jaw

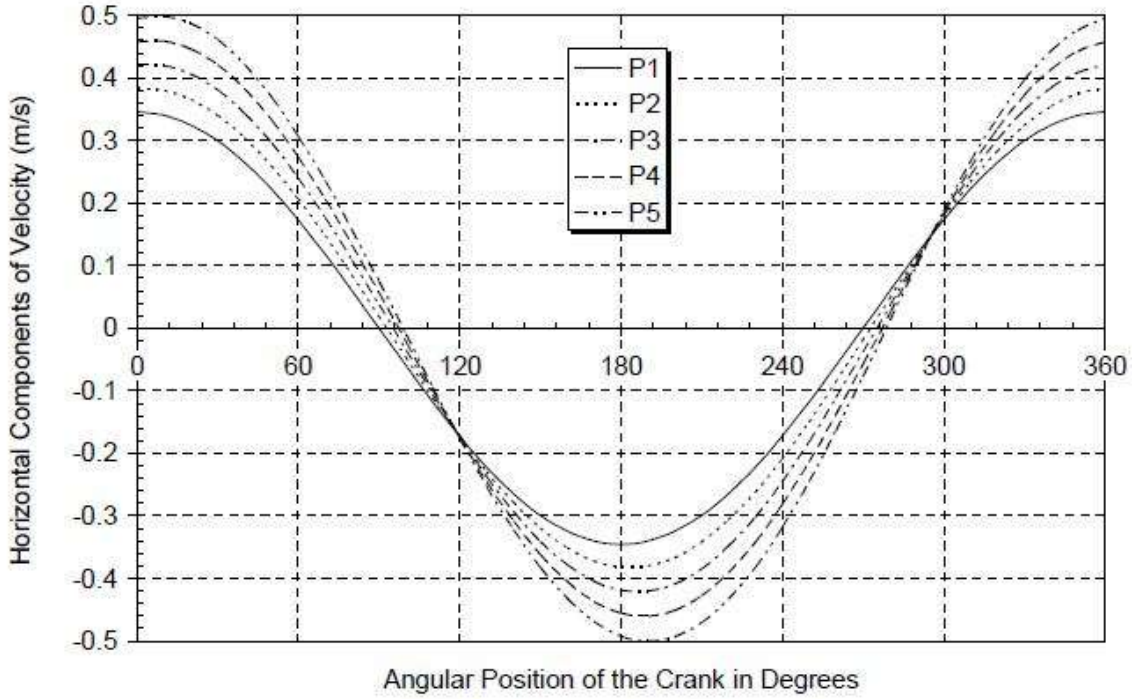

Figure 3.16: Horizontal Components of Velocity of Points in the Swing Jaw

In Table 3.20, negative values of velocity indicate that the swing jaw is moving away from the fixed jaw while positive values indicate that the swing jaw is moving towards the fixed jaw. From Table 3.20, the magnitude of the maximum value of the component of velocity in the Z direction increases at an almost constant rate, as we move from point *P1* to *P5*. Moreover, as we move from point *P1* to *P5*, the maximum value of the component of velocity in the *Z* direction appears to remain unchanged, whether the swing jaw is moving towards the fixed jaw or away from the fixed jaw.

The horizontal components of velocity for points *P1* to *P5* are compared graphically in Figure 3.16, for one complete rotation of the crank. Again, the instances when the angular oscillation of the swing jaw instantaneously stops are evidenced in Figure 3.16 by the crank positions at which all the points in the swing jaw have equal horizontal (as well as vertical) components of velocity.

In Figures 3.15 and 3.16, it can be seen that, for approximately the first quarter of rotation of the crank, the swing jaw moves vertically downward and horizontally towards the fixed jaw, thus forcefully feeding the charge of material into the crushing chamber and simultaneously crushing it. For the second quarter of rotation of the crank, the swing jaw still moves vertically downward but horizontally away from the fixed jaw, thus letting the crushed material fall through the crushing chamber. For the third quarter of rotation of the crank, the swing jaw moves vertically upwards and horizontally away from the fixed jaw, still letting the crushed material fall through the crushing chamber. Finally, in the last quarter of rotation of the crank, the swing jaw continues to move vertically upwards but horizontally towards the fixed jaw, thus beginning another crushing cycle.

3.3.5. Angular Acceleration Analysis of the Swing Jaw

An expression for the angular acceleration of the coupler can be obtained by differentiating equation (3.33) with respect to time, in doing so, it should be in mind that $r_1, \theta_1, r_2, r_3, r_4$ and ω_2 are all constants with respect to time. The result of the differentiation is then as follows:

$$\left.\begin{aligned} r_1 r_2 \omega_2^2 \cos(\theta_2 - \theta_1) + r_2 r_3 \omega_3 (\omega_3 - \omega_2) \cos(\theta_3 - \theta_2) \\ + r_2 r_3 \sin(\theta_3 - \theta_2) \frac{d\omega_3}{dt} + r_3 r_1 \omega_3^2 \cos(\theta_3 - \theta_1) \\ + r_3 r_1 \sin(\theta_3 - \theta_1) \frac{d\omega_3}{dt} \\ = r_2 r_3 \omega_2 (\omega_3 - \omega_2) \cos(\theta_3 - \theta_2) \end{aligned}\right\} \quad \ldots\ldots\ldots\ldots\ldots\ldots\ldots\ldots (3.39)$$

Here, the following additional notation can be introduced:

$$\frac{d\omega_3}{dt} = \alpha_3 \qquad \ldots\ldots\ldots\ldots\ldots\ldots\ldots\ldots\ldots\ldots (3.40)$$

With the use of equation (3.40), equation (3.39) can now be re-arranged into the following:

$$\left.\begin{aligned} r_1 r_2 \omega_2^2 \cos(\theta_2 - \theta_1) + r_2 r_3 (\omega_3 - \omega_2)^2 \cos(\theta_3 - \theta_2) \\ + r_3 r_1 \omega_3^2 \cos(\theta_3 - \theta_1) \\ = -[r_2 r_3 sin(\theta_3 - \theta_2) + r_3 r_1 \sin(\theta_3 - \theta_1)] \alpha_3 \end{aligned}\right\} \ldots\ldots\ldots\ldots\ldots\ldots (3.41)$$

Equation (3.41) can be divided through by $r_2 r_3$to obtain the following:

$$\left.\begin{aligned} &\frac{r_1}{r_3}\omega_2^2\cos(\theta_2-\theta_1)+(\omega_3-\omega_2)^2\cos(\theta_3-\theta_2)\\ &\qquad+\frac{r_1}{r_3}\omega_3^2\cos(\theta_3-\theta_1)\\ &\qquad=-\left[sin(\theta_3-\theta_2)+\frac{r_1}{r_2}\sin(\theta_3-\theta_1)\right]\alpha_3 \end{aligned}\right\} \quad \ldots\ldots\ldots\ldots\ldots\ldots (3.42)$$

Now. by letting $\omega_2 = 28.8$ radians per second, as was done before, and using the data in Table 6.1, equation (6.39) may be re-written as follows:

$$\left.\begin{aligned} \alpha_3 &= (K_1+K_2+K_3)/K_4\\ K_1 &= 624.56\cos(\theta_2-\theta_1)\\ K_2 &= (\omega_3-28.8)^2\cos(\theta_3-\theta_2)\\ K_3 &= 68.08\omega_3^2\cos(\theta_3-\theta_1)\\ K_4 &= -sin(\theta_3-\theta_2)+[68.08\sin(\theta_3-\theta_1)] \end{aligned}\right\} \ldots\ldots\ldots\ldots\ldots\ldots (3.43)$$

With the values of θ_3 and ω_3 that correspond to given values of θ_2 having been determined, equations (3.43) were used to determine the values of α_3 as $\theta_2$was varied from 0° to 360°. The calculated values are given in Table 3.21. A graph of variation of α_3 with θ_2 is shown in Figure 3.17.

Table 3.21: Analytically Determined Values of α_3, for Given Values of θ_2

$\boldsymbol{\theta_2}$ (degrees)	$\boldsymbol{\alpha_3}$(rad/s^2)	$\boldsymbol{\theta_2}$(degrees)	$\boldsymbol{\alpha_3}$(rad/s^2)
0	5.415	195	-3.315
15	2.362	210	0.543
30	-0.767	225	4.384
45	- 3.820	240	7.858
60	-6.657	255	10.659
75	-9.175	270	12.573
90	-11.150	285	13.490
105	-12.538	300	13.406
120	-13.179	315	12.401
135	-12.960	330	10.617
150	-11.813	345	8.226
165	-9.741	360	5.435
180	-6.841		

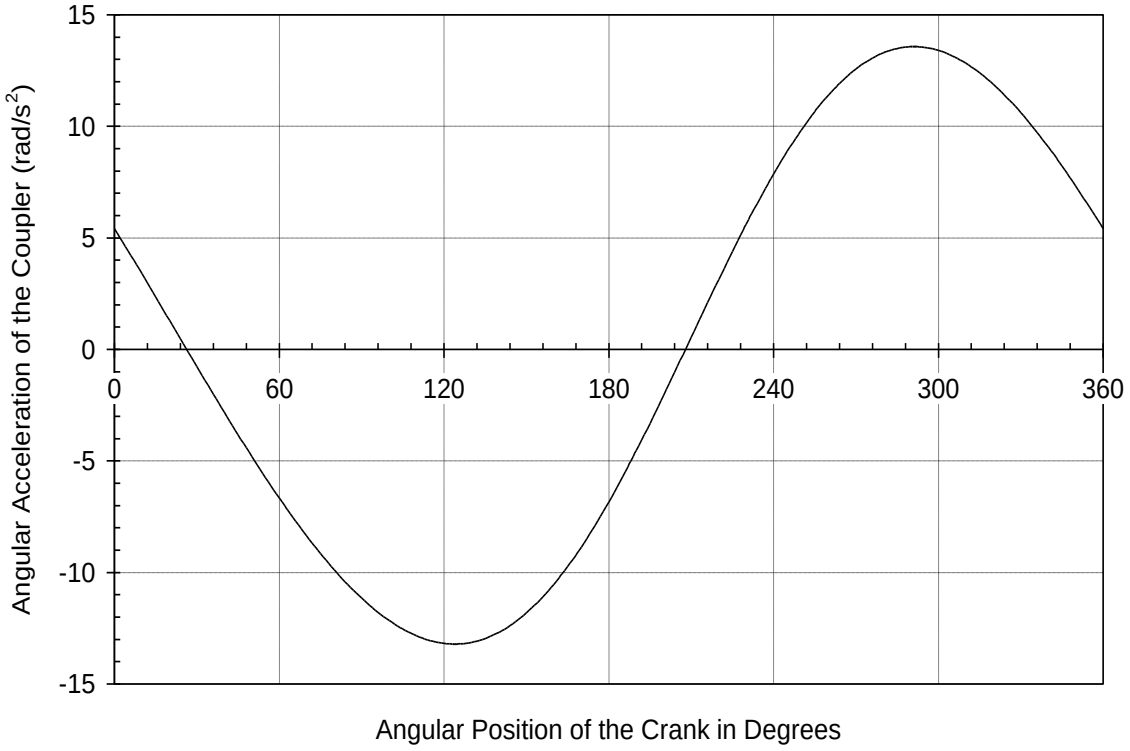

Figure 3.17: Angular Accelerations of the Coupler versus Crank Angle

For one complete cycle of motion of the swing jaw, the minimum value of its angular acceleration occurred at $\theta_2 = 123.9^{\circ}$ and was found to be -13.208 radians per square second while the maximum value of its angular acceleration occurred at $\theta_2 = 291.2^{\circ}$and was found to be 13.573 radians per square second. Thus, the angular acceleration of the swing jaw can attain substantial magnitudes. Cao *et al.*, (2006) found that the minimum values of angular acceleration of the swing jaw occurred at $\theta_2 = 124°$ and was found to be -13 radians for square second while the maximum angular acceleration occurred at θ_2 = 291°and was found to be 14 radians per square second. Therefore, the values obtained using the Vector Loop Closure Method are fairly in agreement with those of Cao *et al.*, (2006).

3.3.5.1 Acceleration of a Point in the Swing Jaw

The vertical and horizontal components of the acceleration of a point on line O_3O_4 in Figure 3.8 can be determined by differentiating equations (3.37) with respect to time, to obtain the following:

$$\left.\begin{aligned} a_{PV} = \ddot{y}_p &= -\omega_2^2 r_2 \cos\theta_2 - \omega_3^2 r_5 \cos\theta_3 - \alpha_3 r_5 \sin\theta_3 \\ a_{PH} = \ddot{z}_P &= -\omega_2^2 r_2 \sin\theta_2 - \omega_3^2 r_5 \sin\theta_3 + \alpha_3 r_5 \cos\theta_3 \end{aligned}\right\} \quad \text{..... (3.44)}$$

In equations (3.44), if r_5 is given, then, for any given value of θ_2, the corresponding values of θ_3, ω_3 and α_3 can be determined, and therefore the acceleration components $a_{PV}$and a_{PH}can also be determined.

For the values of r_5 given in Table 3.15, the values of the acceleration components $a_{PV}$and a_{PH}were determined using equations in (3.44) for one complete cycle of motion of the mechanism. The data shown in Tables 3.22 and 3.23 are the results obtained.

Table 3.22: Accelerations in the Y Direction

Point	***P1***	***P2***	***P3***	***P4***	***P5***
$\ddot{y}_{min}$(m/s^2)	-9.953	-10.467	-11.092	-11.817	-12629
$\ddot{y}_{max}$(m/s^2)	9.953	10.647	11.420	12.252	13.132

Table 3.23: Accelerations in Z Direction

Point	***P1***	***P2***	***P3***	***P4***	***P5***
$\ddot{z}_{min}$(m/s^2)	-9.953	-8993	-8.064	-7.176	-6.339
$\ddot{z}_{max}$(m/s^2)	9.953	8.807	7.716	6.720	5.887

In Table 3.22, negative values indicate an acceleration that is directed vertically downward and would either slow down the vertical component of velocity of the swing jaw, if it were moving in the upward direction, or speed up the vertical component of velocity of the swing jaw, if it were moving in the downward direction. Positive values indicate an acceleration that is directed vertically upward and would either slow down the vertical component of velocity of the swing jaw, if it were moving in the downward direction, or speed up the vertical component of velocity of the swing jaw, if it were moving in the upward direction. From Table 3.22, the magnitude of the maximum value of the component of acceleration in the *Y* direction increases at a slightly increasing rate, as we move from point *P1* to *P5* . Moreover, as we move from point *P1* to *P5*, the maximum value of the component of acceleration in the *Y* direction is almost unchanged, whether it is directed vertically upwards or vertically downwards.

In Table 3.23, negative values indicate an acceleration that is directed horizontally away from the fixed jaw and would either slow down the horizontal component of velocity of the swing jaw, if it were moving towards the fixed jaw, or speed up the horizontal component of velocity of the swing jaw, if it were moving away from the fixed jaw. Positive values indicate an acceleration that is directed horizontally towards the fixed jaw and would either slow down the horizontal component of velocity of the swing jaw, if it were moving away from the fixed jaw, or speed up the horizontal component of velocity of the swing jaw, if it were moving towards the fixed jaw. From Table 3.23, the magnitude maximum value of the component of acceleration in the *Z* direction decreases at a slightly decreasing rate, as we move from point *P1* to *P5*. Moreover, as we move from point *P1* to *P5*, the maximum value of the component of acceleration in the *Z* direction is almost unchanged, whether it is directed towards the fixed jaw or away from the fixed jaw.

The vertical components of acceleration for points *P1* to *P5* are compared graphically in Figure 3.18, for one complete rotation of the crank.

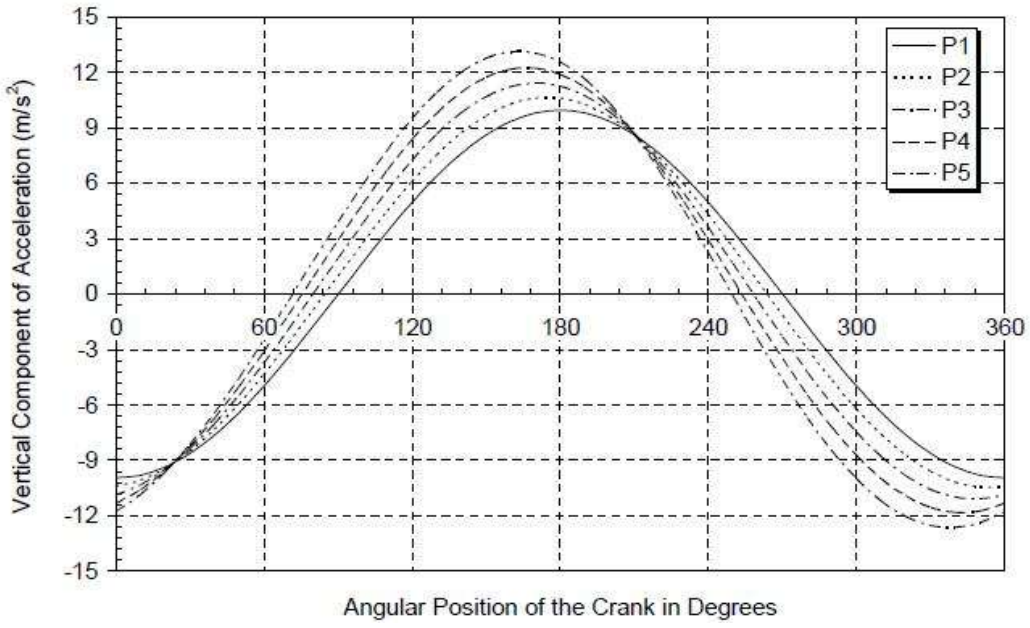

Figure 3.18: Vertical Components of Acceleration of Points in the Swing Jaw

It can be seen in Figure 3.17that the angular acceleration of the swing jaw instantaneously becomes zero when $\theta_2 \cong 26.32°$ and when $\theta_2 \cong 207.92°$. At these instances, the acceleration of the swing jaw becomes a purely translational and all the points in it have the same vertical components of acceleration, as can be seen in Figure 3.18.

The horizontal components of acceleration for points *P1* to *P5* are compared graphically in Figure 3.19, for one complete rotation of the crank. Again, it can be seen in Figure 6.15 that the angular acceleration of the swing jaw instantaneously becomes zero when $\theta_2 \cong 26.32°$ and when $\theta_2 \cong 207.92°$. At these instances, the acceleration of the swing jaw becomes a purely translational and all the points in it have the same horizontal components of acceleration, as can be seen in Figure 3.19.

Cao *et al.,* (2006) in their work found that the angular acceleration of the swing jaw instantly becomes zero when the angular position of the crank become $\theta_2 \cong 26°$ and when $\theta_2 \cong 208°$ which is fairly in agreement with the result of this research work.

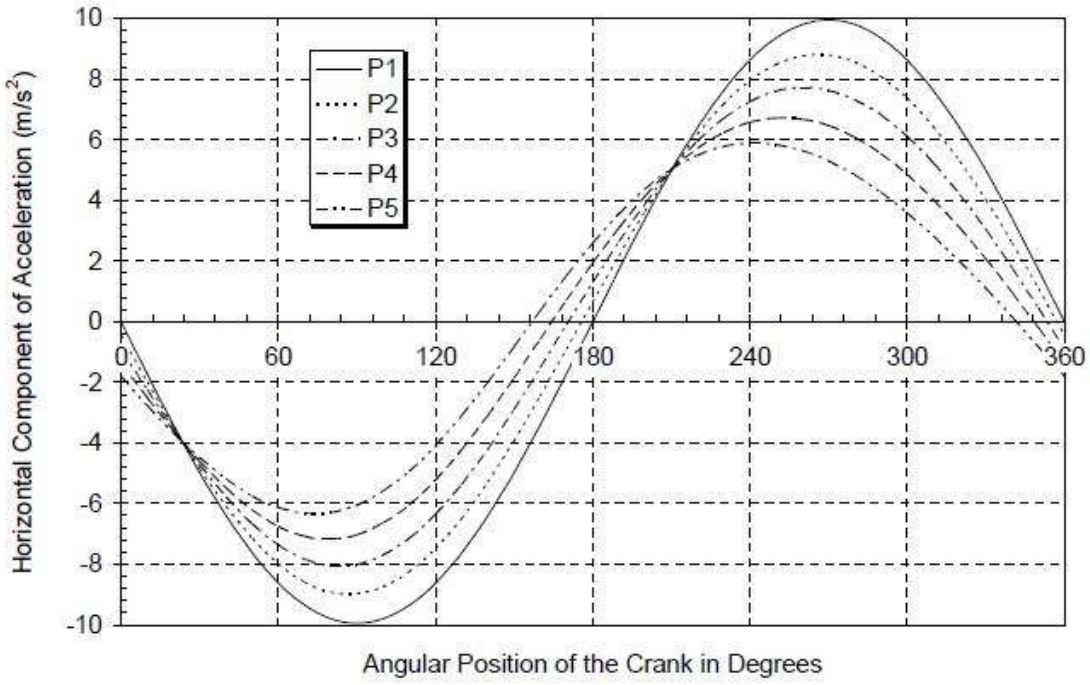

Figure 3.19: Horizontal Components of Acceleration of Points in the Swing Jaw

3.4 ANALYSIS OF THE SINGLE TOGGLE JAW CRUSHER FORCE TRANSMISSION CHARACTERISTICS

3.4.1 Introduction

Ham *et al.,* (1958) stated that "in analyzing forces in any machine system, the basic assumption is that, "the system is composed of all external forces and all the inertial forces that act upon any member of the machine is a system that is in equilibrium."

Since the mechanism is being treated as a planar, therefore all the forces are taken similarly to be planar. In this analysis, it is assumed that:

(i) The forces arising due to acceleration of the machine components are extraneous hence negligible.

(ii) The frictional forces are negligible as there is use of antifriction bearings in the revolute joints (Abhary, 2008).

(iii) In the 4R mechanism, the efficiency is 100% (Erdman and Sandor, 1991; Norton, 1991; Shigley and Vicker, 1980)

(iv) There is equilibrium of the forces acting on the moving joints of the mechanism and can easily be related to the input torque as well as the load torque (Abhary, 2008)

The presentation by Shigley and Vicker Jr. (1980) defined the Mechanical Advantage as the ratio of the output torque to the input torque, which led to a slightly different expressions for the Mechanical Advantage, as compared to Erdman and Sandor (1991) and Norton (1992), who defined Mechanical Advantage as the ratio of output force to input force.

The methods presented by Erdman and Sandor (1991), Norton (1992), Shigley and Vicker (1980) give no indication of the actual forces that are sustained by the members of the mechanisms, knowledge of which would be necessary at the design stage. The method in this presentation include the following:

i) A static force analysis that neglects the frictional and inertia forces

ii) All the forces and moments are assumed to be coplanar.

iii) Consider on the moving joints of the mechanism and relating them to the input torque as well as the load torque. This may be compared to the method presented by Abhary (2008).

As a result of the analysis, a characteristic Mechanical Advantage of the Single Toggle Jaw Crusher may be used as a criterion for selecting such mechanism.

3.4.2 A Review of the Single Toggle Jaw Crusher Kinematics.

In the kinematical model of the Single Toggle Jaw Crusher, which is illustrated in Figure 3.20, the acentric shaft is modelled as a short crank, of length r_2 that continuously rotates about a fixed axis, at 0_2. The swing jaw is modelled as the coupler link O_3O_4, of length r_3, which moves with a complex planar motion that has both rotational and translation components. The toggle link is modelled as the rocker O_4O_1 which oscillates about the

fixed axis at 0_1. The fixed jaw is considered to be an integral part of the frame of the machine.

Oduori *et al.*, (2015) analyzed the kinematics of the Single Toggle Jaw Crusher, as modelled in Figure 3.20 and found the following expression:

$$2r_1r_2\cos(\theta_2 - \theta_1) + 2r_1r_2\cos(\theta_3 - \theta_1)$$

$$+2r_3r_1\cos(\theta_3 - \theta_1) = r_4^2 - r_3^2 - r_2^2 - r_1^2 \quad \ldots\ldots\ldots\ldots\ldots\ldots\ldots\ldots\ldots\ldots\ldots \text{(3.45)}$$

In this study, we used the dimensional data for a PE 400 x 600 Single Toggle Jaw Crusher shown (Cao *et al.*, 2006). Given $r_1 = 817mm$ and $\theta_1 = 3.18^{\circ}$; substituting the data into equation (3.45), the following is obtained:

$$0.753\ cos\ (\theta_2 - 3.18^{\circ}) + cos\ (\theta_3 - \theta_2)$$

$$+\ 68.08\ cos\ (\theta_3 - 3.18^{\circ}) = -62.894 \ldots\ldots\ldots\ldots\ldots\ldots\ldots\ldots\ldots\ldots\ldots\ldots \text{(3.46)}$$

Equation (3.46) can be used to determine values of θ_3 for any given value of θ_2, which represents the input motion.

In the cycle of motion of the Single Toggle Jaw Crusher mechanism, two phases known as the toggle phases are of particular interest. In each of the toggle phases, the crank and the coupler link fall in a single straight line, therefore, the toggle phases occur when $\theta_2 = \theta_3$ and when $\theta_2 = \theta_3 + 180^{\circ}$. For the first toggle phase, equation (3.46) can be reduced to the following.

$$68.833\ cos\ (\theta_2 - 3.18^{\circ}) = -62.894 \ldots\ldots\ldots\ldots\ldots\ldots\ldots\ldots\ldots\ldots\ldots\ldots .. \text{(3.47)}$$

Solving equation (3.47) gives $\theta_2 = 161.34^{\circ}$ for the first toggle phase.

Similarly, for the second toggle phase equation 3.46) can be reduced to the following;

$$67.327\ cos\ (\theta_2 - 3.18^{\circ}) = +61.894 \ldots\ldots\ldots\ldots\ldots\ldots\ldots\ldots\ldots\ldots\ldots\ldots \text{(3.48)}$$

Equation (3.48) too is readily solved to give $\theta_2 = 340^{\circ}$ for the second toggle phase.

3.4.3 Force Transmission Model

3.4.3.1 Static Force Analysis

The forces and moments acting on the links of the Toggle Jaw Crusher Mechanism are all assumed to be coplanar and compressive and illustrated in Figure 3.20.

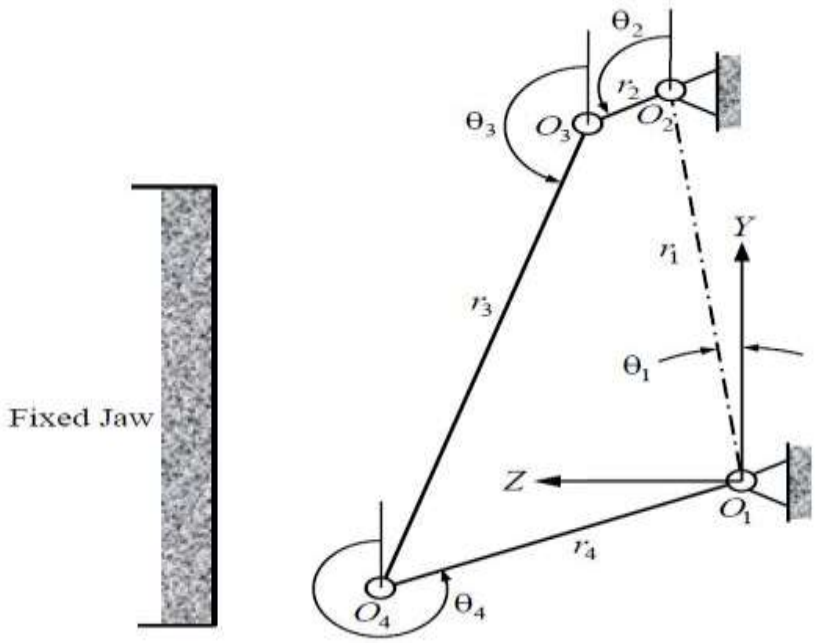

Figure 3.20: Kinematical Model of the Single Toggle Jaw Crusher

In performing the static force analysis, it is assumed that the masses of the links, as well as friction are negligible. In Figure 3.21 T_2 is the driving torque applied at the crank axis O_1 to drive the crank and the entire crusher mechanism. T_3 is the torque, acting along the axis of O_3 due to the resistance of the feed materials against being crushed. F_2, F_3, and F_4 are the forces in links 2, 3 and 4 respectively and they are assumed to be compressive. The system of forces and moments are assumed to be equilibrium in every phase of motion of the mechanism.

The forces acting at the moving joints O_3 and O_4 are shown in Figure. 3.22.

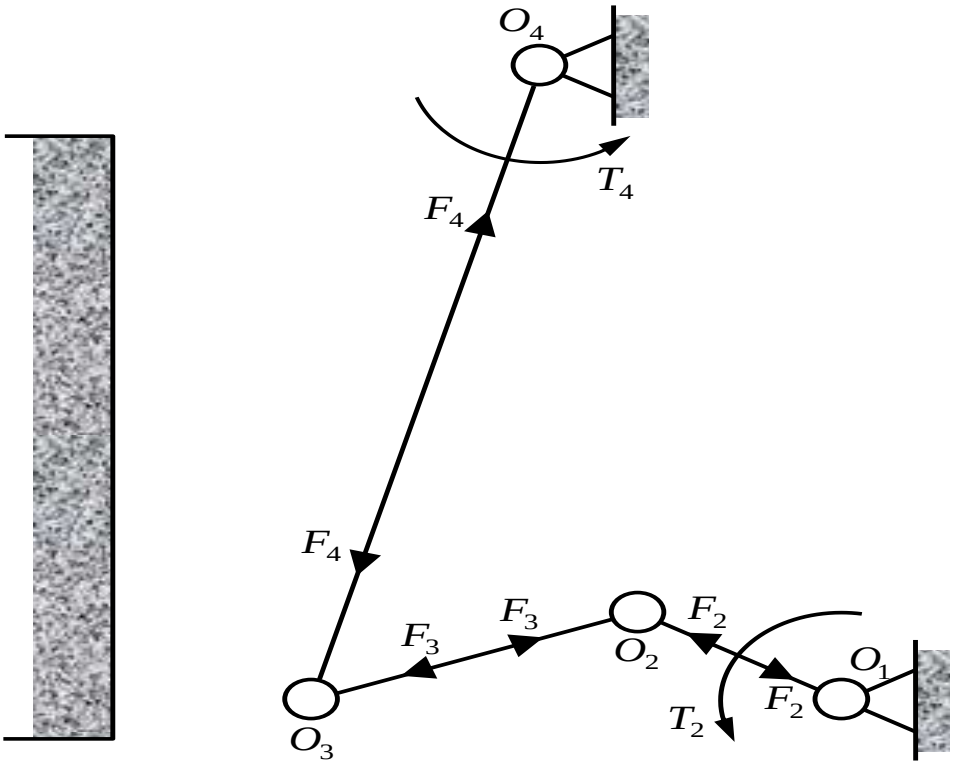

Figure 3.21: Model for Static Force Analysis

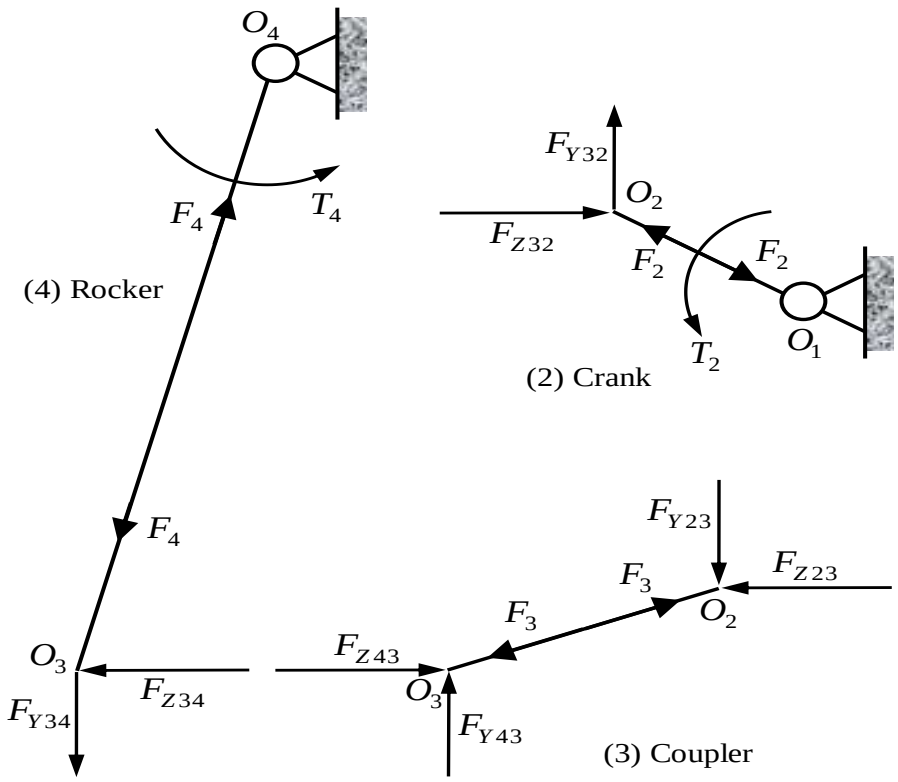

Figure 3.22: Free-body Diagrams of the Crank, the Coupler and the Rocker

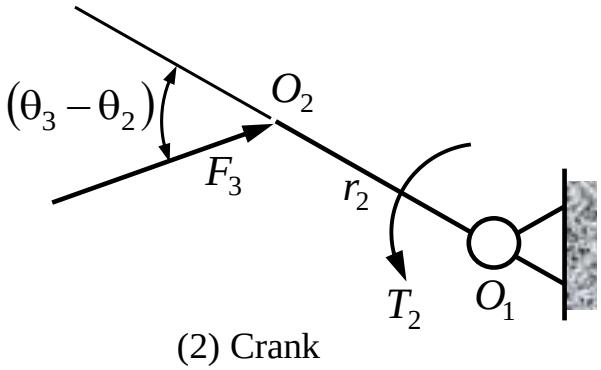

Figure 3.23: Balance of Moment on the Crank

Start by considering the crank. Static force analysis is based on the assumption that there are no accelerations in the mechanism. Referring to Figures (3.21. 3.22 and 3.23, the equilibrium of moments acting on the crank, about the fixed joint O_2, leads to the following result:

$$\left.\begin{aligned} 0 &= -F_{Y32}r_2\sin\theta_2 - F_{Z32}r_2\cos\theta_2 + T_2 \\ T_2 &= [F_{Z32}\cos\theta_2 + F_{Y32}\sin\theta_2]r_2 \end{aligned}\right\} \quad \ldots\ldots\ldots\ldots\ldots\ldots\ldots\ldots (3.49)$$

Now consider the coupler. The equilibrium of forces at joint O_3 leads to the following:

$$\left.\begin{aligned} F_{Y23} + F_3\cos(180^\circ - \theta_3) &= 0 \\ F_{Y23} &= F_3\cos\theta_3 \\ F_{Y23} = -F_{Y23} &= -F_3\cos\theta_3 \end{aligned}\right\} \quad \ldots\ldots\ldots\ldots\ldots\ldots\ldots\ldots (3.50)$$

$$\left.\begin{aligned} F_{Z23} + F_3\sin(180^\circ - \theta_3) &= 0 \\ F_{Z23} &= F_3\sin\theta_3 \\ F_{Z23} = -F_{Y23} &= -F_3\sin\theta_3 \end{aligned}\right\} \quad \ldots\ldots\ldots\ldots\ldots\ldots\ldots\ldots (3.51)$$

From equations (3.49), (3.50) and (3.51), it follows that:

$$\left.\begin{aligned} T_2 &= (F_3\sin\theta_3\cos\theta_2 - F_3\cos\theta_3\sin\theta_2)r_2 \\ &= F_2r_2\sin(\theta_3 - \theta_2) \end{aligned}\right\} \quad \ldots\ldots\ldots\ldots\ldots\ldots\ldots\ldots (3.52)$$

The statement of equation (3.52) is illustrated in Figure 3.23.

It is evident from Figures. 3.22 and 3.23 that:

$$F_3\cos(\theta_3 - \theta_2) = -F_2 \quad \ldots\ldots\ldots\ldots\ldots\ldots\ldots\ldots (3.53)$$

Now, in Figure 3.22, by considering the equilibrium of all the forces acting upon the coupler, the following is obtained:

$$\left.\begin{aligned} F_{Y43} + F_{Y23} &= 0 \\ F_{Y43} = -F_{Y23} &= F_3\cos\theta_3 \end{aligned}\right\} \quad \ldots\ldots\ldots\ldots\ldots\ldots\ldots\ldots (3.54)$$

$$\left.\begin{aligned} F_{Z43} + F_{Z23} &= 0 \\ F_{Z43} &= -F_{Z23} = F_3 \sin\theta_3 \end{aligned}\right\} \quad \ldots\ldots\ldots\ldots\ldots\ldots (3.55)$$

In Figure 3.22, the equilibrium of moments acting on the coupler, about the joint O_3 , leads to the following result:

$$\left.\begin{aligned} 0 &= -F_{Y43} r_3 \sin\theta_3 + F_{Z43} r_3 \cos\theta_3 + T_3 \\ T_3 &= [F_{Y43} \sin\theta_3 + F_{Z43} \cos\theta_3] r_3 \end{aligned}\right\} \quad \ldots\ldots\ldots\ldots\ldots\ldots\ldots\ldots (3.56)$$

From equations (3.54), (3.55) and (3.56), it follows that:

$$T_3 = F_3 r_3 \sin(2\theta_3) \qquad \ldots\ldots\ldots\ldots\ldots\ldots\ldots\ldots\ldots\ldots\ldots\ldots\ldots\ldots\ldots\ldots 3.57)$$

A relationship between T_3 and T_2 can now be obtained from equations (3.52) and (3.57), as follows;

$$f(\theta_2) = \frac{T_3 r_2}{T_2 r_3} = -\frac{sin(2\theta_3)}{sin(\theta_3 - \theta_2)} \quad \ldots\ldots\ldots\ldots\ldots\ldots\ldots\ldots \qquad (3.58)$$

Equation (3.58) is in dimensionless form. The left-hand side of equation (3.58) can be regarded as a force transmission ratio that compares the nominal transmitted force, $T_2/r_3$to the nominal input force, T_2/r_2. This ratio is an indicator of the theoretical force transmission potential for any given phase of motion of the mechanism.

For a given crusher mechanism, the values of θ_2, and θ_3 can be determined from purely kinematical considerations, by use of equation (3.45) along with the dimensional data of the mechanism, and then the value of the right-hand side of equation (3.58) will be determined.

Using the dimensional data of the mechanism, given in Table 6.1, along with given values of θ_2, the corresponding values of θ_3 were computed and then used in equation (3.58) to determine the corresponding force transmission ratios, for one and a half cycles of motion of the crank. The results are plotted in Figure 3.24.

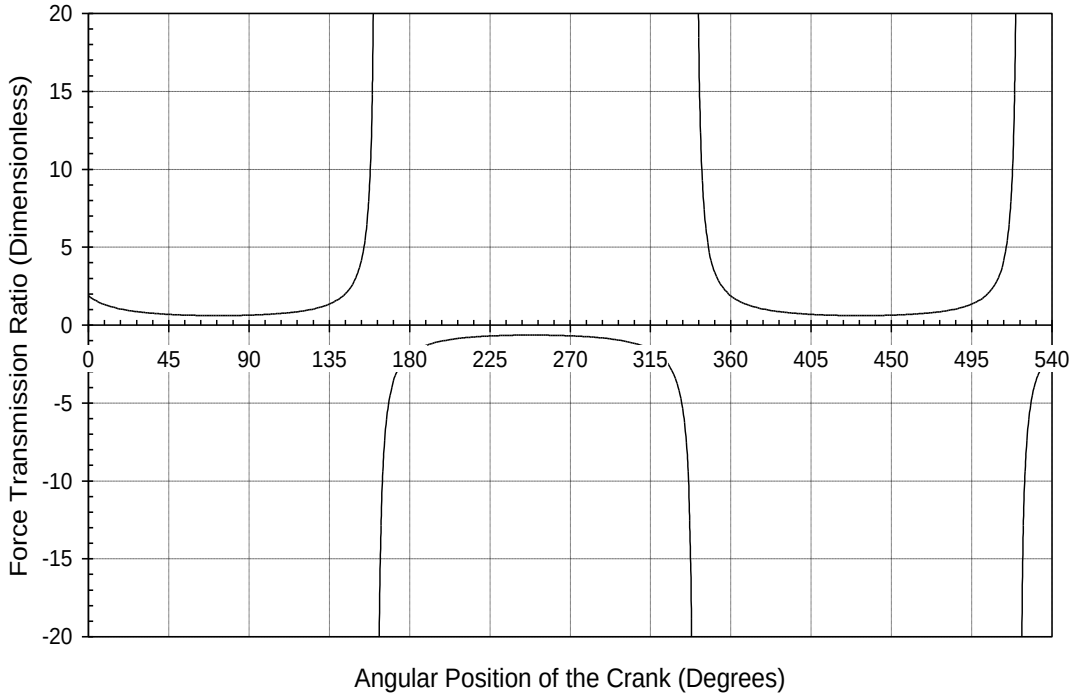

Figure 3.24: Variation of Force Transmission Ratio with Crank Angle θ_2

The first spike in Figure 3.24 indicates the great amplification of the crushing force that occurs at the first toggle position, which corresponds to a crank angle of about 161.34º. Theoretically, the crushing force amplification should be infinite at this toggle phase. Moreover, there occurs an abrupt reversal of the sign of the force transmission ratio from positive to negative, at this toggle phase. The second spike in Figure 3.24, which is also accompanied by a reversal in the sign of the force transmission ratio, occurs at a crank angle of about 340º. This spike corresponds to the second toggle phase of the mechanism.

The great amplification of transmitted force, accompanied by the abrupt reversal of the sign of the force transmission ratio, at each of the toggle phases, may be compared with the phenomenon of resonance, in mechanical vibrations, which also features great amplification of the responding motion, accompanied by a reversal of the phase between the forcing and the responding functions.

As the crank rotates from $\theta_2 = 161.34^\circ$ to $\theta_2 = 340^\circ$the crusher would be on the idle stroke with the swing jaw being retracted and no work being done in crushing the feed material. This is evidenced by the negative values of the force transmission ratio, between these two angular positions of the crank, in Figure 3.24. Useful work is done as the crank rotates from $\theta_2 = 340^\circ$to $\theta_2 = 521.34^\circ$, in a succeeding cycle of motion of the crank. Thus, during each cycle of motion of the crank, the useful working stroke of the mechanism lasts for about $181.34^\circ$of rotation of the crank, which is very slightly greater than half the cycle of motion of the crank. On the other hand, during each cycle of motion of the crank, the idle stroke lasts for 178.66º of rotation of the crank, which is very slightly less than half the cycle of motion of the crank. Thus, the mechanism has a quick return feature that is hardly noticeable since the crushing stroke lasts for 50.31% of the complete cycle of its motion, while the idle stroke lasts for 49.63% of the complete cycle of the motion of the mechanism.

3.4.3.2 Force Transmission Ratio and the Transmitted Torque

In the preceding section, we have seen that the crushing stroke lasts for only about 50% of each complete cycle of motion of the Single Toggle Jaw Crusher. For the other 50% of the complete cycle of motion, the swing jaw is being retracted in preparation for the next crushing stroke.

In Figure 3.24, it can be seen that the force transmission ratio varies from a very high value, at the beginning of the crushing stroke, that initially falls very rapidly and then levels off to reach a minimum value of less that unity (about 0.6), about halfway through the crushing stroke. The latter half of the crushing stroke appears to be a mirror image of the earlier half, in which the force transmission ratio first rises gradually and then spikes to a very high value at the end of the crushing stroke. Sample values of the force transmission ratio during the useful crushing stroke are given in Table 3.24.

Cao *et al.,* (2006) found that the useful working stroke of the mechanism lasts about 180° *(*from $\theta_2 \cong 340^\circ \; to \; \theta_2 \cong 521^\circ$) *with* the stroke as the crank rotates from $\theta_2 \cong 161^\circ \; to \; \theta_2 \cong 340^\circ$. These results agree with those in this thesis.

Table 3.24: Some Values of Force Transmission Ratio During the Crushing Stroke

$\boldsymbol{\theta_2}$ (degrees)	Force Transmission Ratio. $\boldsymbol{f(\theta_2)}$ (Dimensionless)	$\boldsymbol{\theta_2}$ (degrees)	Force Transmission Ratio, $\boldsymbol{f(\theta_2)}$ (Dimensionless)
340	2,418,327	440	0.612
350	4.649	450	0.6.16
360	1.882	460	0.684
370	1.280	470	0.766
380	0.989	480	0.904
390	0.323	490	1.148
400	0.772	500	1.642
410	0.660	510	3.046
420	0.624	520	26.030
410	0.609	521.31	3,268.45

The fact that the crushing stroke commences with a very high value of the force transmission ratio is advantageous when crushing brittle material, which is often the case. Since brittle materials fracture without undergoing significant deformation, actual crushing of brittle materials in a Single Toggle Jaw Crusher would occur soon after commencement of the crushing stroke, where the force transmission ratio is high.

According to Chinese jaw crusher manufacturer's data (Henan Hongxing Mining Machinery Company Limited, 2013), the PE 400 by 600 Single Toggle Jaw Crusher has 30kW motor power and an input eccentric shaft speed of 28.7979 radians per second. Assuming that the input speed is constant, the input torque is found to be 1.0417kNm. By using this information, along with the data in Table 3.24 and equation (3.58) the transmitted torque, in kilo newtons meter, can be estimated to be the following:

$$T_3 = -94.19\left[\frac{sin(2\theta_3)}{sin(\theta_3-\theta_2)}\right] \quad \text{.....(3.59)}$$

The above calculation assumes a 100% power transmission efficiency. Equation (3.59) was used to calculate the values of the transmitted torque that are given in Table 3.25.

Table 3.25: Sample Values of the Transmitted Torque During Crushing Stroke

θ_2 (degrees)	Torque kNm.	θ_2 (degrees)	Torque kNm.
340	227,784.124	440	57.685
350	350.770	450	59.917
360	196.420	460	64.441
370	120.544	470	72.195
380	93.110	480	85.183
390	77.544	490	108.106
400	68.000	500	154.632
410	62.120	510	286.930
420	58.741	520	2451.743
430	57.325	521	307,8854,93

The above calculations reveal that the minimum value of the transmitted torque will be about 55 times; as big as the input torque, with the theoretical maximum value being infinity. It is for this reason that a material that cannot be crushed will lead to breakage of the toggle link.

The values of the transmitted torque, as calculated by use of equation (3.59), are plotted in Figure 3.25, for one complete active crushing stroke.

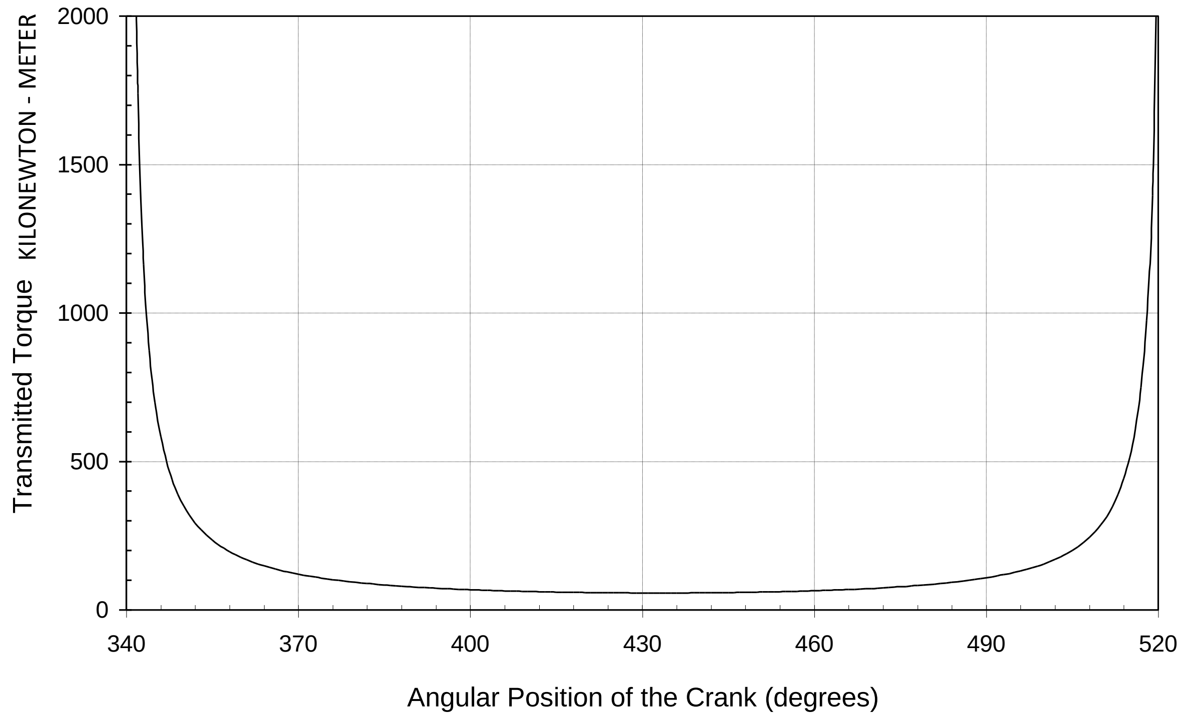

Figure 3.25: Variation of Transmitted Torque during a Crushing Stroke.

3.4.3.3 Characteristic Mechanical Advantage

A force transmission ratio that would characterize the Single Toggle Jaw Crusher was calculated as the mean value of the force transmission ratio over a complete useful crushing stroke, which does not include the retraction stroke.

According to the Mean Value Theorem of the Integral Calculus (Larson *et al.,* 1994), if a function $y = f(x)$ is continuous on the closed interval $[a, b]$ then the mean value of y for that interval can be determined as follows;

$$\bar{y} = \frac{1}{b-a}\int_a^b f(x)dx \quad \ldots\ldots\ldots\ldots\ldots\ldots\ldots\ldots\ldots\ldots\ldots\ldots\ldots\ldots\ldots\ldots\ldots\ldots\ldots\ldots(3.60)$$

In this case the transmitted torque T_3 is continuous over the interval of 340° and 521.31°, therefore, determining the Characteristic Mechanical Advantage, the mean value of the force transmission ratio was determined as follows:

$$\bar{f}(\theta_2) = \frac{1}{18.31^\circ} \int_{340^\circ}^{521.31^\circ} \frac{sin(2\theta_3)}{sin(\theta_3 - \theta_2)} \, d\theta_2 \quad \dots\dots\dots\dots\dots\dots\dots\dots\dots\dots\dots\dots\dots\dots\dots\dots \, (3.61)$$

The integral in equation (3.61) was evaluated numerically by use of the composite trapezoidal rule (Chaprar, 2012). For $340^\circ \leq \theta_2 \leq 520^\circ$, taken at one-degree intervals, the integral was evaluated as follows:

$$I_1 = \frac{1}{2}\left[f(340^\circ) + 2\sum_{\theta_2=341^\circ}^{\theta_2=519^\circ} f(\theta_2) + f(340^\circ)\right] = 1{,}559.709 \dots\dots\dots\dots\dots\dots \, (3.62)$$

For $520^\circ \leq \theta_2 \leq 521.31^\circ$, taken as three unequal intervals, the integral was evaluated as follows:

$$I_1 = \left[\frac{f(520^\circ) + 1.3f(521^\circ) + 0.31f(521.3^\circ) + 0.01f(521.31^\circ)}{2}\right] = 358.8177 \dots\dots.. \ (3.63)$$

In equations (3.62) and (3.63), $f(340^\circ)$, for instance, is the value of $f(\theta_2)$ for the case where $\theta_2 = 340^\circ$. The total integral was then determined as follows:

$$I = I_1 + I_2 = 1{,}918.527 \dots\dots\dots\dots\dots\dots\dots\dots\dots\dots\dots \quad (3.64)$$

Thus, the characteristic mechanical advantage was determined as follows:

$$\bar{f}(\theta_2) = \frac{I}{18.31^\circ} = 10.581 \dots\dots\dots\dots\dots\dots\dots\dots\dots\dots\dots\dots.. \quad (3.65)$$

From the preceding analysis, the following force transmission characteristics can be summed up for the *PE* 400 by 600 Single Toggle Jaw Crusher Mechanism as shown in Table 3.26.

Table 3.26: Force Transmission Characteristic of the Single Toggle Jaw Crusher.

Characteristic	Value (dimensionless)	Corresponding Crank Angle (degrees)
Minimum Force Transmission Ratio	0.608	433
Maximum Force Transmission Ratio	3268.446	521.31
Mean Force Transmission Ratio	10.58	Non-applicable

The minimum force transmission ratio occurs at about the midpoint of the active crushing stroke, while the maximum force transmission ratio occurs at the end of the active crushing stroke. However, the force transmission ratio at the beginning of the active crushing stroke is also very high- about 74% of the value at the end of the crushing stroke.

Given a number of different mechanism designs, the characteristics given in Table 3.26 may be calculated for each candidate mechanism and used, among others, as criteria in the selection of a suitable jaw crusher mechanism for a given application.

3.5 THE ANALYSIS OF THE KINEMATICS AND MECHANICAL ADVANTAGE OF THE DOUBLE TOGGLE JAW CRUSHER

3.5.1 Introduction

The swing jaw drive mechanism of a Double Toggle Jaw Crusher is modelled as a planar six bar mechanism with the swing jaw modelled as an oscillating rock link. Starting with two position Vector Loop Closure, mathematical equations describing the displacement, the angular position, angular velocity and angular acceleration of the swing jaw are obtained. Having obtained the kinematical equations, the mechanical advantage of the mechanism in derived therefrom.

3.5.2. Kinematical Model of Double Toggle Jaw Crusher

The concept of the Double Toggle Jaw Crusher is illustrated in Figure 3.26.

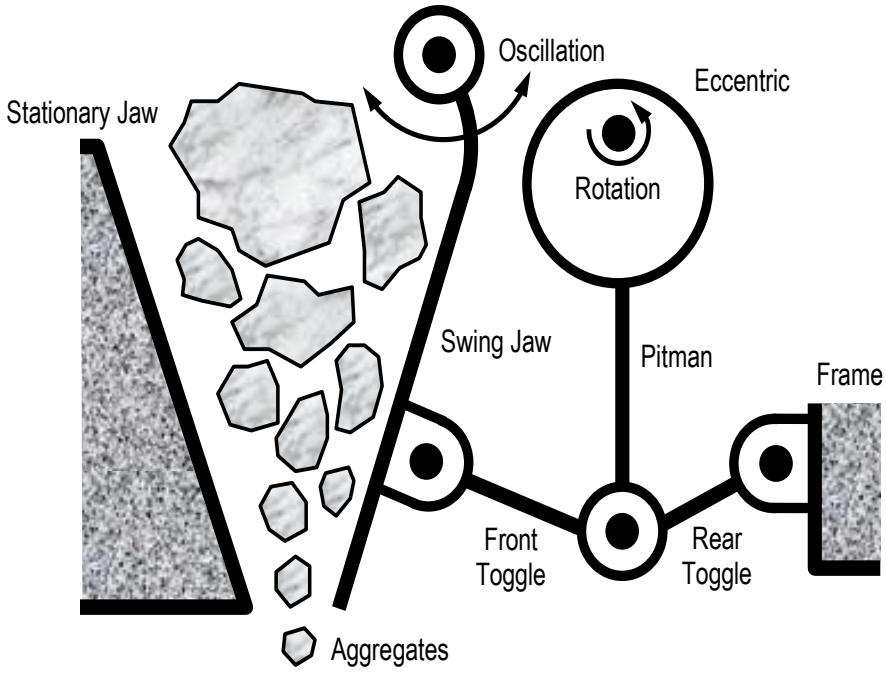

Figure 3.26: The Blake Double Toggle Jaw Crusher Design Concept

The swing jaw drive mechanism which include the eccentric shaft, the pitman, the toggle links, the swing jaw and the frame, can be modeled as a planar six bar linkage mechanism. Except for the frame, all links in the mechanism are connected to two joints and they are, therefore, binary links. The frame is connected to three joints, the first linking it to the near toggle; the second linking it to the eccentric shaft and the third linking it to the upper end of the swing jaw. The frame is therefore, a tertiary link.

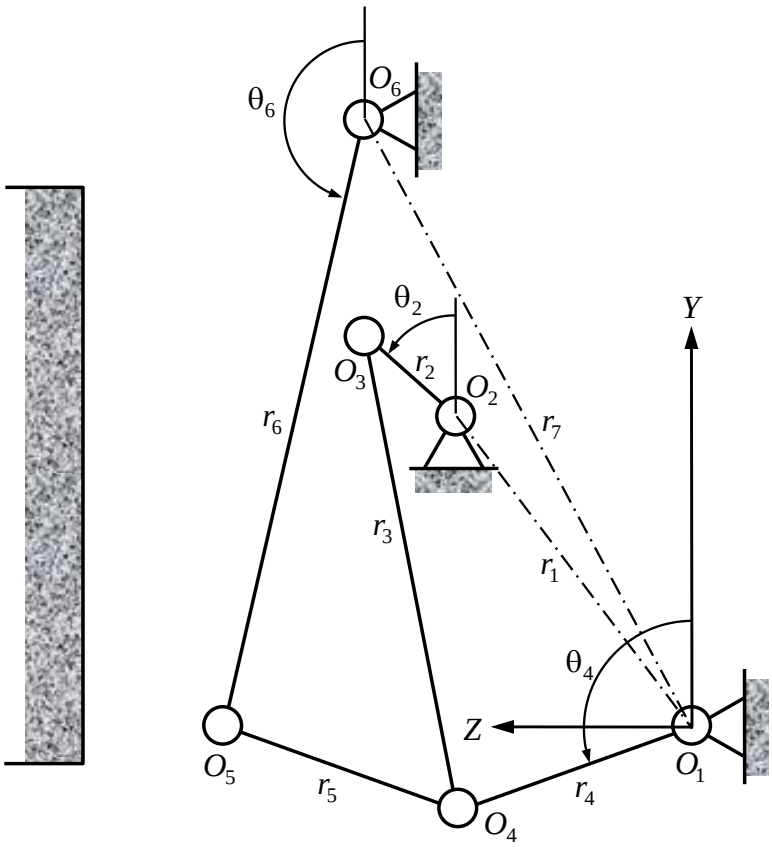

Figure 3.27: Kinematic Model of Double Toggle Jaw Crusher

In the kinematical model, which is illustrated in Figure 3.27, the eccentric shaft is modelled as a short crank, of length r_2 that continuously rotates about a fixed axis, at O_2. The Pitman is modelled as the coupler link O_3O_4, of length r_3, which executes a complex planar motion that has both rotational and translational components. The rear toggle link of length r_4 rocks about the fixed axis at O_1. The front toggle link of length r_5 is modelled as the coupler link O_4O_5 of length r_5 which also executes a complex planar motion that has both rotational and translational components. The swing jaw is modelled as the rocker O_5O_6, of length r_6, which oscillates about the fixed axis at O_6. However, the line O_5O_6 does not represent the crushing surface of the swing jaw. The fixed jaw is considered to be an integral part of the frame of the machine. Thus, two closed loops, $O_1O_2O_3O_4O_1$ and $O_1O_4O_5O_6O_1$can be identified in the kinematical model.

In studying the kinematics of the Double Toggle Jaw Crusher, it is particularly important to understand the motion of the rocker link O_5O_6, relative to the fixed jaw, as the crank rotates through a complete cycle. The coordinate reference frame that is illustrated in Figure 8.3 will be used in the analysis. The *X* axis is perpendicular to the plane of the figure and it points at the reader. Angular displacements are taken counter-clockwise, relative to the positive *Y* direction, which is the vertically upward direction.

3.5.2.1 Kinematical Analysis – The First Loop Vector Closure

The kinematical analysis that follow shall be based on the Vector Loop Closure Method (Erdman and Sandor, 1991; Kimbrell, 1991; Norton 1992; Shigley and Vicker, 1980). The first Vector Loop to be treated is illustrated in Figure 3.28. The resulting closure equation for this Vector Loop can be written as follows:

$$\bar{r}_1 + \bar{r}_2 - \bar{r}_3 - \bar{r}_4 = 0 \quad \text{.....} \quad (3.66)$$

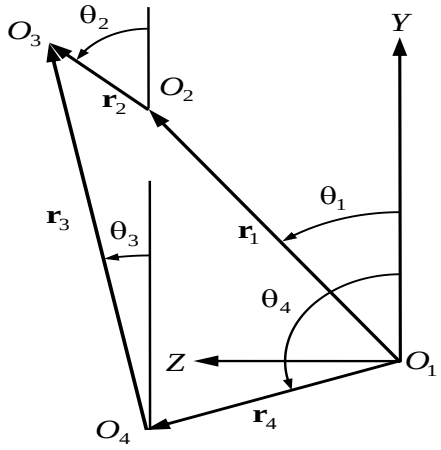

Figure 3.28: The First Vector Loop Closure

Equation (3.66) can be expressed in complex exponential notation as follows:

$$r_1 e^{j\theta_1} + r_2 e^{j\theta_2} - r_3 e^{j\theta_3} - r_4 e^{j\theta_4} = 0 \quad \text{.....} \quad (3.67)$$

The Euler identities state as follows (Carmichael and Smith, 1962):

$$\left.\begin{aligned} e^{j\theta} &= \cos\theta + j\sin\theta \\ e^{-j\theta} &= \cos\theta - j\sin\theta \end{aligned}\right\} \quad \text{(3.68)}$$

The following notations shall be used for conciseness:

$$\left.\begin{aligned} \cos\theta_i &= c_i \\ \sin\theta_i &= s_i \end{aligned}\right\} \quad \text{(3.69)}$$

By using equations (3.68) and (3.69), equation (3.67) can be re-written as follows:

$$r_1(c_1 + js_1) + r_2(c_2 + js_2) - r_3(c_3 + js_3) - r_4(c_4 + js_4) = 0 \quad \text{(3.70)}$$

In equation (3.70), if the real terms and the imaginary terms are considered separately, the following two equations are readily obtained:

$$\left.\begin{aligned} r_1c_1 + r_2c_2 &= r_3c_3 + r_4c_4 \\ r_1s_1 + r_2s_2 &= r_3s_3 + r_4s_4 \end{aligned}\right\} \quad \text{(3.71)}$$

By squaring each of the equations in (3.71), the following is obtained:

$$\left.\begin{aligned} r_1^2\,c_1^2 + 2r_1r_2c_1c_2 + r_2^2\,c_2^2 &= r_3^2\,c_3^2 + 2r_3r_4c_3c_4 + r_4^2\,c_4^2 \\ r_1^2\,s_1^2 + 2r_1r_2s_1s_2 + r_2^2\,s_2^2 &= r_3^2\,s_3^2 + 2r_3r_4s_3s_4 + r_4^2\,s_4^2 \end{aligned}\right\} \quad \text{(3.72)}$$

By adding corresponding terms of the equations in (3.72), and noting that $c_i^2 + s_i^2 = 1$, the following is obtained:

$$r_1^2 + 2r_1r_2(c_1c_2 + s_1s_2) + r_2^2 = r_3^2 + 2r_3r_4(c_3c_4 + s_3s_4) + r_4^2 \quad \text{(3.73)}$$

Now, the equations in (3.71) can be rearranged into the following:

$$\left.\begin{aligned} r_3c_3 &= r_1c_1 + r_2c_2 - r_4c_4 \\ r_3s_3 &= r_1s_1 + r_2s_2 - r_4s_4 \end{aligned}\right\} \quad \text{(3.74)}$$

It is well known from trigonometry (Carmichael and Smith, 1962) that:

$$\cos\theta_i\cos\theta_k + \sin\theta_i\sin\theta_k = \cos(\theta_i - \theta_k) \quad \text{(3.75)}$$

By substituting the equations in (3.74) into equation (3.73), and using the identity in equation (3.75), the following is obtained:

$$\left.\begin{aligned} 2r_1r_2\cos(\theta_1-\theta_2)+2r_1r_4\cos(\theta_1-\theta_4)+r_1^2+r_2^2-r_3^2+r_4^2 \\ =2r_2r_4\cos(\theta_2-\theta_4) \end{aligned}\right\} \quad \text{.....(3.76)}$$

In Figure 3.28, θ_1 is a fixed quantity. The motion of the crank O_2O_3 is the input motion and may be considered to be a rotation at uniform angular velocity, ω_2. Thus, at an instant in time, *t*, after commencement of the motion, the value of θ_2, in radians, will be determined as follows:

$$\theta_2(t) = \omega_2 t \qquad \text{..... (3.77)}$$

For given values of r_1, r_2, r_3, r_4, and θ_1 equation (3.76) can be used to determine the value of θ_4 that corresponds to any given value of θ_1. In that case, equation (3.76) will therefore describe all the possible phases of motion of the mechanism whose vector loop is illustrated in Figure 3.28.

In the special case where $\theta_1 = 0$, equation (3.76) reduces to the following:

$$2r_1r_2\cos\theta_2-2r_1r_4\cos\theta_4+r_1^2+r_2^2-r_3^2+r_4^2=2r_2r_4\cos(\theta_4-\theta_2) \quad \text{.....(3.78)}$$

Each of the terms in equation (3.78) can he divided by $2r_2r_4$ and the resulting equation can be re-arranged to obtain the following;

$$\frac{r_1}{r_4}\cos\theta_4-\frac{r_1}{r_2}\cos\theta_2+\frac{r_1^2+r_2^2-r_3^2+r_4^2}{2r_2r_4}=\cos(\theta_4-\theta_2) \text{..... (3.79)}$$

Equation (3.79) can be re-written as follows:

$$\left.\begin{aligned} K_1\cos\theta_2+K_2\cos\theta_4+K_3=\cos(\theta_4-\theta_2) \\ K_1=\frac{r_1}{r_2} \\ K_2=\frac{r_1}{r_4} \\ K_3=\frac{r_1^2+r_2^2-r_3^2+r_4^2}{2r_2r_4} \end{aligned}\right\} \text{.....} \quad (3.80)$$

Equation (3.80) is a well-known Freudcnstein's equation that has been commonly used in the synthesis of four bar mechanisms (Erdman and Sandor, 1991; Kimbrell, 1991; Norton, 1992; Shigley and Vicker, 1980).

3.5.2.2 Kinematical Analysis – The Second Loop Vector Closure

The second position Vector Loop to be treated is illustrated in Figure 3.29. The resulting closure equation for this second loop may be expressed as follows:

$$\bar{r}_4 + \bar{r}_5 - \bar{r}_6 - \bar{r}_7 = 0 \quad \ldots\ldots\ldots\ldots\ldots\ldots\ldots\ldots\ldots\ldots\ldots\ldots \quad (3.81)$$

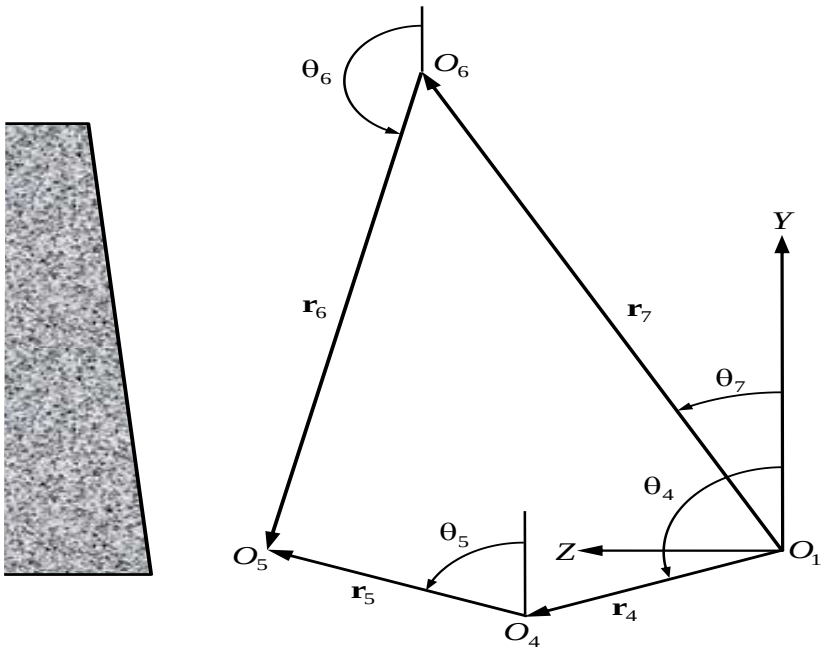

Figure 3.29: The Second Vector Loop Closure

Equation (3.81) can be re-written in complex exponential notation as follows:

$$r_4 e^{j\theta_4} + r_5 e^{j\theta_5} - r_6 e^{j\theta_6} - r_7 e^{j\theta_7} = 0 \quad \ldots\ldots\ldots\ldots\ldots\ldots\ldots\ldots \quad (3.82)$$

By using equations (3.68) and (3.69), equation (3.82) can be re-written as follows:

$$r_4(c_4 + js_4) + r_5(c_5 + js_5) - r_6(c_6 + js_6) - r_7(c_7 + js_7) = 0 \quad \ldots\ldots\ldots\ldots (3.83)$$

In equation (3.83), if the real terms and the imaginary terms are considered separately, the following two equations are readily obtained:

$$\left.\begin{aligned} r_4c_4 + r_5c_5 &= r_6c_6 + r_7c_7 \\ r_4s_4 + r_5s_5 &= r_6s_6 + r_7s_7 \end{aligned}\right\} \quad \text{……..……(3.84)}$$

By squaring each of the equations in (3.84), the following equations are obtained:

$$\left.\begin{aligned} r_4^2\ c_4^2 + 2r_4r_5c_4c_5 + r_5^2\ c_5^2 &= r_6^2\ c_6^2 + 2r_6r_7c_6c_7 + r_7^2\ c_7^2 \\ r_4^2\ s_4^2 + 2r_4r_5s_4s_5 + r_5^2\ s_5^2 &= r_6^2\ s_6^2 + 2r_6r_7s_6s_7 + r_7^2\ s_7^2 \end{aligned}\right\} \text{……..……(3.85)}$$

By adding corresponding terms of the in equations in (3.85), and noting that $c_i^2 + s_i^2 = 1$, the following is obtained:

$$r_4^2 + 2r_4r_2(c_4c_5 + s_4s_5) + r_5^2 = \ r_6^2 + 2r_6r_7(c_6c_7 + s_6s_7) + \ r_7^2 \quad \text{…..……(3.86)}$$

Now, the equations in (3.84) can be rearranged into the following:

$$\left.\begin{aligned} r_5c_5 &= r_6c_6 + \ r_7c_7 - r_4c_4 \\ r_5s_5 &= r_6s_6 + r_7s_7 - r_4s_4 \end{aligned}\right\} \quad \text{……..…… (3.87)}$$

By substituting the equations in (3.87) into equation (3.86), and using the identity in equation (3.75), the following is obtained:

$$\left.\begin{aligned} 2r_6r_7\cos(\theta_6 - \theta_7) + 2r_4r_7\cos(\theta_4 - \theta_7) + \ r_4^2 - \ r_5^2 + \ r_6^2 + \ r_7^2 \\ = 2r_4r_6\cos(\theta_4 - \theta_6) \end{aligned}\right\} \text{…….(3.88)}$$

In Figure 3.29, θ_7 is a fixed quantity. Given the motion of the crank O_2O_3, the corresponding motion of the rocker O_1O_4, and hence θ_4, can be determined by use of equation (3.76). Once θ_4 is known, the corresponding value of θ_6 can be determined by use of equation (3.88), so long as r_4, r_5, r_6, r_7 and θ_7 are known. Thus, for given values of the lengths of all the links in the mechanism, along with θ_1 and θ_7, equations (3.76) and (3.88) contain all the information that is necessary to determine all the phases of motion of the mechanism.

3.5.3 Angular Displacement of the Swing Jaw

The data in Table 3.27 shall be used to demonstrate application of the kinematical equations (Cao *et al.,* 2006).

Table 3.27: DB 6-4 (425 by 600) Double-Toggle Jaw Crusher Dimensions (Cao et al., 2006)

r_1 (mm)	r_2 (mm)	r_3 (mm)	r_4 (mm)	r_5 (mm)	r_6 (mm)	r_7 (mm)	θ_1 (decrees)	θ_7 (decrees)
662.5	28.5	609.5	503.5	503.5	1166	1537	45	40

The data in Table 3.27 can be used after manipulating algebraically the trigometrical terms in equation (3.76) to give:

$$\left.\begin{array}{c} f_1(\theta_2)\cos\theta_4 + f_2(\theta_2)\sin\theta_4 = f_3(\theta_2) \\ f_1(\theta_2) = 16.437 + \cos\theta_2 \\ f_2(\theta_2) = 16.437 + \sin\theta_2 \\ f_3(\theta_2) = 11.211 + 0.93\,(\cos\theta_2 + \sin\theta_2) \end{array}\right\} \quad \text{.....(3.89)}$$

In equation (3.89), for given values of θ_2, the functions $f_1(\theta_2), f_2(\theta_2)$ and $f_3(\theta_2)$ take on definite values, denoted by k_1, k_2andk_3, respectively, and the following can be obtained from equations in (3.89):

$$\left.\begin{array}{c} a\cos^2\theta_4 - b\ \cos\theta_4 + c = 0 \\ a = K_1^2 + K_2^2 \\ b = 2K_1K_3 \\ c = K_3^2 - K_2^2 \end{array}\right\} \quad \text{.....(3.90)}$$

For any given value of θ_2 equations in (3.90) yield two values of θ_4. Thus, mathematically, there are two possible configurations of the four-bar mechanism, whose vector loop is illustrated in Figure 3.28, for any possible value of θ_2. However, in practice only one of these configurations is applicable. By reviewing the configuration of the Double Toggle Jaw Crusher mechanism in Figure 3.27, it should be evident that the applicable

configuration of the mechanism should not have a value of θ_3 that is substantially greater than zero, or a value of θ_4 that is somewhat close to zero. Microsoft Excel Worksheet was used to calculate the non-trivial values of θ_4 that correspond to given values of θ_2, for one complete cycle of rotation of the crank. A sample of the results is given in Table 3.28 and the relationship between θ_2 and θ_4 is plotted in Figure 3.30.

Table 3.28: Values of θ_4 for Given Values of θ_2

θ_2 (degrees)	θ_4 (degrees)	θ_2(degrees)	θ_4 (degrees)
0	102.868	195	109.542
15	103.006	210	109.172
30	103.357	225	108.589
45	103.892	240	107.840
60	104.582	255	106.983
75	105.384	270	106.080
90	106.250	285	105.199
105	107.123	300	104.399
120	107.455	315	103.732
135	108.659	330	103.238
150	109.212	345	102.945
165	109.560	360	102.868
130	109.674		

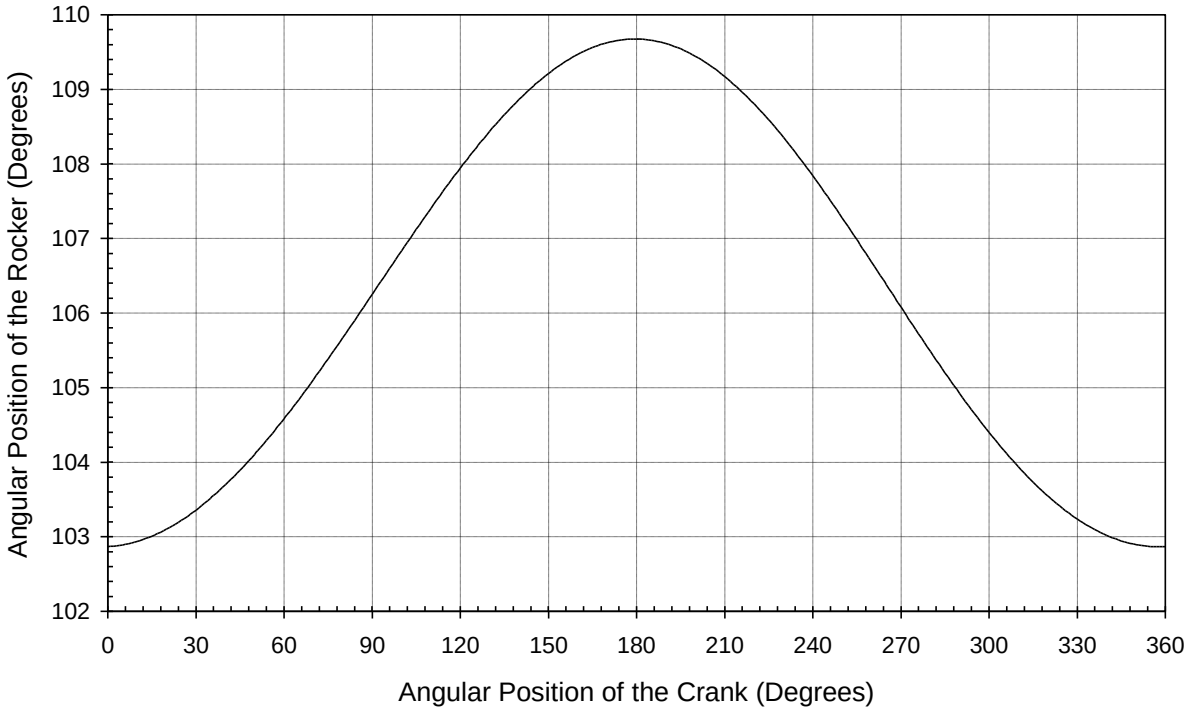

Figure 3.30: Variation of Back Toggle Angle θ_3 with Crank Angle θ_2

Similarly, by using the data in Table 3.28, after manipulating algebraically the trigonomical terms in equation (3.27) reduces to the following:

$$\left.\begin{gathered} g_1(\theta_4)\cos\theta_6 + g_2(\theta_4)\sin\theta_6 = g_3(\theta_4) \\ g_1(\theta_4) = 2.33845 - \cos\theta_4 \\ g_2(\theta_4) = 19622 - \sin\theta_4 \\ g_3(\theta_4) = 1.01\cos\theta_4 + 0.84731\sin\theta_4 - 3.169856 \end{gathered}\right\} \quad \ldots\ldots\ldots\ldots\ldots\ldots\ldots\ldots\ldots\ldots \quad (3.91)$$

In equations (3.91), for given values of θ_4, the functions $g_1(\theta_4), g_2(\theta_4)$and $g_3(\theta_4)$ take on definite values, denoted by K_1, K_2 and K_3 respectively and the following can be obtained from equations (3.91).

$$\left.\begin{gathered} A\cos^2\theta_6 - B\cos\theta_6 + C = 0 \\ A = K_1^2 + K_2^2 \\ B = 2K_1K_3 \\ C = K_3^2 - K_2^2 \end{gathered}\right\} \quad \ldots\ldots\ldots\ldots\ldots\ldots\ldots\ldots\ldots\ldots\ldots\ldots (3.92)$$

Mathematically, for any given value of θ_4, there will be two possible configurations of the part of the mechanism, whose vector loop is illustrated in Figure 3.29. However only one of these configurations is applicable, that is, the one giving values of θ_4 that are close to 90° and values of θ_6 that are close to 180º, which should be evident by reviewing the configuration of the Double Toggle Jaw Crusher Mechanism.

Microsoft Excel was used to calculate the non-trivial values of θ_6 that correspond to given values of θ_2, for one complete cycle of rotation of the crank. A sample of the results is given in Table 3.29 and the relationship between θ_2 and θ_6 is plotted in Figure 3.31.

Table 3.29: Values of θ_6 for Given Values of θ_2

θ_2 (degrees)	θ_6(degrees)	θ_2 (degrees)	θ_6 (degrees)
0	180.443	195	182.138
15	180.471	210	182.025
30	180.544	225	181.854
45	180.659	240	181.640
60	180.813	255	181.407
75	181.002	270	181.173
90	181.216	285	180.957
105	181.444	300	130.772
120	181.670	315	180.624
135	181.874	330	180519
150	181.037	345	130.458
165	182.143	360	180.443
180	182.178		

The minimum value of θ_6 is about 180.443° and it occurs at a crank angle of zero. The maximum value of θ_6 is about 182.178° and it occurs at a crank angle of about 180º. As can be discerned in Table 3.29 and Figure 3.31 the range of variation of the inclination of the swing jaw to the vertical is only about 1.735º. With the length of the swing jaw being 1166mm, this range of angular oscillation of the swing jaw translates to a throw of about 35mm at the lower end of the swing jaw. However, the throw diminishes proportionately as we move from the bottom of the swing jaw towards the pivot of the swing jaw, at which point it becomes zero. Cao *et al.,* (2006) found the minimum value of θ_6 to be 180° while the maximum value was found to be 182° hence the values calculated in this thesis are in agreement.

It should be noted that θ_6 is the angle of inclination of the line O_5O_6 from the positive Z direction. It is not the angle of inclination of the crushing surface of the swing jaw from the positive Z direction. Therefore, a value of θ_6 that is greater than 180° does not imply the set (outlet opening) of the crushing chamber will be larger than its gape (inlet opening).

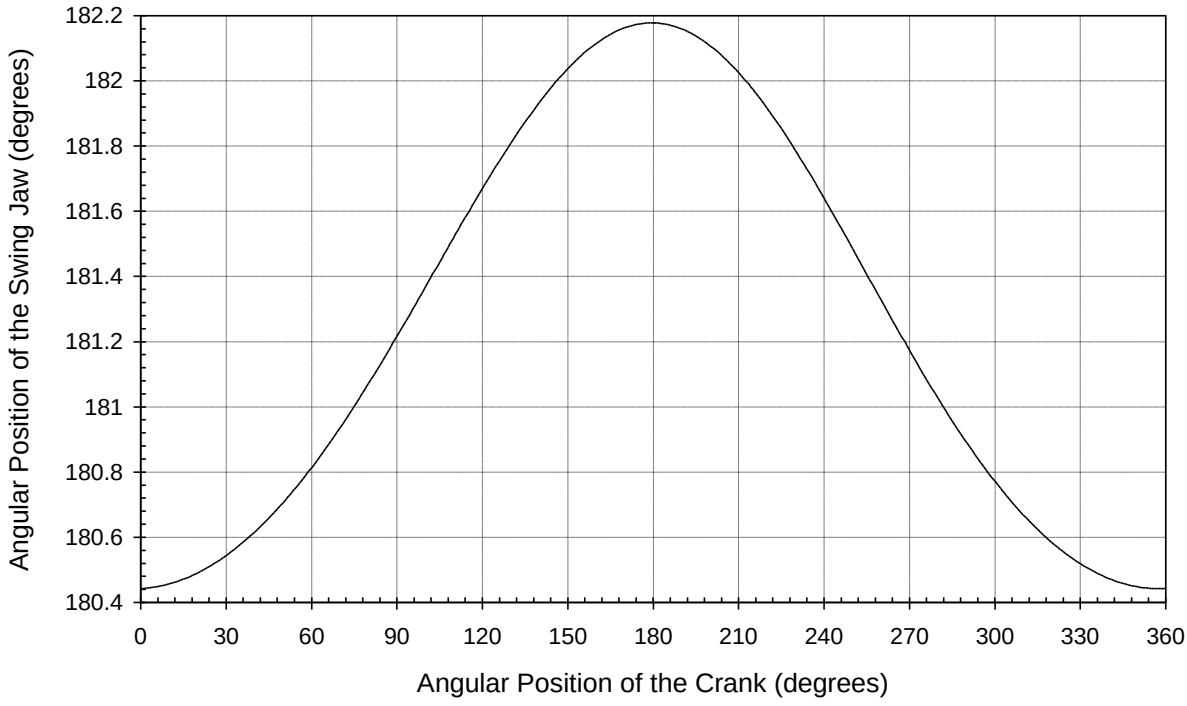

Figure 3. 31: Variation of Swing Jaw Angle θ_6 with Crank Angle θ_2

3.5.4 Angular displacement of the Pitman

Referring to the vector loop illustration in Figure 3.28, it should be evident that for given values of θ_2, the angular position of the coupler link O_3O_4 is determined as follows:

$$\theta_3 = \sin^{-1}\left[\frac{r_1 \sin\theta_1 + r_2 \sin\theta_2 - r_4 \sin\theta_4}{r_3}\right] \qquad \ldots\ldots\ldots\ldots\ldots\ldots\ldots \quad (3.93)$$

The data in Table 3.29 were used in a Microsoft Excel environment to calculate the values of θ_3 that correspond to given values of θ_2, for one complete cycle of rotation of the crank. A sample of the results is given in Table 3.30 and the relationship between θ_2 and θ_3 is plotted in Figure 3.32.

Table 3.30: Values of θ_3 for Given Values of θ_2

$\boldsymbol{\theta_2}$ (degrees)	$\boldsymbol{\theta_3}$ (degrees)	$\boldsymbol{\theta_2}$ (degrees)	$\boldsymbol{\theta_3}$ (degrees)
0	-2.106	195	-1.261
15	-1.386	210	-2.009
30	-0.674	225	-2.720
45	-0.015	240	-3.340
60	0.551	255	-3.821
75	0.990	270	-4.125
90	1.276	285	-4.230
105	1.392	300	-4.131
120	1.329	315	-3.838
135	1.088	330	-3.378
150	0.681	345	-2.786
165	0.131	360	-2.106
180	-0.531		

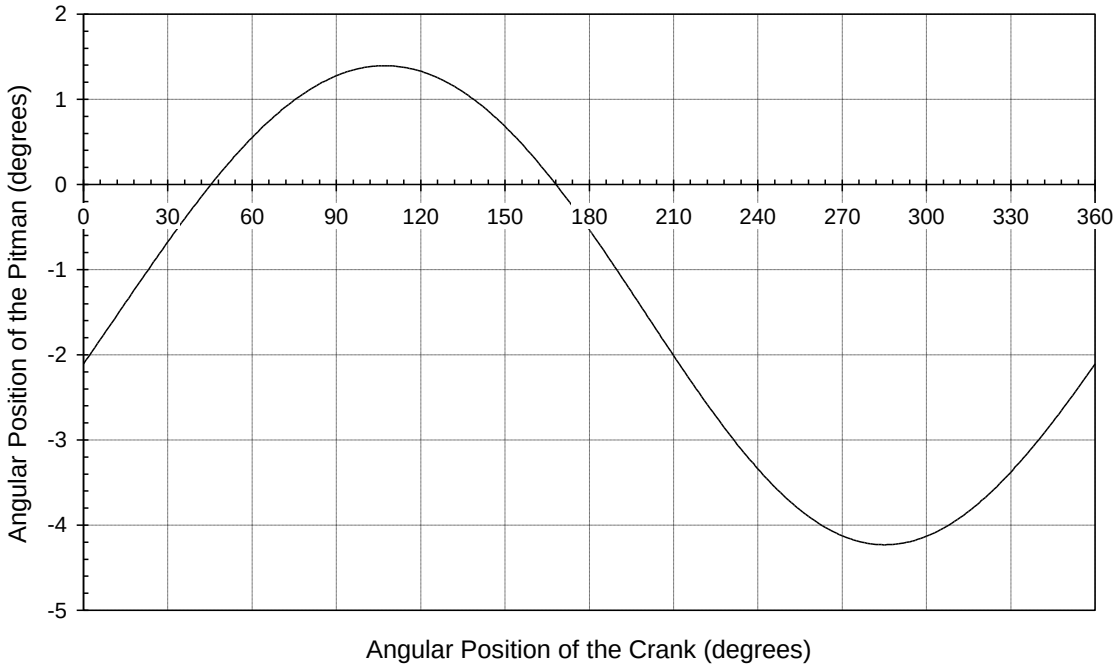

Figure 3.32: Variation of Swing Jaw Angle θ_3 with Crank Angle θ_3

In a completely symmetrical configuration of the pitman and the two-toggle links, one would expect the angular oscillation of the pitman to be symmetrically centred about the vertical (the zero degrees line). However, from the results obtained here, it is evident that the angular oscillation of the pitman is slightly skewed towards the negative angular direction and centred around an angle of about $-1{,}415°$. This result could be in part due to the fact that the lengths of the links in the mechanism were determined through measurements that could be subject to some small error. However, a deviation of less than $\pm 1.5^{\circ}$ is acceptable for our purposes.

3.5.5. Angular Displacement of the Front Toggle Link

Referring to the vector loop illustration in Figure 3.29, it should be evident that, for given values of θ_2 the angular position of the front toggle link O_4O_5 is determined as follows:

$$\theta_5 = \cos^{-1}\left[\frac{r_7\cos\theta_7 + r_6\cos\theta_6 - r_4\sin\theta_4}{r_5}\right] \quad \text{..... (3.94)}$$

The data in Table 3.27 were used in a Microsoft Excel was used to calculate the values of $\theta_5$that correspond to given values of θ_2 for one complete cycle of rotation of the crank. A sample of the results is given in Table 3.30 and the relationship between θ_2 and θ_5, is plotted in Figure 3.33.

Table 3.31: Values of θ_5 for Given Value of θ_2

θ_2 (degrees)	θ_5 (degrees)	θ_2 (degrees)	θ_5 (degrees)
0	75793	195	68.975
15	75.651	210	69.159
30	73.298	225	69.961
45	74.757	240	70.732
60	74.058	255	71.612
75	73.243	270	72.534
90	72.362	285	73.432
105	71.469	300	74.244
120	70.625	315	74.919
135	69.890	330	75.419
150	69.318	345	75.715
165	68.957	360	75.793
180	68.838		

The values of θ_4 and θ_5 obtained in the above calculations indicate that the actual configuration of the Double Toggle Jaw Crusher mechanism is really like the illustration in Figures. 3.27, 3.28 and 3.29, with θ_4 being an obtuse angle and θ_5 being an acute angle.

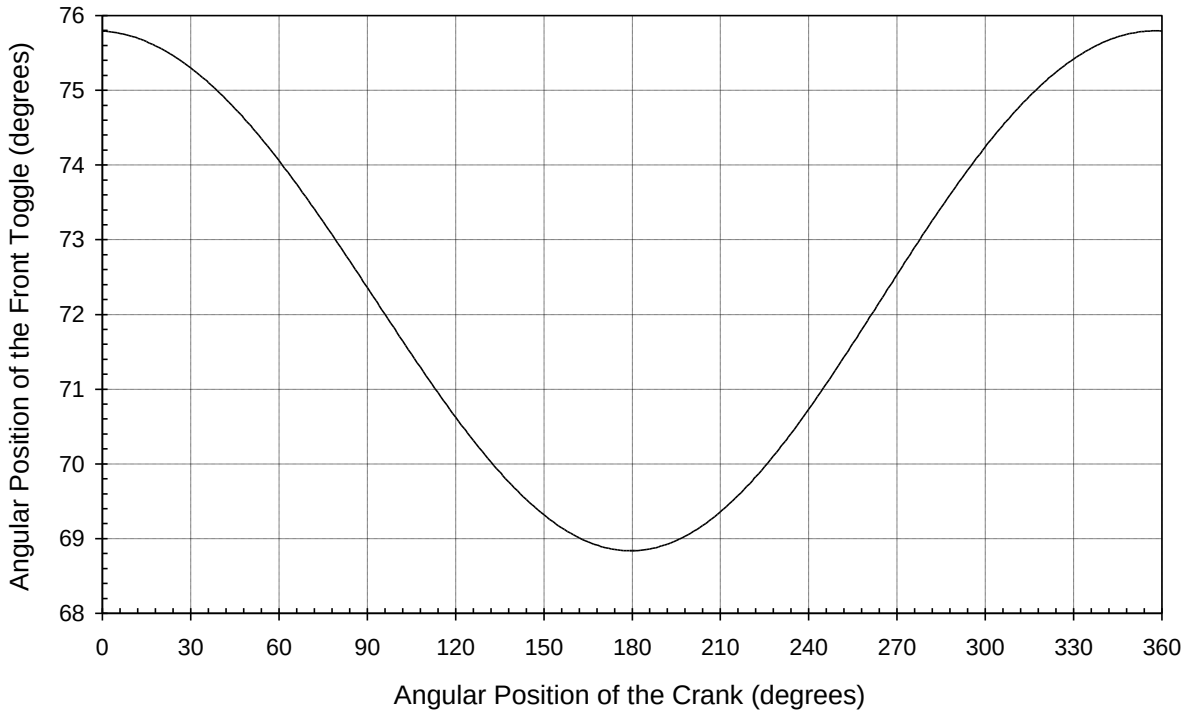

Figure 3.33: Variation of Front Toggle Angle θ_5 with Crank Angle θ_2

Thus, given the lengths of the links that comprise the mechanism, along with θ_1 and θ_7, equations 3.76, 3.93 and 3.94 contain all information that is necessary to determine all the phases of motion of the entire Double Toggle Jaw Crusher Mechanism.

3.5.6 Velocity Closure for the First Loop

The velocity closure equation for the first loop is obtained by differentiating equation (3.67) with respect to time, to obtain the following:

$$\left.\begin{aligned} jr_1 e^{j\theta_1}\frac{d\theta_1}{dt} + jr_2 e^{j\theta_2}\frac{d\theta_2}{dt} - jr_3 e^{j\theta_3}\frac{d\theta_3}{dt} - jr_4 e^{j\theta_4}\frac{d\theta_4}{dt} = 0 \\ r_1 e^{j\theta_1}\frac{d\theta_1}{dt} + r_2 e^{j\theta_2}\frac{d\theta_2}{dt} - r_3 e^{j\theta_3}\frac{d\theta_3}{dt} - r_4 e^{j\theta_4}\frac{d\theta_4}{dt} = 0 \end{aligned}\right\} \quad \text{.....(3.95)}$$

Here, again, we use the Euler identities given in equations (3.68) and the abbreviations in equations (3.69). Let us introduce the following notation:

$$\frac{d\theta_i}{dt} = \omega_i \text{.....(3.96)}$$

Now, equation (3.95) may be re-written as follows

$$r_1\omega_1(c_1 + js_1) + r_2\omega_2(c_2 + js_2) - r_3\omega_3(c_3 + js_3) - r_4\omega_4(c_4 + js_4) = 0 \quad \text{……..(3.97)}$$

In equation (3.97), while noting that to $\omega_1 = 0$, if the real terms and the imaginary terms are considered separately, the following two equations are readily obtained:

$$\left.\begin{aligned} \omega_2 r_2 c_2 &= \omega_3 r_3 c_3 + \omega_4 r_4 c_4 \\ \omega_2 r_2 s_2 &= \omega_3 r_3 s_3 + \omega_4 r_4 s_4 \end{aligned}\right\} \text{……..(3.98)}$$

Each of equations in (3.98) may be re-arranged to obtain the following:

$$\frac{\omega_2 r_2 c_2 - \omega_4 r_4 c_4}{r_3 c_3} = \frac{\omega_2 r_2 c_2 - \omega_4 r_4 s_4}{r_3 s_3} = \omega_3 \quad \text{…….. (3.99)}$$

Equation (3.99) can be manipulated algebraically to obtain the following:

$$\omega_2 r_2 c_2 s_3 - \omega_4 r_4 s_3 c_4 = \omega_2 r_2 c_3 s_2 - \omega_4 r_4 c_3 s_4 \text{……..……..} \quad (3.100)$$

Further, equation (3.100) can be rearranged into the following:

$$\omega_2 r_2 (s_3 c_2 - c_3 s_2) = \omega_4 r_4 (s_3 c_4 - c_3 s_4) \quad \text{……..…..} \quad (3.101)$$

Recall that (Carmichael and Smith, 1962):

$$\sin\theta_k \cos\theta_i - \cos\theta_k \sin\theta_i = sin(\theta_k - \theta_i) = -\sin(\theta_i - \theta_k) \text{ … … … … … … … …} \quad (3.102)$$

By using the identities in equation (3.102), the following can be obtained from equation (3.101):

$$G_1 = \frac{\omega_4}{\omega_2} = \frac{r_2 sin(\theta_3 - \theta_2)}{r_4 sin(\theta_3 - \theta_4)} = \frac{r_2 sin(\theta_2 - \theta_3)}{r_4 sin(\theta_4 - \theta_3)} \quad \text{… … … … … … … … … … … … … ….} \quad (3.103)$$

We have seen, earlier on, how to determine the values of θ_3 and θ_4, for any given value of θ_2. Thus, for given values of $r_1, r_2, r_3, r_4,$ and θ_1, equation (3.103) can be used to determine the value of G_1 that corresponds to any given value of θ_2. We have also seen that the motion of the crank O_2O_3 is the input motion and may be considered to be a rotation at uniform

angular velocity, ω_2, and that, at an instant in time, ***t***, after commencement of the motion, the value of θ_2, in radians, will be determined from equation (3.77).

Thus, for given values of $r_1, r_2, r_3, r_4, \theta_1$ and ω_2, equation (3.103) can be used to determine the value of ω_4, that corresponds to any given vaiue of θ_2.

The data in Table 3.32 were used in a Microsoft Excel was used to calculate the values of G_1 that correspond to given values of θ_2 for one complete cycle of rotation of the crank. A sample of the results is given in Table 3.32 and the relationship between, θ_2, and the angular velocity ratio, G_1 is plotted in Figure. 3.34.

Table 3.32: Values of the Angular Velocity Ratio G_1 for Given Values of θ_2

θ_2 (degrees)	G_1 (dimensionless)	θ_2(degrees)	G_1 (dimensionless)
0	0.00215	195	-001696
15	0.01649	210	-0.03218
30	0.02976	225	-0.04495
45	0.04124	240	-0.05425
60	0.05025	255	-0.05940
75	0.05618	270	-006016
90	0.05858	285	-0.05667
105	0.05716	300	-0.04942
120	0.05716	315	-00390S
135	0.04277	330	-0.02647
150	0.03046	345	-0.01244
165	0.01567	360	0.00215
180	0.00056		

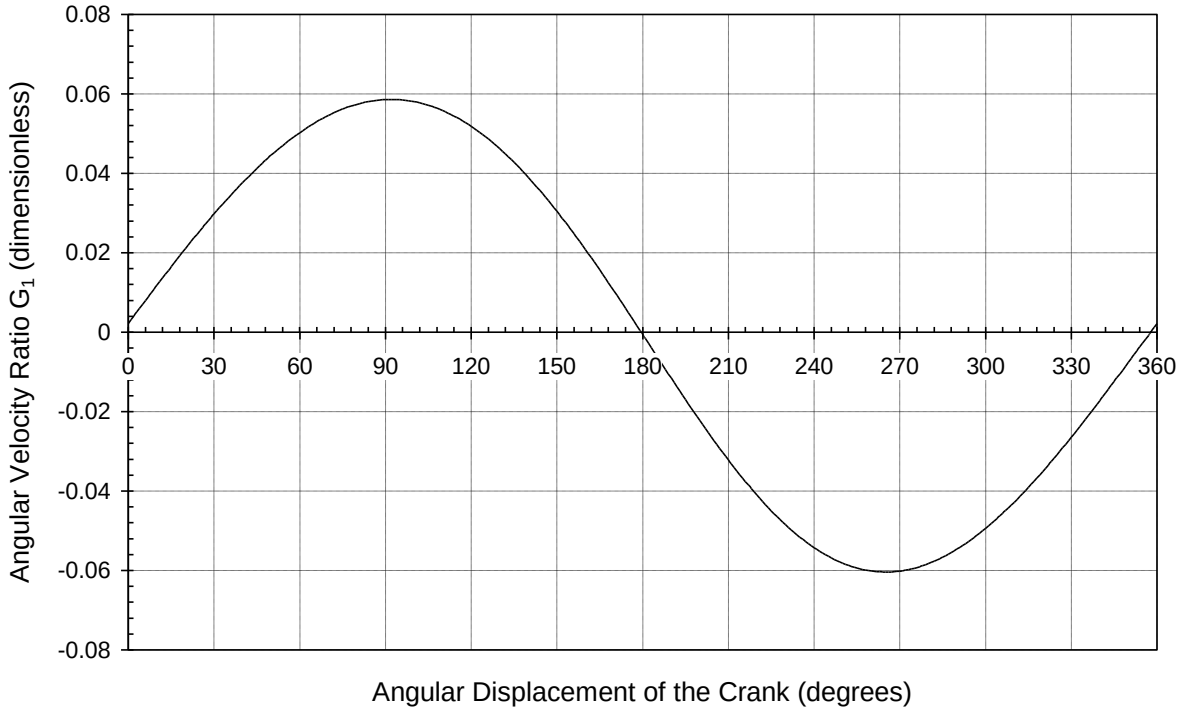

Figure 3.34: Variation of Angular Velocity Ratio G_1 with Crank Angle θ_2

The results in Table 3.32 and Figure 3.34 indicate that the mechanism whose vector loop is illustrated in Figure 3.29 has two toggle phases. The first toggle phase occurs when θ_2= 179.5º, to good approximation. The second toggle phase occurs when $\theta_2 = 357.8^{o}$, again to good approximation. At the toggle phases, the angular velocity ratios become zero. Beyond the toggle phases, the direction of the angular motion of the driven link, in this case link 4, reverses. The graph in Figure 3.34 is nearly, but not quite, symmetrical about the *x* axis. Moreover, the angular velocity ratio is nearly, but not quite, equal to zero, when $\theta_2 = 0^{\circ}$.

3.5.7 Velocity Closure for the Second Loop

The velocity closure equation for the Second Velocity Vector Loop is obtained by differentiating equation (3.82) with respect to time, to obtain the following;

$$r_4 e^{j\theta_4}\frac{d\theta_4}{dt} + r_5 e^{j\theta_5}\frac{d\theta_5}{dt} - r_6 e^{j\theta_6}\frac{d\theta_6}{dt} - r_7 e^{j\theta_7}\frac{d\theta_7}{dt} = \quad \text{.....(3.104)}$$

By using equations (3.68), (3.69) and (3.96), equation (3.104) can be re-written as follows:

$$r_4\omega_4(c_4 + js_4) + r_5\omega_5(c_5 + js_5) - r_6\omega_6(c_6 + js_6) - r_7\omega_7(c_7 + js_7) = 0 \ldots\ldots (3.105)$$

In equation (3.105), while noting that to $\omega_7 = 0$, if the real terms and the imaginary terms are considered separately, the following two equations are readily obtained

$$\left.\begin{array}{l} \omega_4 r_4 c_4 + \omega_5 r_5 c_5 = \omega_6 r_6 c_6 \\ \omega_4 r_4 s_4 + \omega_5 r_5 s_5 = \omega_6 r_6 s_6 \end{array}\right\} \ldots\ldots\ldots\ldots\ldots\ldots\ldots\ldots (3.106)$$

Each of equations in (3.106) may be re- arranged to obtain the following:

$$\frac{\omega_6 r_6 c_6 - \omega_4 r_4 c_4}{r_5 c_5} = \frac{\omega_6 r_6 s_6 - \omega_4 r_4 s_4}{r_5 s_5} = \omega_5 \quad \ldots\ldots\ldots\ldots\ldots\ldots\ldots\ldots (3.107)$$

Equation (3.107) can be manipulated algebraically to obtain the following:

$$\omega_6 r_6 s_6 c_6 - \omega_4 r_4 s_5 c_4 = \omega_6 r_6 c_5 s_6 - \omega_4 r_4 c_5 s_4 \ldots\ldots\ldots\ldots\ldots\ldots\ldots (3.108)$$

Further, equation (3.108) can be rearranged into the following:

$$\omega_6 r_6 (s_5 c_6 - c_5 s_6) = \omega_4 r_4 (s_5 c_4 - c_5 s_4) \ldots\ldots\ldots\ldots\ldots\ldots\ldots\ldots\ldots\ldots\ldots (3.109)$$

Recall that (Carmichael and Smith, 1962):

$$\sin\theta_k \cos\theta_i - \cos\theta_k \sin\theta_i = sin(\theta_k - \theta_i) = -\sin(\theta_i - \theta_k) \ldots\ldots\ldots\ldots\ldots\ldots\ldots (3.110)$$

By using the identities in equations (3.102), equation (3.109) can be re- written as follows:

$$G_2 = \frac{\omega_6}{\omega_4} = \frac{r_4 sin(\theta_5 - \theta_4)}{r_6 sin(\theta_5 - \theta_6)} = \frac{r_4 sin(\theta_4 - \theta_5)}{r_6 sin(\theta_6 - \theta_5)} \ldots\ldots\ldots\ldots\ldots\ldots\ldots\ldots\ldots\ldots\ldots (3.111)$$

We have already seen how to calculate the values of θ_4, θ_5 and θ_6 for given values of the lengths of all the links, the angles θ_1, θ_7 and the input angular displacement θ_2. Thus, equation (3.111) can be used to determine the value of G_2, that corresponds to any given value of θ_2. Microsoft Excel was used to calculate the values of G_2 that correspond to given values of θ_2, for one complete cycle of rotation of the crank. A sample of the results is

given in Table 3.33 and the relationship between θ_2 and the angular velocity ratio, $G_2$is plotted in Figure 3.35.

Table 3.33: Values of the Angular Velocity Ratio $G_2$for Given Values of θ_2

θ_2 (degrees)	G_2(dimensionless)	θ_2 (degrees)	G_2(dimensionless)
0	0.20315	195	0.30545
18	0.20527	210	0.29962
30	0.21053	225	0.29052
45	0.21861	240	0.27889
60	0.22904	255	0.26566
75	0.24122	270	0.25183
90	0.25442	285	0.23841
105	0.26718	300	0.22627
120	0.28050	315	0.21619
135	0.29160	330	0.20873
150	0.30025	345	0.20432
165	0.30571	360	0.20315
180	0.30753		

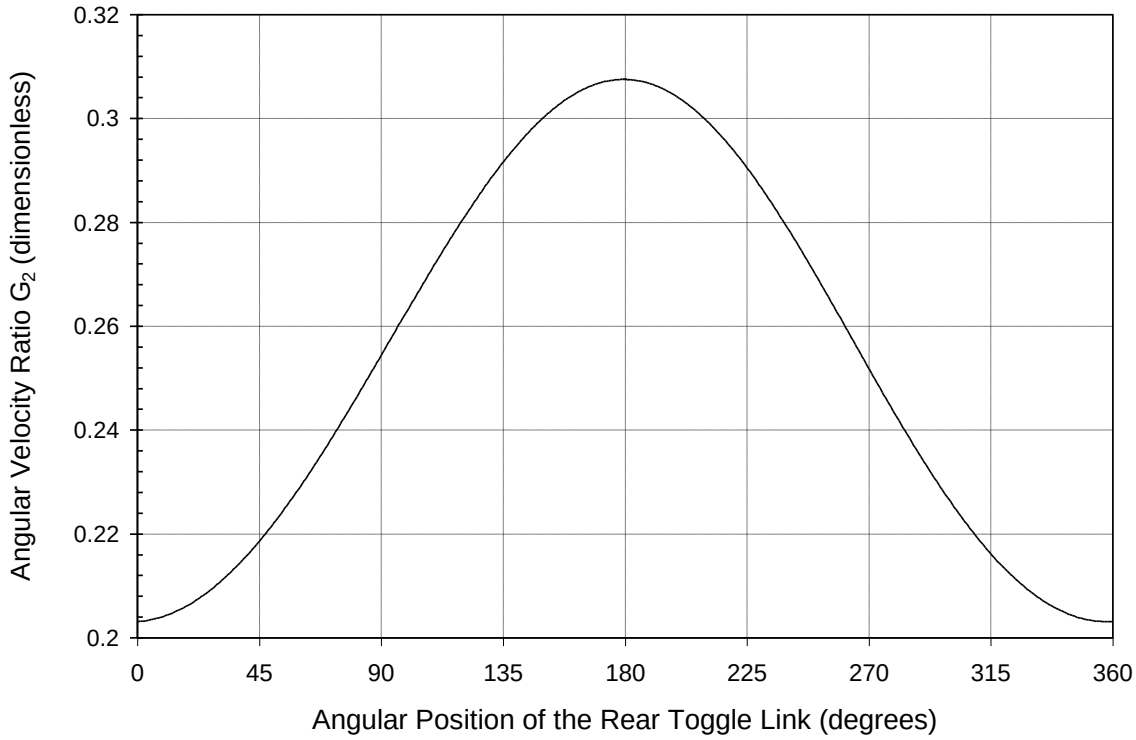

Figure 3.35: Variation of Angular Velocity Ratio G_2 with Crank Angle θ_2

Equations (3.103) and (3.111) can now be used to obtain the following:

$$G = \frac{\omega_6}{\omega_2} = G_1 G_2 = \frac{r_2 sin(\theta_2 - \theta_3)}{r_6 sin(\theta_4 - \theta_3)} \frac{sin(\theta_4 - \theta_5)}{sin(\theta_6 - \theta_5)} \quad \text{.....(3.112)}$$

For given values of $r_1, r_2, r_3, r_4, r_5, r_6, \theta_1$ and θ_7 equation (3.112) can be used to determine the value of *G* that corresponds to any given value of θ_2. This was done using Microsoft Excel and a sample of the results that were obtained is given in Table 3.34. The relationship between θ_2, and the angular velocity ratio, *G*, is plotted in Figure 3.36.

Note that positive values of the angular velocity of the swing jaw correspond to increasing values of the angle denoted by θ_6, in Figure 3.27. These values occur during the idle stroke, while the swing jaw is receding from the fixed jaw and letting the crushed material to fall through the crushing chamber. On the other hand, negative values of the angular velocity of the swing jaw correspond to reducing values of the angle θ_6 . These values occur during the active crushing stroke, when the swing jaw is approaching the fixed jaw and compressing the material being crushed. The two instances when the angular velocity of

the swing jaw becomes zero are the toggle phases of the mechanism. These phases occur when the angle θ_2 is approximately 0 degrees and when θ_2 is approximately 180 degrees.

Table 3.34: Values of the Angular Velocity Ratio G for Given Values of θ_2

$\boldsymbol{\theta_2}$ (degrees)	G (Dimensionless)	$\boldsymbol{\theta_2}$ (degrees)	*G* (Dimensionless)
0	0.00044	195	-0.00518
15	0.0033S	210	-0.00964
30	0.00627	225	-0.01306
45	0.00902	240	-0.01513
60	0.01151	255	-0.01578
75	0.01355	270	-0.01515
90	0.01490	285	-0.01351
105	0.01531	300	-0.01118
120	0.01454	315	-0.00845
135	0.01247	330	-0.00553
180	0.00914	345	-0.00254
165	0.00479	360	000044
180	-0.00017		

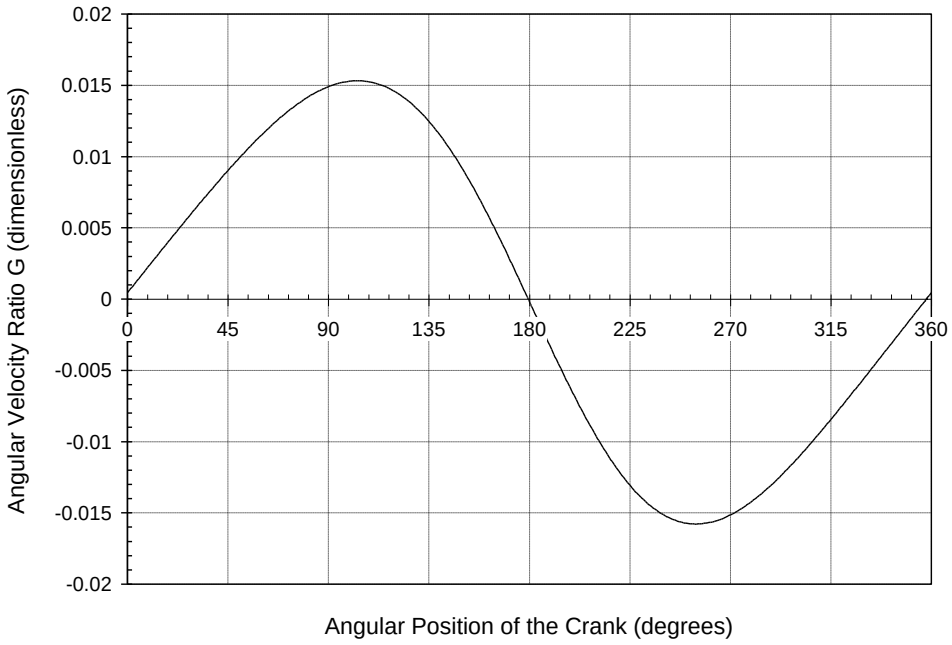

Figure 3.36: Variation of Angular Velocity Ratio G with Crank Angle θ_2

3.5.8 The Force Transmission Characteristics of the Double Toggle Jaw Crusher

The forces acting in the links of the Double Toggle Jaw Crusher mechanism are illustrated in Figure 3.37.

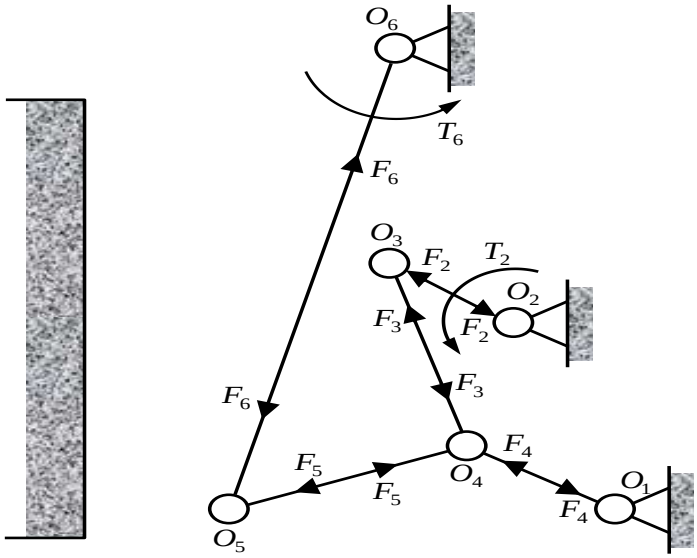

Figure 3.37: Model for Static Force Analysis

In performing the static force analysis, it shall be assumed that the masses of the links, as well as friction forces are negligible. In Figure 3.37, T_2 is the driving torque, applied about the crank axis O_2 to drive the crank and the entire crusher mechanism. T_6 is the torque, acting about the swing jaw axis O_6, due to the resistance of the feed material against being crushed, and its value shall be assumed to be predetermined. F_2, F_3, F_4, F_5 and F_6 are the forces in links 2, 3, 4, 5 and 6 respectively and they are all assumed to be compressive.

3.5.8.1 Static Force Analysis

The free-body diagrams of the toggle mechanism consisting of links 1, 3, 4 and 5 in a partly assembled configuration as can be seen in Figure 3.38.

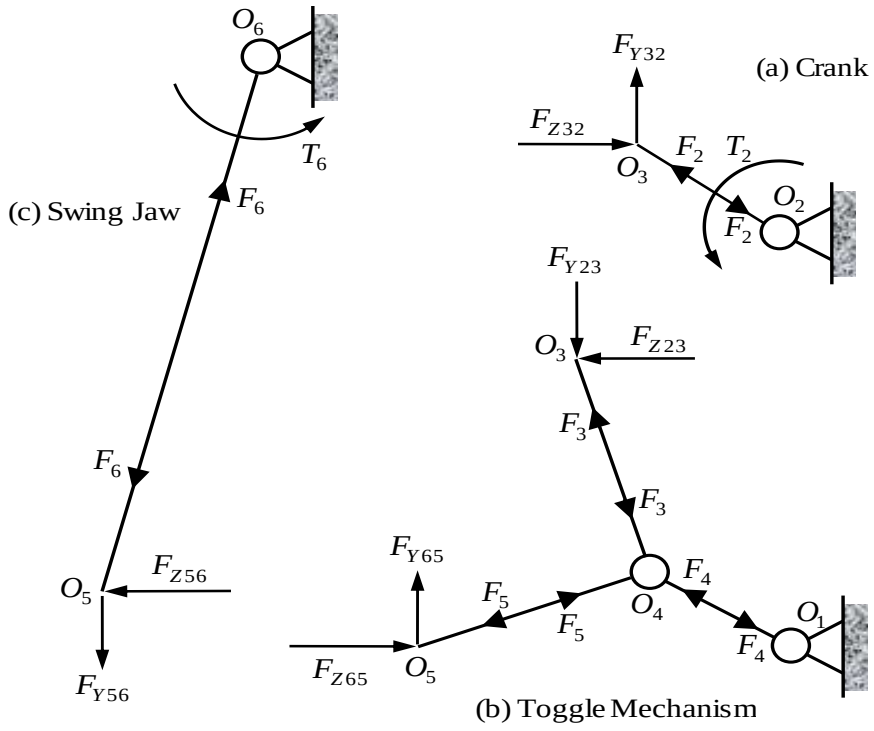

Figure 3.38: Free Body Diagrams of the Moving Links

Let us start by considering the crank. The equilibrium of moments on the crank, about the joint O_1 as shown in Figure 3.38 leads to the following result:

$$\left.\begin{aligned} 0 &= -F_{Y32} r_2 \sin\theta_2 - F_{Z32} r_2 \cos\theta_2 + T_2 \\ T_2 &= \left[F_{Z32}\cos\theta_2 + F_{Y32}\sin\theta_2\right] r_2 \end{aligned}\right\} \quad \text{.....(3.113)}$$

In equation (3.113), r_2 is the length of the crank.

Next, consider the assemblage that is labelled the toggle mechanism. The equilibrium of forces at joint O_3 requires that the following equations be satisfied:

$$\left.\begin{aligned} -F_{Y23} + F_3\cos\theta_3 &= 0 \\ F_{Y23} &= F_3\cos\theta_3 \\ F_{Y32} &= -F_{Y23} = -F_3\cos\theta_3 \end{aligned}\right\} \quad \text{.....(3.114)}$$

$$\left.\begin{aligned} F_{Z23} + F_3\sin\theta_3 &= 0 \\ F_{Z23} &= -F_3\sin\theta_3 \\ F_{Z32} &= -F_{Z23} = F_3\sin\theta_3 \end{aligned}\right\} \quad \text{.....(3.115)}$$

From equations (3.113), (3.114) and (3.115), it follows that:

$$\left.\begin{aligned} T_2 &= \left(F_3\sin\theta_3\cos\theta_2 - F_3\cos\theta_3\sin\theta_2\right) r_2 \\ &= F_3 r_2 \sin\left(\theta_3 - \theta_2\right) \\ &= -F_3 r_2 \sin\left(\theta_2 - \theta_3\right) \end{aligned}\right\} \quad \text{.....(3.116)}$$

The statement of equation (3.116) is illustrated in Figure 3.39.

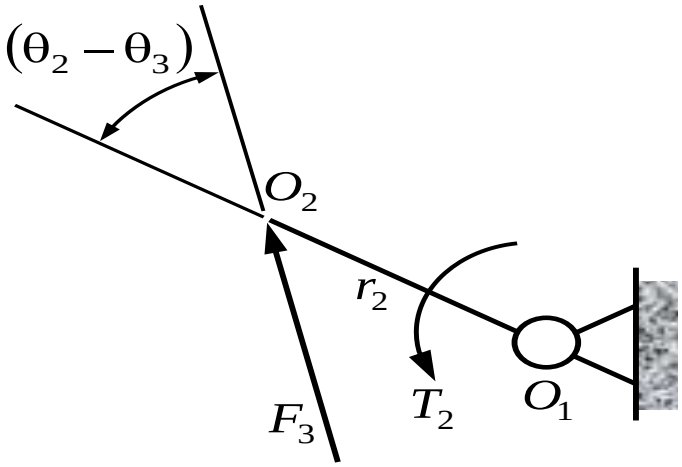

Figure 3.39: Balance of Movements on the Crank

Similarly, equilibrium of forces at joint, O_5, as shown in Figure 3.38 leads to the following:

$$\left.\begin{aligned} F_{Y65} + F_5\cos\theta_5 = 0 \\ F_{Y65} = -F_5\cos\theta_5 \\ F_{Y56} = -F_{Y65} = F_5\cos\theta_5 \end{aligned}\right\} \text{.....(3.117)}$$

$$\left.\begin{aligned} -F_{Z65} + F_5\sin\theta_5 = 0 \\ F_{Z65} = F_5\sin\theta_5 \\ F_{Z56} = -F_{Z65} = -F_5\sin\theta_5 \end{aligned}\right\} \text{.....(3.118)}$$

In Figure 3.38, equilibrium of the forces acting at joint O_4 requires that the vectors of the forces F_3, F_4 and F_5 form a closed triangle since these three forces are concurrent at O_4. The closed triangle is shown in Figure 3.40.

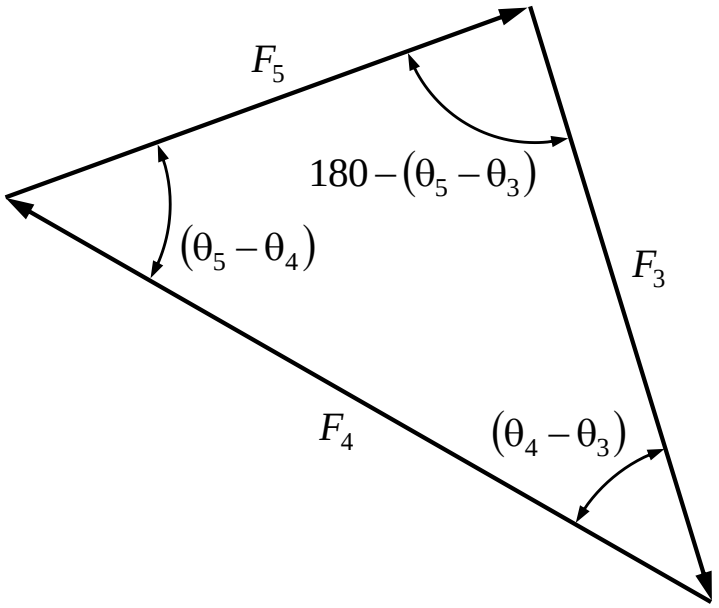

Figure 3.40: The Polygon of Forces in the Toggle mechanism

Applying the Sine rule to the triangle in Figure 3.40 leads to the following result:

$$\frac{F_3}{\sin(\theta_5-\theta_4)}=\frac{F_4}{\sin(\theta_5-\theta_3)}=\frac{F_5}{\sin(\theta_4-\theta_3)} \quad \text{.....(3.119)}$$

Hence:

$$F_5=\frac{F_3\sin(\theta_4-\theta_3)}{\sin(\theta_5-\theta_4)} \quad \text{.....(3.120)}$$

Now let us consider the swing jaw. The equilibrium of moments on the swing jaw, about the joint O_6, in Figure 3.38 leads to the following result:

$$\left.\begin{aligned} 0&=F_{Y56}r_6\sin(180-\theta_6)-F_{Z56}r_6\sin(\theta_6-90)+T_6\\ T_6&=\left[-F_{Z56}\cos\theta_6-F_{Y56}\sin\theta_6\right]r_6 \end{aligned}\right\} \quad \text{.....(3.121)}$$

From equations (3.117), (3.118) and (3.121), it follows that:

$$T_6 = -F_5 r_6 \sin(\theta_6 - \theta_5) \quad \text{(3.122)}$$

The statement of equation (3.122) is illustrated in Figure 3.41. In this figure, the angle $(\theta_6 - \theta_5)$ is known as the transmission angle and it should preferably be as close to 90^0 as possible.

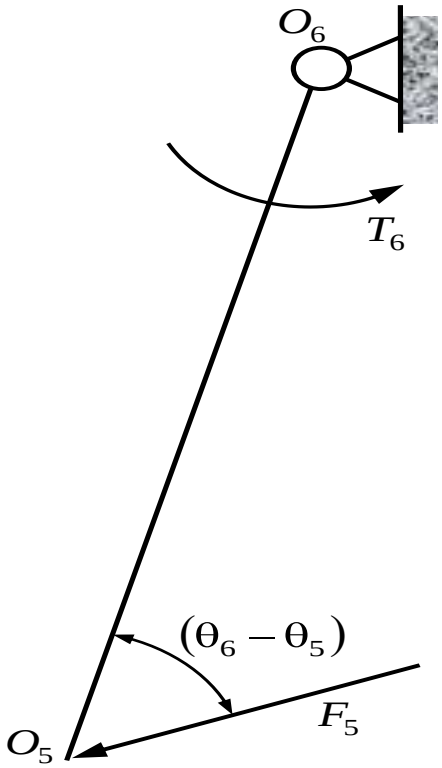

Figure 3.41: Balance of Moments on the Swing Jaw

It should be evident from Figures. 3.38 and 3.41 that:

$$F_6 \cos(\theta_6 - \theta_5) = -F_6 \quad \text{(3.123)}$$

From equations (3.119) and (3.122), it follows that:

$$T_6 = -\frac{F_3 r_6 \sin(\theta_4 - \theta_3)\sin(\theta_6 - \theta_5)}{\sin(\theta_5 - \theta_4)} \quad \text{.....(3.124)}$$

A relationship between T_6 and T_2 can be obtained from equations (3.116) and (3.124), as follows:

$$\frac{T_6 r_2}{T_2 r_6} = \frac{\sin(\theta_4 - \theta_3)\sin(\theta_6 - \theta_5)}{\sin(\theta_2 - \theta_3)\sin(\theta_5 - \theta_4)} \quad \text{.....(3.125)}$$

Equation (3.125) is in dimensionless form. For a given crusher mechanism, values of θ_2, θ_3 θ_4, θ_5 and θ_6 can be determined from purely kinematical considerations and then the value of the right-hand side of equation (3.125) can be determined.

Let us use the following values for the crusher mechanism, which were also used in the analysis of the Double Toggle Jaw Crusher kinematics Cao *et al.*, 2006) as shown in Table 3.35.

Table 3.35: DB 6-4 (425 by 600) Double-Toggle Jaw Crusher Dimensions

r_1 (mm)	r_2 (mm)	r_3 (mm)	r_4, (mm)	r_5 (mm)	r_6 (mm)	r_7 (mm)	θ_1 (degrees)	θ_7 (degrees)
662.5	28.5	609.5	503.5	503.5	1166	1537	45	40

With the data given in Table 3.35, given the values of θ_2, the corresponding values of θ_3 θ_4, θ_5 and θ_6 were computed and then used in equation (3.125) to determine the corresponding force transmission ratios. The results are plotted in Figure 3.42.

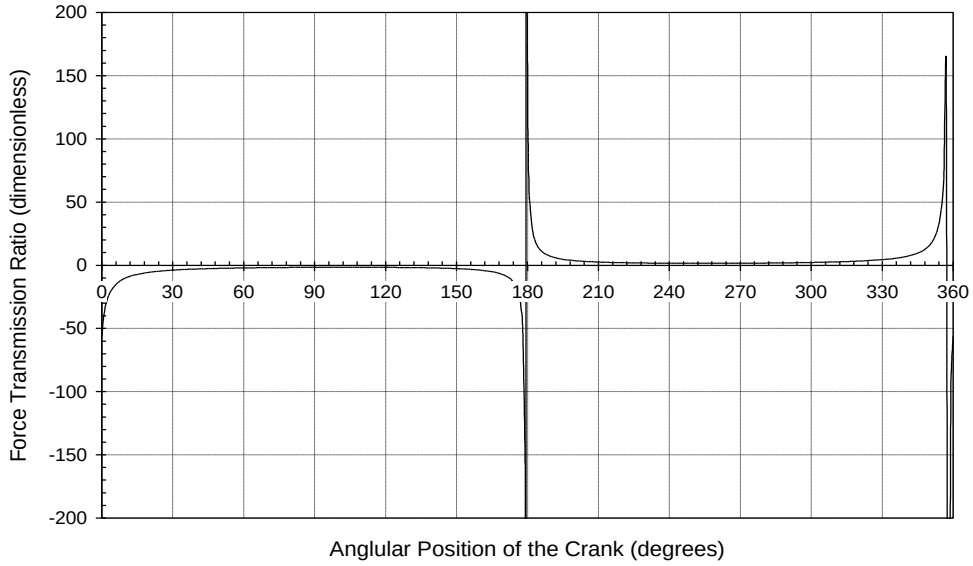

Figure 3.42: Variation of Normalized Torque Ratio with crank Angle θ_2

The first spike in Figure 3.42 indicates the great amplification of the crushing force that occurs at the toggle position, which corresponds to a crank angle of about 180^0. Theoretically, the crushing force amplification should be infinite at this toggle position. The second spike in Figure 3.42 occurs at a crank angle of about 360^0. This spike corresponds to the second toggle position of the mechanism. However, as the crank rotates from $\theta_2 = 0^0$ to $\theta_2 = 180^0$, the crusher would be on the idle stroke with the swing jaw being retracted and no work being done in crushing the feed material. Cao *et al.,* (2006) established that the amplification force occurs at the toggle position which occurs to a crank angle of 180° and 360° respectively. This thesis establishes the same values using the Vector Loop Closure method.

3.5.8.2 The Mechanical Advantage of the Crusher

If we assume that power is transmitted from the input end to the output end of the crusher, with 100 percent mechanical efficiency, then we may write the following:

$$H = T_2\omega_2 = -T_6\omega_6 \quad \ldots\ldots\ldots\ldots\ldots\ldots\ldots\ldots\ldots\ldots \quad (3.126)$$

In equation (3.126).

- H is the input power, which is also equal to the transmitted power, in watts;
- T_2 is the input torque, in Newton-metres.
- ω_2 is The angular velocity of the input crank, in radians per second?
- T_6 is the load torque, which occurs due to the resistance of the charge material against being crushed. It is measured in Newton-metres,
- ω_6 is the angular velocity of the swing jaw, in radians per second.

The negative sign in equation (3.126) arises because the load torque is directed opposite to the angular velocity, ω_6. The load torque T_6 is positive when the angle θ_2 is decreasing, during the active crushing stroke. Conversely, the load torque is negative when the angle θ_6 is increasing, during the idle stroke. From equations (3.112 and 3.126), the following is readily obtained:

$$\frac{T_6}{T_2} = -\frac{\omega_2}{\omega_6} = -\frac{1}{G} = \frac{r_6 sin(\theta_4 - \theta_3)}{r_2 sin(\theta_2 - \theta_3)} \frac{sin(\theta_6 - \theta_5)}{sin(\theta_4 - \theta_5)} \quad \text{.....(3.127)}$$

Thus, a mechanical advantage of the crusher may be defined as follows (Oduori *et al.*, 2016):

$$MA = \frac{T_6 r_2}{T_2 r_6} = \frac{sin(\theta_4 - \theta_3)}{sin(\theta_2 - \theta_3)} \frac{sin(\theta_6 - \theta_5)}{sin(\theta_4 - \theta_5)} \quad \text{.....(3.128)}$$

Microsoft Excel is used to calculate values of mechanical advantage as defined in equation (3.128) for given values of the crank angle, θ_2 as it rotates through one complete cycle of motion. Sample values of Mechanical Advantage (MA) are given in Table 3.36and a plot of the mechanical advantage of the crusher, against θ_2, is given m Figure 3.43.

Table 3.36: Values of the Mechanical Advantage, MA, for Given Values of θ_2

θ_2, (degrees)	*MA* (dimensionless)	θ_2, (degrees)	*MA* (dimensionless)
0	-93,533.5	195	7,899.6
15	-12,089.7	210	4.243.6
10	-6,259.0	225	3,132.7
45	-4,537.6	240	2,704.1
60	-3,555.0	255	2,592.6
75	-3,019.1	270	2,700.4
90	-2,745.1	285	3,028.0
105	-2,672.8	300	3,658.9
120	-2,814.2	315	4,842.7
135	-3,280.2	330	7,404.8
180	-4,473.1	345	18,094.5
165	-8,541.36	360	-93,533.5
180	283,019.3		

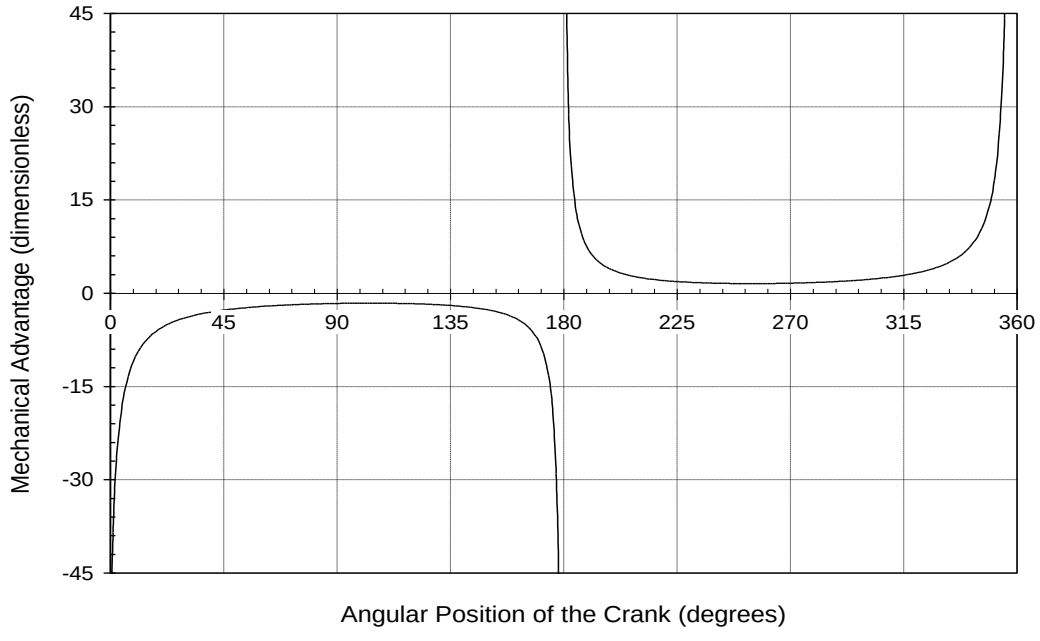

Figure 3.43: Variation of Mechanical Advantage MA with Crank Angle θ_2

It is evident in Figure 3.43 that as the input crank rotates from *0* degrees to about 180 degrees, the swing jaw is moving away from the fixed jaw This is why the mechanical advantage is negative. At a crank angle of about 180 degrees, there occurs a sudden spike in the value of the mechanical advantage, accompanied by a reversal in sign from negative to positive. This is evidence of a toggle phase, which coincide with the commencement of the active crushing stroke Another toggle phase occurs at the end of the active crushing stroke, which coincides with the commencement of the succeeding idle stroke. Between the toggle phases, during the active crushing stroke, the mechanical advantage initially decreases rapidly, remains at a low value for most of the stroke and then increases rapidly towards the end of the stroke. In this respect, the idle stroke is a mirror image of the active crushing stroke.

3.5.9. Acceleration Closure for the First Loop

The acceleration closure equation for the first Vector Loop Closure is obtained by differentiating equation (3.95) with respect to time. But before doing so, note that in equation (3.95):

$$r_1 e^{j\theta_1} \frac{d\theta_1}{dt} = 0 \qquad \text{.....(3.129)}$$

In Figure 3.27, since the input motion is a rotation of the crank O_2O_3 at uniform angular velocity, it follows that:

$$\frac{d^2\theta_2}{dt^2} = \frac{d\omega_2}{dt} = 0 \qquad \text{.....(3.130)}$$

Thus, equation (3.130) can be differentiated, with respect to time, to obtain the following:

$$\left.\begin{aligned} r_2 e^{j\theta_2}\left[j\left(\frac{d\theta_2}{dt}\right)^2 + \frac{d^2\theta_2}{dt^2}\right] - r_3 e^{j\theta_3}\left[j\left(\frac{d\theta_3}{dt}\right)^2 + \frac{d^2\theta_3}{dt^2}\right] \\ -r_4 e^{j\theta_4}\left[j\left(\frac{d\theta_4}{dt}\right)^2 + \frac{d^2\theta_4}{dt^2}\right] = 0 \end{aligned}\right\} \text{..... (3.131)}$$

From equations (3.96), (3.130) and (3.131), it follows that;

$$r_2 e^{j\theta_2}[j\omega_2^2] - r_3 e^{j\theta_3}\left[j\omega_3^2 + \frac{d\omega_3}{dt}\right] - r_4 e^{j\theta_4}\left[j\omega_4^2 + \frac{d\omega_4}{dt}\right] = 0 \ldots\ldots\ldots\ldots\ldots (3.132)$$

Here, we introduce the following notation:

$$\frac{d\omega_i}{dt} = \alpha_i \qquad \ldots\ldots\ldots\ldots\ldots\ldots\ldots\ldots\ldots\ldots (3.133)$$

Thus, equation (3.131) can be re-written as follows

$$jr_2\omega_2^2 e^{j\theta_2} - jr_3\omega_3^2 e^{j\theta_3} - jr_3\alpha_3 e^{j\theta_3} - jr_4\omega_4^2 e^{j\theta_4} - jr_4\alpha_4 e^{j\theta_4} = 0 \ldots\ldots\ldots\ldots\ldots (3.134)$$

Here, again, we use the Euler identities given in equations (3.68) and the abbreviations in equations (3.69). Thus

$$\left.\begin{aligned} r_2\omega_2^2(jc_2 - s_2) - r_3\omega_3^2(jc_3 - s_3) - r_3\alpha_3(c_3 + js_3) \\ -r_4\omega_4^2(jc_4 - s_4) - r_4\alpha_4(c_4 + js_4) = 0 \end{aligned}\right\} \quad \ldots\ldots\ldots\ldots\ldots\ldots\ldots (3.135)$$

In equation (3.135), if the real terms and the imaginary terms are considered separately, the following two equations are readily obtained:

$$\left.\begin{aligned} r_2\omega_2^2 s_2 = r_3\omega_3^2 s_3 - r_3\alpha_3 c_3 + r_4\omega_4^2 s_4 - r_4\alpha_4 c_4 \\ r_2\omega_2^2 c_2 = r_3\omega_3^2 c_3 + r_3\alpha_3 s_3 + r_4\omega_4^2 c_4 + r_4\alpha_4 s_4 \end{aligned}\right\} \quad \ldots\ldots\ldots\ldots\ldots\ldots\ldots (3.136)$$

The expressions of ω_3 given in equation (3.99), can be substituted into each of the equations in (3.136) to obtain the following:

$$\left.\begin{aligned} r_2\omega_2^2 s_2 = \frac{(\omega_2 r_2 s_2 - \omega_4 r_4 s_4)^2}{r_3 s_3} - r_3\alpha_3 c_3 + r_4\omega_4^2 s_4 - r_4\alpha_4 c_4 \\ r_2\omega_2^2 c_2 \frac{(\omega_2 r_2 c_2 - \omega_4 r_4 c_4)^2}{r_3 c_3} + r_3\alpha_3 s_3 + r_4\omega_4^2 c_4 + r_4\alpha_4 s_4 \end{aligned}\right\} \ldots\ldots\ldots\ldots\ldots\ldots (3.137)$$

Each of equations (3.137) may be manipulated algebraically and re-arranged to obtain the following:

$$\left.\begin{aligned} r_3^2 c_3 s_3 \alpha_3 &= +(\omega_2 r_2 s_2 - \omega_4 r_4 s_4)^2 - r_3 s_3 [r_2 \omega_2^2 s_2 - r_4 \omega_4^2 s_4 + r_4 \alpha_4 c_4] \\ &= -(\omega_2 r_2 s_2 - \omega_4 r_4 c_4)^2 + r_3 c_3 [r_2 \omega_2^2 c_2 - r_4 \omega_4^2 c_4 + r_4 \alpha_4 s_4] \end{aligned}\right\} \ldots\ldots \quad (3.138)$$

The right-hand sides of equations (3.138) can be expanded and re-arranged to obtain the following.

$$\left.\begin{aligned} r_3^2 c_3 s_3 \alpha_3 = {} & + r_2^2 s_2^2 \omega_2^2 - 2 r_2 r_4 s_2 s_4 \omega_2 \omega_4 + r_4^2 s_4^2 \omega_4^2 - r_2 r_3 s_2 s_4 \omega_2^2 \\ & + r_3 r_4 s_3 s_4 \omega_4^2 - r_3 r_4 s_3 c_4 \alpha_4 \\ = {} & - r_2^2 c_2^2 \omega_2^2 + 2 r_2 r_4 c_2 c_4 \omega_2 \omega_4 - r_4^2 c_4^2 \omega_4^2 + r_2 r_3 c_2 c_4 \omega_2^2 \\ & - r_3 r_4 c_3 c_4 \omega_4^2 - r_3 r_4 c_3 s_4 \alpha_4 \end{aligned}\right\} \ldots\ldots\ldots\ldots \quad (3.139)$$

Now, by using well known trigonometric identities, equations (3.139) can be reduced to the following:

$$\left.\begin{aligned} & r_2^2 \omega_2^2 - 2 r_2 r_4 \omega_2 \omega_4 \cos(\theta_2 - \theta_4) + r_4^2 \omega_4^2 - r_2 r_3 \omega_2^2 \cos(\theta_2 - \theta_3) \\ & + r_3 r_4 \omega_4^2 \cos(\theta_3 - \theta_4) \\ & = r_3 r_4 \alpha_4 \sin(\theta_3 - \theta_4) \end{aligned}\right\} \quad \ldots\ldots\ldots (3.140)$$

Thus, the angular acceleration of the rear toggle link $O_1 O_4$ can he expressed as follows:

$$\left.\begin{aligned} \alpha_4 = {} & \left[\frac{r_2^2 \omega_2^2 + r_4^2 \omega_4^2}{r_3 r_4 \sin(\theta_3 - \theta_4)}\right] - \left[\frac{2 r_2 \omega_2 \omega_4 \cos(\theta_2 - \theta_4)}{r_3 \sin(\theta_3 - \theta_4)}\right] \\ & - \left[\frac{r_2 \omega_2^2 \cos(\theta_2 - \theta_3)}{r_4 \sin(\theta_3 - \theta_4)}\right] + \left[\frac{\omega_4^2 \cos(\theta_3 - \theta_4)}{\sin(\theta_3 - \theta_4)}\right] \end{aligned}\right\} \ldots\ldots\ldots \quad (3.141)$$

Now, by using the notation in equation (3.103), equation (3.141) can be reduced to the following normalized (dimensionless) form:

$$\alpha_{n4} = \frac{\alpha_4}{\omega_2^2} = \left.\begin{aligned} &\left[\frac{r_2^2 + G_1^2 r_4^2}{r_3 r_4 \sin(\theta_3 - \theta_4)}\right] - \left[\frac{2 r_2 G_1 \cos(\theta_2 - \theta_4)}{r_3 \sin(\theta_3 - \theta_4)}\right] \\ &- \left[\frac{r_2 \cos(\theta_2 - \theta_3)}{r_4 \sin(\theta_3 - \theta_4)}\right] + \left[\frac{G_1^2 \cos(\theta_3 - \theta_4)}{\sin(\theta_3 - \theta_4)}\right] \end{aligned}\right\} \ldots\ldots\ldots\ldots\ldots\ldots\ldots\ldots (3.142)$$

In equation (3.142) the units of measurements of α_{n4} can be stated as rad^{-1}. However, since the radian measure is a ratio of two lengths, and therefore dimensionless, α_{n4} is indeed dimensionless. Given the lengths of all the links in the mechanism, the angles θ_1, and θ_7, the right-hand side of equation (3.142) can be evaluated for any value of θ_2. Moreover the value of ω_2 is usually predetermined and therefore equation (3.142) can be used to determine the angular acceleration α_4 for any phase of motion of the mechanism. Microsoft Excel was used to calculate the normalized acceleration α_{n4}, of the rear Toggle link for given values of the angular position of the crusher, denoted by θ_2. The results are given in Table 3.37 and a plot of this normalized acceleration against the crank angle θ_2, is shown in Figure 3.44.

Table 3.37: Normalized Rear Toggle Acceleration for Given Values of θ_2

$\boldsymbol{\theta_2}$. (degrees)	$\boldsymbol{\alpha_{n4}}$ (Dimensionless)	$\boldsymbol{\theta_2}$. (degrees)	$\boldsymbol{\alpha_{n4}}$ (Dimensionless)
0	0.05576	195	-0.06124
15	0.05323	210	-0.05422
30	0.04774	225	-0.04271
45	0.03952	240	-0.02789
60	0.02886	255	-0.01131
75	0.01616	270	0.00542
90	0.00199	285	0.02090
105	-0.01292	300	0.03409
120	-0.02767	315	0.04436
135	-0.04120	330	0.05142
150	-0.05236	345	0.05520
165	-0.06000	360	0.05576
180	-0.06315		

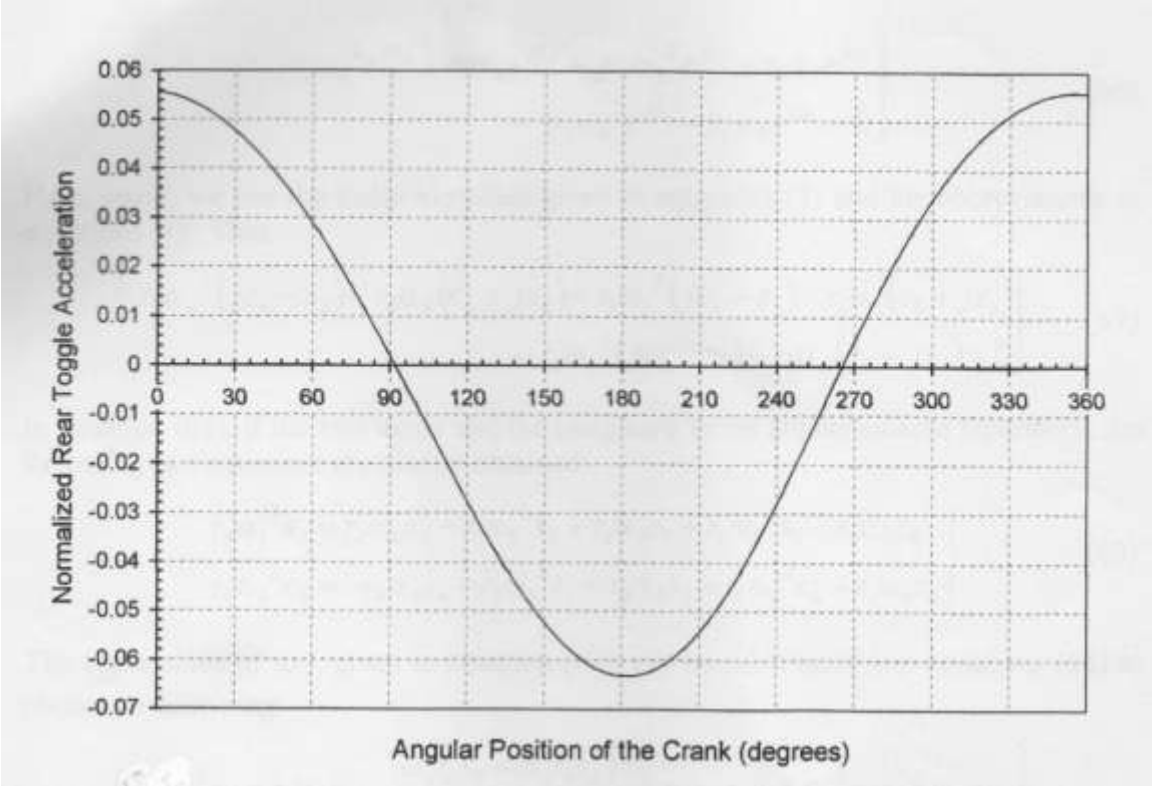

Figure 3.44: Normalized Rear Toggle Acceleration α_{n6} versus Crank Angle θ_2

3.5.10 Acceleration Closure for the Second Loop

The acceleration closure equation for the second loop is obtained by differentiating equation (3.104) with respect to time. Again, note that in equation (3.104).

$$r_7 e^{j\theta_7} \frac{d\theta_7}{dt} = 0 \quad \text{.....(3.143)}$$

Thus, equation (3.104) can be differentiated, with respect to time, to obtain the following:

$$\left.\begin{aligned} r_4 e^{j\theta_2}\left[j\left(\frac{d\theta_4}{dt}\right)^2 + \frac{d^2\theta_4}{dt^2}\right] + r_5 e^{j\theta_5}\left[j\left(\frac{d\theta_5}{dt}\right)^2 + \frac{d^2\theta_5}{dt^2}\right] \\ -r_6 e^{j\theta_6}\left[j\left(\frac{d\theta_6}{dt}\right)^2 + \frac{d^2\theta_6}{dt^2}\right] = 0 \end{aligned}\right\} \quad \text{.....(3.144)}$$

By using the notations in equations (3.96) and (3.133), equation (3.144) can be re-written as follows.

$$\left.\begin{aligned} jr_4\omega_4^2 e^{j\theta_4} + r_4\alpha_4 e^{j\theta_4} + jr_5\omega_5^2 e^{j\theta_5} + r_5\alpha_5 e^{5} \\ -jr_6 e^{j\theta_6} - r_6\alpha_6 e^{j\theta_6} = 0 \end{aligned}\right\} \ldots\ldots\ldots\ldots (3.145)$$

Here, again, we use the Euler identities given in equations (3.68) and the abbreviations in equations (3.69). Thus:

$$\left.\begin{aligned} r_4\omega_4^2(jc_4 - s_4) + r_4\alpha_4(c_4 + js_4) + r_5\omega_5^2(jc_5 + s_5) + r_5\alpha_5(c_5 + js_5) \\ -r_6\omega_6^2(jc_6 - s_6) - r_6\alpha_6(c_6 + js_6) = 0 \end{aligned}\right\} \ldots\ldots\ldots (3.146)$$

In equation (3.146), if the real terms and the imaginary terms are considered separately, the following two equations are readily obtained:

$$\left.\begin{aligned} r_4\omega_4^2 s_4 = r_4\alpha_4 c_4 - r_5\omega_5^2 s_5 + r_5\alpha_5 c_5 + r_6\omega_6^2 s_6 - r_6\alpha_6 c_6 \\ r_4\omega_4^2 c_4 = r_4\alpha_4 s_4 - r_5\omega_5^2 c_5 - r_5\alpha_5 s_5 + r_6\omega_6^2 c_6 + r_6\alpha_6 s_6 \end{aligned}\right\} \ldots\ldots\ldots\ldots\ldots\ldots (3.147)$$

The expression of ω_5, given in equation (3.107), can be substituted into equations (3.147) to obtain the following:

$$\left.\begin{aligned} r_4\omega_4^2 s_4 = r_4\alpha_4 c_4 - \frac{(\omega_6 r_6 s_6 - \omega_4 r_4 s_4)^2}{r_5 s_5} + r_5\alpha_5 c_5 + r_6\omega_6^2 s_6 - r_6\alpha_6 c_6 \\ r_4\omega_4^2\, c_4 = -r_4\alpha_4 s_4 - \frac{(\omega_6 r_6 c_6 - \omega_4 r_4 c_4)^2}{r_5 c_5} - r_5\alpha_5 s_5 + r_6\omega_6^2 c_6 + r_6\alpha_6 s_6 \end{aligned}\right\} \ldots\ldots\ldots\ldots (3.148)$$

Each of equations (3.148) may be manipulated algebraically and re-arranged to obtain the following.

$$\left.\begin{aligned} r_5^2 c_5 s_5 \alpha_5 = (\omega_6 r_6 s_6 - \omega_4 r_4 s_4)^2 \\ -r_5 s_5[r_4\alpha_4 c_4 - r_4\omega_4^2 s_4 + r_6\omega_6^2 s_6 - r_6\alpha_6 c_6] \\ = -(\omega_6 r_6 c_6 - \omega_4 r_4 c_4)^2 \\ -r_5 c_5[r_4\alpha_4 s_4 + r_4\omega_4^2 c_4 - r_6\omega_6^2 c_6 - r_6\alpha_6 s_6] \end{aligned}\right\} \ldots\ldots\ldots\ldots\ldots (3.149)$$

The right-hand side of equation (3.149) can be expanded and re-arranged to obtain the following.

$$\left.\begin{aligned} r_5^2 c_5 s_5 \alpha_5 = {} & r_6^2 s_6^2 \omega_6^2 - 2 r_4 r_6 s_4 s_6 \omega_4 \omega_6 + r_4^2 s_4^2 \omega_4^2 - r_4 r_5 c_4 s_5 \alpha_4 \\ & + r_4 r_5 s_4 s_5 \omega_4^2 + r_5 r_6 s_5 c_6 \alpha_6 - r_5 r_6 s_5 s_6 \omega_6^2 \\ = {} & - r_6^2 c_6^2 \omega_6^2 + 2 r_4 r_6 c_4 c_6 \omega_4 \omega_6 - r_4^2 c_4^2 \omega_4^2 - r_4 r_5 s_4 c_5 \alpha_4 \\ & - r_4 r_5 c_4 c_5 \omega_4^2 + r_5 r_6 c_5 s_6 \alpha_6 + r_5 r_6 c_5 c_6 \omega_6^2 \end{aligned}\right\} \quad \text{..... (3.150)}$$

Now. by using well known trigonometric identities, equation (3.150) can be reduced to the following:

$$\left.\begin{aligned} & r_4^2 \omega_4^2 - 2 r_4 r_6 \omega_4 \omega_6 \cos(\theta_4 - \theta_6) + r_6^2 \omega_6^2 + r_4 r_5 \alpha_4 \sin(\theta_4 - \theta_5) \\ & + r_4 r_5 \omega_4^2 \cos(\theta_4 - \theta_5) - r_5 r_6 \omega_6^2 \cos(\theta_5 - \theta_6) \\ & = -r_5 r_6 \alpha_6 \sin(\theta_5 - \theta_6) \end{aligned}\right\} \quad \text{..... (3.151)}$$

Thus, the angular acceleration of the swing jaw O_5O_6 can be expressed as follows:

$$\left.\begin{aligned} \alpha_6 = {} & \left[\frac{r_4^2\omega_4^2 + r_6^2\omega_6^2}{r_5 r_6 \sin(\theta_5 - \theta_6)}\right] + \left[\frac{2 r_4 \omega_4 \omega_6 \cos(\theta_4 - \theta_6)}{r_5 \sin(\theta_5 - \theta_6)}\right] \\ & - \left[\frac{r_4 \alpha_4 \sin(\theta_4 - \theta_5)}{r_6 \sin(\theta_5 - \theta_6)}\right] - \left[\frac{r_4 \omega_4^2 \cos(\theta_4 - \theta_5)}{r_6 \sin(\theta_5 - \theta_6)}\right] \\ & + \left[\frac{\omega_6^2 \cos(\theta_5 - \theta_6)}{r_6 \sin(\theta_5 - \theta_6)}\right] \end{aligned}\right\} \quad \text{.....(3.152)}$$

Now, by using the notation in equations (3.103) and (3.112), equation (3.152) can be reduced to the following dimensionless form

$$\left.\begin{aligned} \alpha_{n6} = \frac{\alpha_6}{\omega_2^2} = {} & - \left[\frac{G_1^2 r_4^2 + G^2 r_6^2}{r_5 r_6 \sin(\theta_5 - \theta_6)}\right] + \left[\frac{2 r_4 G G_1 \cos(\theta_4 - \theta_6)}{r_5 \sin(\theta_5 - \theta_6)}\right] \\ & - \left[\frac{r_4 \alpha_{n4} \sin(\theta_4 - \theta_5)}{r_6 \sin(\theta_5 - \theta_6)}\right] - \left[\frac{r_4 G_1^2 \cos(\theta_4 - \theta_5)}{r_6 \sin(\theta_5 - \theta_6)}\right] \\ & + \left[\frac{G^2 \cos(\theta_5 - \theta_6)}{\sin(\theta_5 - \theta_6)}\right] \end{aligned}\right\} \quad \text{.....(3.153)}$$

Given the lengths of all the links in the mechanism, the angles θ_1, and θ_7 the right-hand side of equation (3.153) can be evaluated for any value of $\theta_{2.}$ Moreover, the value of ω_2 is usually predetermined and therefore equation (3.153) can be used to determine the angular acceleration, α_6 for any phase of motion of the mechanism.

Microsoft Excel was used to calculate the normalized acceleration, α_{n6}, of the swing jaw, for given values of the angular position of the crank, denoted by $\theta_{2.}$ Sample results are given m Table 3.38 and a plot of this normalized acceleration against the crank angle, $\theta_{2.}$, is given in Figure 3.45.

Table 3.38: Normalized Swing Jaw Acceleration for Given Values of θ_2

$\theta_{2.}$ (degrees)	α_{n6} (dimensionless)	$\theta_{2.}$ (degrees)	α_{n6} (dimension less)
0	-0.02430	195	0.02771
15	-0.02297	210	0/02518
30	-0.02007	225	0.02084
45	-0.01580	240	0.01499
60	-0.01045	255	0.00311
75	-0.00435	270	0.00078
90	0.00213	285	-0.00638
105	0.00359	300	-0.0128G
120	0.01467	315	-0.01806
135	0.02000	330	-0.02183
150	0.02425	345	-0.02393
165	0.0271 1	360	-0.02430
180	0 02832		

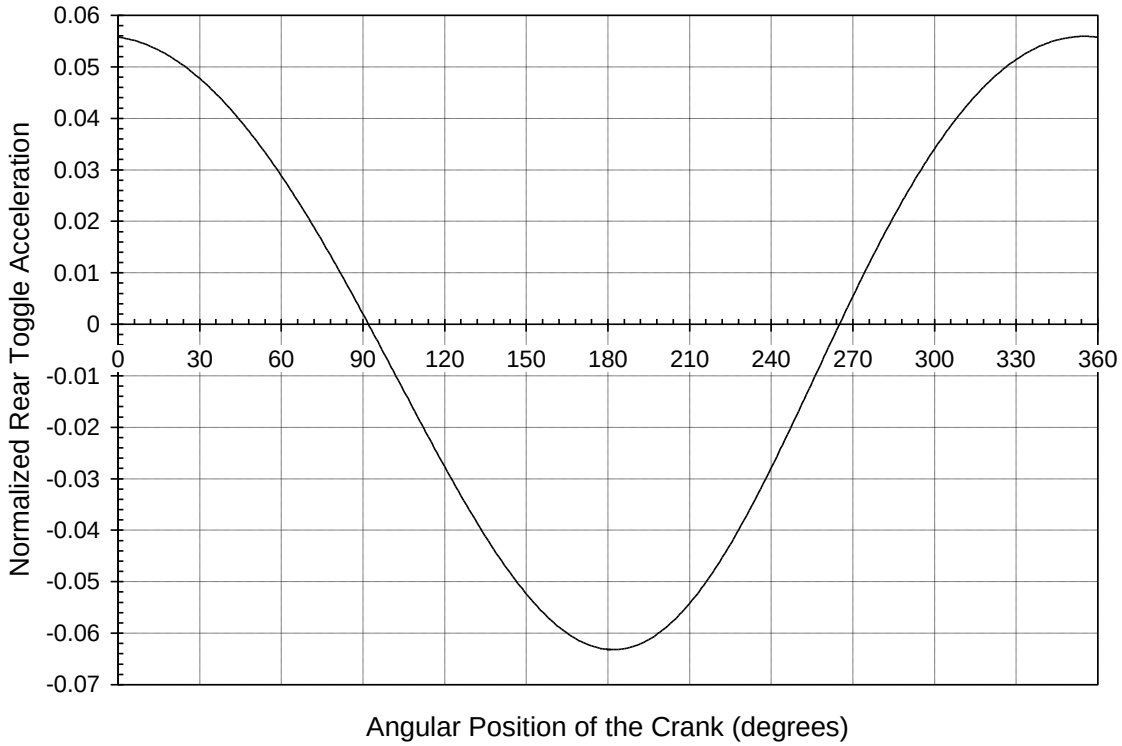

Figure 3.45: Normalized Swing Jaw Acceleration α_{n6} versus Crank Angle θ_2

CHAPTER FOUR

RESULTS AND DISCUSSION

4.1 THE COMPRESSIVE STRENGTH OF ROCKS

Table 4.1 shows the compressive strength of the tested rocks, and Figure 4.1 shows the average value of the analyzed data.

From Table 4.1, the error bars show +/-1 standard deviation. The average values of compressive strength of tested rocks show range of results from 23.54MPa to 127.12Mpa.

Table 4.1: The Consolidated Compressive Strength of Rocks

Rock type	Minimum Compressive Strength (MN/m^2)	Average value of Compressive Strength (MN/m^2)	Maximum Compressive Strength (MN/m^2)	Variance (MN/m^2)	Standard Deviation (MN/m^2)
Schist	50.93	78.52	101.88	211	14.52
Gneiss	45.85	91.13	127.12	617	24.58
Tuff	23.54	67.81	104.54	1038	32.22
Granodiorite	34.97	77.10	109.53	690	26.26
Quartzite	32.96	68.40	112.07	697	26.41
Granite	70.42	92.38	122.37	365	19.11
Phonolite	32.0	72.41	112.58	698	26.42
Gray Wecke	29.91	77.81	122.26	770	27.74

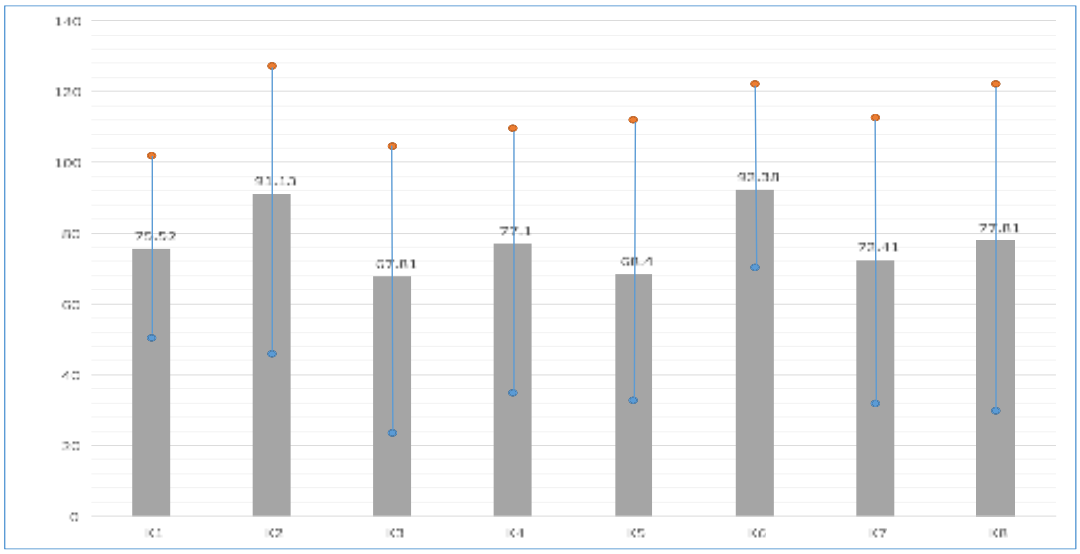

Figure 4.1:The Average Values of Compressive Strength of Analyzed Data (MN/m^2)

In this study, the obtained average value for Tuff is 67.8MPa with that of Gneiss 191.13MPa. The results show high variation in the compressive strength and high values of standard deviation on the same rock type.

The reason for high standard deviation and hence variance in the results could be because of;

i. Different origins of the works
ii. The mineralogical content of sample
iii. The grain size of the rock material
iv. Although the particles in the samples are loaded pre-dominantly in compression, significant magnitude of tensile stresses are induced within the particle (King, 2001). It is those tensile catastrophic splitting cracks that are responsible for the particle breakage. This could contribute to the large variance in crushing loads. However, around the loading point, there is progressive localized crushing caused by the high compressive stress.
v. The fact that although the particles in the samples are loaded pre-dominantly
vi. Other properties that might have had avoidable effect on the results

4.2 ANALYSIS OF THE SINGLE TOGGLE JAW CRUSHER KINEMATICS

In this thesis, the crushing mechanism of the Single Toggle Jaw Crusher is modelled as a planar crank and rocker mechanism, with the eccentric shaft being modelled as a short crank, the swing jaw of the crusher being modelled as the coupler link and the toggle link being modelled as the rocker. Starting with a suitable right-handed Cartesian coordinate reference frame, a unique Single Toggle Jaw Crusher of the Kinematical Model was established. The Vector Loop Closure Method and the differential calculus were then used to derive from first principles the equations of position, velocity and acceleration for any specified point in the Swing Jaw of the Crusher. The derived equations were validated by the use of the dimensions of a practical Single Toggle Jaw Crusher. Further, it is demonstrated, with the aid of graphical plots, that the movement of the swing jaw of the Single Toggle Jaw Crusher would have both vertical and horizontal components, relative to the material being crushed. Thus, the swing jaw applies a direct compressive crushing force as well as a rubbing force upon the stones being crushed. The downward, rubbing force increases the throughput of the crusher but also increases the rate of wear of the crushing surfaces of the wear plates of the jaws. The equations derived can be used to investigate the effects of any alterations in the design of the crusher mechanism, upon its kinematics.

4.3 THE ANALYSIS OF THE SINGLE TOGGLE JAW CRUSHER FORCE TRANSMISSION CHARACTERISTICS

In this thesis, a static force analysis of the mechanisms of the Single Toggle Jaw Crusher mechanism was carried out. The method used is systematic, clear and simple to follow and use. As a result of the static force analysis, some force transmission characteristics of the Single Toggle Jaw Crusher mechanism were obtained. The analysis can also be used to determine the forces that are sustained by each of the components of the Single Toggle Jaw Crusher Mechanism, provided that the values of the input torque and load torque are known.

Using the dimensional data of the PE 400 by 600 jaw crusher, the maximum value of the force transmission ratio is found to be about 3268, the minimum value of the force transmission ratio is found to be about 0.61 and the mean value of the force transmission ratio was found to be about 10.6. These metrics can be used as criteria in the selection of a suitable mechanism design to be used in a given application, from among different alternatives.

The study shows that the force transmission ratio is very high at the beginning of the active crushing stroke, drops off rapidly and then levelled off at about the minimum value, remains at the low value for about two thirds of the active crushing stroke and then rises rapidly to a very high value at the end of the active crushing stroke. That the force transmission ratio is very high at the beginning of the active stroke is advantageous in crushing brittle materials which fracture without undergoing appreciable deformation.

In this study, the Single Toggle Jaw Crusher is suitable for Small and Medium Scale Entrepreneurs because of ease to operate and maintain. It is also relatively cheaper compared to the Double Toggle Jaw Crusher.

4.4. THE KINEMATICS AND MECHANICAL ADVANTAGE OF THE DOUBLE TOGGLE JAW CRUSHER

In this thesis, the crushing mechanism of the Double Toggle Jaw Crusher is modelled as a planar mechanism with six links and six revolute joints, with the eccentric shaft being modelled as a short crank and the swing jaw being modelled as a rocker. Except for the frame of the mechanism each of the six links is connected to only two joints and is therefore a binary link. The frame of the mechanism is connected to three joints and is therefore a tertiary link.

A suitable right-handed Cartesian coordinate reference frame is established and used in the kinematical analysis of the Crusher Mechanism. The position vector loop closure method is used to derive the position vector loop closure equation, which is then used to obtain the angular position of the swing jaw for any angular position of the input crank. By differentiating the position vector loop closure equation, with respect to time, the velocity

closures equation was obtained and subsequently used to obtain the angular velocity ratio of the swing jaw (output link) and the eccentric shaft (input link), for any given angular position of the crank. By assuming a 100% mechanical efficiency of power transmission in the mechanism, in this thesis, the angular velocity ratio is used to derive the mechanical advantage of the mechanism, for any given angular position of the crank. Further, by differentiating the velocity closure equation, with respect to time, an acceleration closure equation is obtained that is subsequently used to obtain the angular velocity of the swing jaw for any given angular position of the crank. Thus, a comprehensive analysis of the kinematics of the swing jaw of the Double Toggle Jaw Crusher is achieved.

Using the data *(Cao et al., 2006*), it is demonstrated that at crank angle of 180°, there occurs a certain spike in the value of mechanical advantage accompanied by reversal in sign from negative to positive. This is the toggle phase which consider with the active crushing stroke of the crusher when the mechanical advantage is very large. The equations derived in this thesis can be used to investigate the effects of any alterations in the design of the crusher mechanism, upon its kinematics.

4.5. THE SINGLE TOGGLE JAW CRUSHER VERSUS THE DOUBLE TOGGLE JAW CRUSHER

The linkage mechanisms of the Single Toggle Jaw Crusher were modelled as a planar four bar mechanism consisting of four revolute joints (4R). However, the movement (motion) of the swing jaw is elliptical in nature hence applies both compressive and a rubbing force on the stones being crushed. This action causes heavy wear on the plates of stationary and swing jaws compared to the Double Toggle Jaw Crusher where the moving Swing jaw applies an almost direct compressive force of the stones being crushed. This implies that the wear on the swing and stationary jaws is minimal. This makes the Double Toggle Jaw Crusher to be used for crushing abrasive and hard stones. The criteria for the comparison of different jaw crusher mechanism can be based on the force transmission characteristics in order to select the most appropriate design for use in particular application. The equations derived in this thesis can be applied in calculating the forces sustained by the machine load bearing components.

CHAPTER FIVE

CONCLUSIONS, LIMITATIONS AND RECOMMENDATIONS

5.1 CONCLUSIONS

5.1.1 The Mechanics of Stone Crushing

The main types of stones found in Kenya and mostly used in the building and construction industry include sandstones, coral limestone, shade, tuff, gneiss, phonolite, granitoid, granite, quartzite, marble and laterite/murram. These stones in their natural conditions are brittle hence in the assessment of their crushing characteristics, one needs to look at the fracture mechanics of materials.

This thesis notes that stone crushes whether manual or mechanical break up stones through attrition, impact, shear and/or compression or a combination of these. In all these cases, the stones are broken up by fracture propagation caused by the applied compression and shear forces. The pre- existing cracks or defects in the rocks relate very well to fracture propagation. It is therefore proper to extend the fracture mechanics to rocks; the subject hitherto was a preserve of metals. The study realizes that rock masses contain cracks and discontinuities and whereas many rock structures are subjected to compressive stresses during communition and crushing, tensile fracture has been observed in some rocks during crushing (King, 2001).

5.1.2 Experimental Work

In this thesis, the compressive tests for the strength of Gneiss, Phonolite, Quartzite, Granite, Tuff, Granidorite, Schist and Grey Wecke were performed Compressive forces are the stone crushing characteristics that are responsible for catastrophic fracture of rocks in communition process compared to Tensile and Brazilian forces. The results of the laboratory tests confirmed that strength of rocks differ a great deal. Tuff recorded the lowest value of 23MN/m^2while gneiss had the highest value of compressive strength at 127MN/m^2. The standard deviations recorded in both cases were very high. These high

variances could have been attributed to the mineralogical content, grain size, possible pre-existing cracks and other materials properties which might have had considerable effect on the strengths of these rocks. Secondly, although the particles in the samples are loaded predominantly in compression, substantial tensile are often induced within the particle (King, 2001; Oka and Majiwa, 1970). It is these tensile catastrophic splitting cracks that is responsible for the particle breakage. However, around the loading point, there is progressive localized crushing caused by high compressive stresses that cause fracture.

5.1.3. Stone Crusher Design Concept

In this thesis, the design concept proposed were Jaw crushers gyratory crushers and the come crusher. I evaluated these concepts in terms of performance content formulated us technical performance, reliability, maintainability, life cycle costs, development risk, production rate, schedule and safety. Using the design making matrix, the jaw crusher design concept was selected as appropriate for Small and Medium Scale Entrepreneur because of;

i) Easy to operate and maintain
ii) Low power cost and high mechanical efficiency
iii) Suitability to crush hard and abrasive material

5.1.4 Jaw crusher models

The models considered in this study was the modeling of the Jaw crusher capacity, modeling of the power drawn and modeling of the product size. The Bonds equation (after Bond 1952) can be used in determining the work output (KWh/t) the work of Rose and English (1967) can be applied in the determination of the productivity of the Jaw Crusher in terms of the volume or tonnes of the material per hour. The product size modeling after Whitten (1972) can be used for the determination of the products size in metres.

5.1.5 Kinematical, Statical And Force Transmission Analysis of Single Toggle and Double Toggle Jaw Crusher

The second objective of the study was to derive the kinematic, static and force transmission equations for Single Toggle and Double Toggle Jaw Crusher mechanisms. Using the Vector Loop Closure Method, the authenticity of the equations was validated by using the data of the existing PE 400 x 600 and PE 6-4 (425 x 600) jaw crushers (Henan Hongxing Mining Machinery Company Limited, 2013).

In the analysis of the Single Toggle Jaw Crusher Mechanism, the results in this thesis show that, for one full cycle of rotation of the crank, the minimum value of the inclination of the swing jaw to the vertical was 159.7° and the maximum value was found to be 161.6º. Thus, the range of variation of the inclination of the coupler (swing jaw) to the vertical for one complete cycle of rotation of the crank is less than 2º, hence the angular orientation of the swing jaw, during the cycle of motion is insignificant. Again, results show that for one full cycle of rotation of the crank, the minimum value of the velocity of the swing jaw was found to be -0.476 radians per while the maximum value was found to be 0.451 radians per second. Thus, the angular velocity of the coupler (swing jaw) is generally small. The angular acceleration for both vertical and horizontal component becomes zero at the crank angle of approximately 26.32º and 207.92º. At these instances, the acceleration of the swing jaw becomes purely translational and all the points have the same horizontal components of acceleration.

Using the dimensional data of the PE 400 x 600 jaw crusher, the maximum value of the force transmission ratio was found to be 3268 at the active crushing stroke. The minimum value of the force transmission ratio was found to be 0.61 and the mean value was 10.6. The results show that the force transmission ratio is very high at the beginning of the active crushing stroke and is advantageous in crushing very brittle materials which fracture without undergoing appreciable deformation.

The crusher mechanism of the Double Toggle Jaw Crusher in this thesis has been modelled as a planar mechanism with six links and six revolute joints with the eccentric shaft being modeled as a short link and swing jaw being modeled as a rocker. The results of the analysis show that the greatest amplification of the crushing force occurs at the toggle position, which corresponds to the angle of 180º in the first phase and at a crank angle of 360º in the second phase. Using the typical dimensions of practical DB 6-4 (425 x 600) Double Toggle Jaw Crusher (Cao *at el.,* 2006), the mechanical advantage suddenly becomes high at 0º in the first phase and at 180º in the second phase. This is evidence of the toggle phase which coincides with the commencement of the active crushing stroke. The equations derived in this study coupled with the compressive tests results, can be used in the design of a more efficient jaw crusher that optimizes the design parameters.

Although, the vector loop closure method used in this thesis is not new, it has not been used for analysis of the jaw crusher mechanism before. By applying judiciously, the derived equations an efficient jaw crusher which optimizes the design parameters can be developed.

5.2 LIMITATIONS OF THE STUDY

5.2.1 Fracture Toughness of Rocks

In attempting to understand the geomaterial features as regards toughness, K_C and strain, it's important to determine the material toughness. This is normally carried out in laboratory. The most common experiment done is the Charpy or Chevron method whereby the bending of a cylindrical specimen is done (Dziedzic,1999) based on the International Standard for Rock Mechanics (1988). This method is where a V-shaped initial notch in the specimen concentrates stress at the notch and cause crack propagation perpendicular to the direction of the applied load. This creates a triaxial state of stress in which the tensile stress (σ_1) is predominant. Such state of condition leads to the determination K_{IC}, the brittle toughness of the stone of which rock is made.

5.2.2. Correlation between Bond Work Index and the Mechanical Properties of Rocks

The Bond's Work Index is a measure of grindability or crushability of materials. The relationship between the communition energy and the product size obtained for a given feed size has been given by Rittinger (1867), Kick (1885) and Bond (1952), known as three theories of communition. The most widely used relationship is the Bonds Work Index (kWh/t). It involves the Bond ball mill testing, rod milling and batch ball milling down to product size of around P_{80}-25microns. Due to lack of equipment, this experiment was not done.

5.3. RECOMMENDATIONS AND FUTURE WORK

5.3.1 Fracture Toughness Measurement

In the process of crack propagating and in particular, at the crack front, three main fracture modes are identified namely; Tension(σ_I), Direct shear (σ_{II})and Pure shear(σ_{III}), as shown in Figure 5.1

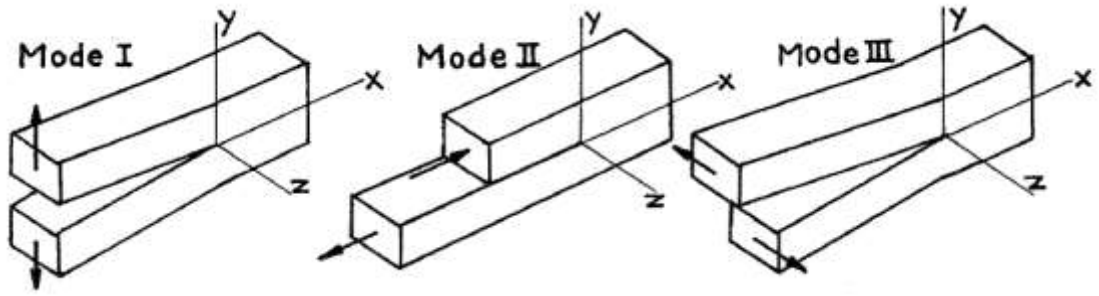

Figure 5.1: The Crack Surface Displacement Modes

As the load is increased in the three modes of loading, the surface energy also increases and therefore the crack tip also modes. In this scenario, there is stress concentration field created (Piniska, 1995). This is measured by what is referred to as stress concentration factors whose critical values are defined as; $K_{IC,}$ K_{IIC} and K_{IIIC} which describe the material Brittle, Fracture Toughness and can be treated as a constant for a particular material as just as Youngs Modulus is also a material contact.

Irwin (1921) reported that the advancement of the crack for a particular surface is given by;

$$\sigma\Gamma = G\sigma_s \quad \text{..... (5.1)}$$

where;

$\sigma\Gamma$ = fracture work needed to create crack surface, σ_s

The energy stream G, which are formed around the crack edge and the characteristics of the geomaterial strain, given by;

(i) Young's Modulus, E
(ii) Poisson's ratio, v

The Stress Intensity Factors, however indicate the stresses, and therefore the energy stream can be defined as;

$$G = \frac{1-v^2}{E}(K_I^2 + K_{II}^2) + \frac{1-v}{E}\ K_{III}^2 \quad \text{..... (5.2)}$$

In the circumstance that G exceeds the critical value, then the crack propagates or advances very fast and the critical value of the energy stream is given by;

$$G_C = \frac{1-v^2}{E}(K_{IC}^2 + K_{IIC}^2) + \frac{1-v}{E}\ K_{IIIC}^2 \quad \text{..... (5.3)}$$

The Chevron band method, can be used to determine the fracture toughness of the geomaterials, including stones (IRSM, 1988; Dziedzic, 1999)

5.3.2 Energy used in Communition Process

a) According to Legendre and Zavenhoven (2014), there have been several attempts to accurately determine the actual energy required for communition process. The most accepted theory is based on the fact that in a size reduction process as the mean particle size decreases, the surface area of the particle increases. Therefore, a measurement of

the energy, E used in the communition process, can be written in mathematical form as follows:

$$\frac{dE}{dS} = kS^n \quad \text{..... (5.4)}$$

where

k , is a constant that is related to the crushing strength of the rock. Differentiate workers have determined the values of parameters *k* and *n*, with the three most important ones being; (i) Rittinger, $n = -2, k = C_R$; (ii) Kick, $n = -1,\ k = C_k$ and (iii) Bond, $n = -1.5, k = C_B$.

It has been suggested that the three approaches to prediction of energy requirement mentioned above are best applicable to certain ranges of product size. These are presented in Table 5.1 (Rhodes, 1998).

Table 5.1: Terminology and Models used in Communition Process (Rhodes, 1998).

Size Range of Product	Description	Adequate Model
1 to 0.1m	**Coarse crushing**	**Kick**
0.1m	Crushing	Kick and Bond
0.01m	Fine Crushing/ Coarse Grinding	Bond
1mm	Intermediate Grinding, Milling	Bond
100microns	Fine Grinding	Bond
10microns	Ultrafine Grinding	Rittinger

For given values of *n*, equation (5.1) can be integrated to obtain the following models (Lindqvist, 2008).

The Bond equation:

$$W_B = C_B \left[\frac{1}{\sqrt{P_{80}}} - \frac{1}{\sqrt{F_{80}}}\right] \quad \text{..... (5.5)}$$

The Kick equation:

$$W_K = -C_K \, in \, \left[\frac{P_{80}}{F_{80}}\right] \quad \text{.....(5.6)}$$

The Rittinger equation:

$$W_R = C_R \left[\frac{1}{\sqrt{P_{80}}} - \frac{1}{\sqrt{F_{80}}}\right] \quad \text{..... (5.7)}$$

where W is the energy consumption per tonne of material crushed, C_B is the so-called Bond Work Index of the rock and it is obtained through measurement. $C_K \, and \, C_R$ are the corresponding Work Indices in Kick and Rittinger formulae, respectively? These models all indicate that as the final product size approaches zero the energy consumption increases towards infinity. Therefore, this thesis recommends that experiments be carried out to determine;

i) The actual Work Indices for commonly used construction materials.
ii) Whether the indices so determined correlate with the well-known mechanical and physical properties of the materials being crushed such as the compressive strength of the materials.

Korman *et al.,* (2015) have described, in detail, a procedure for these measurements, while crushing various materials and attempted to corelate the work Index with some well-known mechanical and physical properties of the materials (Bulk Density, Compressive Strength, Tensile Strength, Hardness and Fracture Toughness).

The energy requirement during the Crushing Process, can also be investigated using the Numerical Methods (Refahi *et al.,* 2007; Refahi *et al.,* 2009; Refahi *et al.,* 2010; Legendre and Zevenhoven, 2014).

5.3.3. The Jaw Crusher Development

Using the Crusher Design Models, the derived Kinematical, Static and Force Transmission Equations and the Uniaxial Compressive Tests Results, a stone crusher can be developed, tested and made available for Small and Medium Scale Entrepreneurs.

REFERENCES

Abhary, K. (2008), "A Simple Analytical Method for Force Analysis of Planar Frictional Tree-like Mechanisms," *In Proceedings of the ASEE Annual Conference and Exposition,* Pittsburgh, Pa, USA.

Al, Chalaby, M. and Huang, C.L (1974), Stress Distribution within a Circular Cylinder in Compression: *International Journal of Rock Mechanics and Geo-Mechanics Abstracts,* Vol. 11 PP. 45-56.

Andrew G.E (1995), Brittle Failure of Rock Materials, *Tests Results and Constituent Models.*

AUBEMA Jaw Crusher (2013), A brochure, available at: www.tlt.as/undersider/documents/jawcrusher.pdf. accessed (May 2013).

Bakke P.S, Hanva R, and Gulsvik A. (2001), "Relation of Occupational Exposure to Respiratory Symptoms as Asthma in a General population Samples" *Am. J Epidemial, Vol. 154, PP. 477-83 13 Wagner.*

Bearman, R.A (1998), The Use of the Point Load Test for the Rapid Estimation of Mode I Fracture Toughness, *International Journal of Rock Mechanics and Mining Sciences,* Vol. 36 PP. 257-263.

Beryl, P., Dantin, EM, and Masacci, P. (1984), Influences of Mechanical Characteristics of Rock on Size Reduction Processing, *Proceedings of Mineral Processing and Extractive Metallurgy,* Beijing, PP. 1526

Bond, F.C (1952), The Third Theory of communition *Transaction of AIME/SME,* Vol. 193, PP. 4884-94.

Brady, B. & Brown. E., (2002), Rock Mechanics for Underground Mining. 3rd ed. *Dordrecht: Kluwer Academic Publishers*; Boston, 628p. ISBN 1-4020-2064-3.

Briggs, C.A and Bearman, R.A (1996), An investigation of Rock Breakage and Damage in Communition Equipment, *Minerals Engineering*, Vol. 9, No. 5, PP. 489-497.

Brown, E.T. (1974), Fracture of Rock under Uniform Biaxial Compression, *Proceedings of the 3rd Congress of ISRM, Denver*, Vol. 2A, PP. 111-117.

Cao, J, Rong X and Yang, S. (2006), Jaw Plate Kinematical Analysis for Single Toggle Jaw Crusher Design. *International Technology and Innovation Conference, Section 1*: Advanced Manufacturing Technology, Hangzhou, PP. 62-66.

Carmichael, R.D. and Smith, E.R. (1962), Mathematical Tables and Formulas, *Dover Publications Incorporated*, New York, NY.

Carmichael, S.R. (1989), *Practical Handbook of Physical Properties of Rhodes and Minerals.*

Carter, R.A. (1999), "New Jaw Crushers are Reliable, Affordable and Transportable," *Rock Products, available at: www.rockproducts.com/index.php.features/51-archives/1240pdf* (accessed May 2013).

Chang, W.T. C-C. Lin, and J.J. Lee, (2003), "Force Transability Performance of Parallel Manipulators," *Journal of Robotic Systems*. Vol. 20, No.11, PP. 659-670.

Chapra, S.C. (2012), Applied Numerical Methods with MATLAB for Engineers and Scientists, Chapter 19, *McGraw Hill, 3rd Edition.*

Coulson, J.M., and Richardson, J.F (1999), Chemical Engineering, 4th Edition, Butterworth- *Heinemann Publishers, Oxford* 2:56.

Crech, W.N. (1974), The Energy Balance Theory and Rock Fracture Measurement for Uniaxial Tension, *The Proceedings of the 3rd Congress of ISRM, Denbver*, Vol. 2A, PP. 167-173.

de la Vergne, J. (2003), Mcintoch Engineering, *Hard Rock Miners Handbook*, North Bay, Ontario, Canada.

Deepak, B.B.V.L (2010), "*Optimum Design and Analysis of the Swinging Jaw Plate of a Single Toggle Jaw Crusher," A Master of Technology Thesis, Department of Mechanical Engineering, National Institute of Technology, Rourkela, Odisha, available at www.scribd.com/doc/37399105/Deepak-project-on-jaw-Ceusher* (accessed May 2013).

Denavit, J.R.S Hartenberg, R. Razi, and J.J, Vicker, (1965) "Velocity, Acceleration, and Static-Force Analyze of Spatial Linkages" *Journal of Applied Mechanics,* Vol.32, No.4, PP.903-910.

Dowling, N.E. (1999), Mechanical Behaviour of Material Engineering Methods for Deformation, Fracture and Fatigue, *Prentice Hall, Upper Saddle River, NJ.*

Durvasula, R. (1990), Occupational Health Information System in Developing Countries – India: *A Case study Present at the Third World; Problems and Policies Baston: Harvard School of Public Health.*

Dziedzic A. (1999). "A New method of Study of Fracture Toughness of Rocks," Prz. Geol., 47 (10): 927-932.

Elisante, E. (2003), Technology Development to Improve Productivity of Women Miners/Processors of Limestone's Aggregate in Dar-es-Salaam City, Tanzania. *Concept Note submitted to Research for Poverty Alleviation (REPOA) Organization, Tanzania.*

Erdman, A.G. and Sandor G.N. (1991), Mechanism Design Volume 1, *Prentice – Hall.*

Fatusi, A. and Erbabor, G. (1996), Occupational Health Status of Saw Mill Workers in Nigeria. *J ray. Soc Health Vo. 116, PP. 232-6.*

Freudenstein, F. (1955), "Approximate Synthesis of Four Bar Linkages" *Transactions of the ASME,* vol. 77, PP. 853-861.

Garnaik, S.K. (2010), "Computer Aided Design of the Jaw Crusher", *A bachelor of Technology Thesis, Department of Mechanical Engineering National Institute of Technology Rourkela, Odisha*.

George, Muir, (2007), The Principles of Single Particle Crushing. *Handbook of Powder Technology,* Vol 12 2007 PP. 117-225.

Government of Kenya, (2013), Ministry of Mining and Natural Resources, *Annual Report 2013.*

Government of Kenya, (2017), Kenya National Bureau of Statistics, *Economic Survey 2017.*

Government of Kenya, (2017), National Environmental Management Authority, *Annual Report, 2017.*

Griffith A.A (1920). "Phenomenon of Rupture and Flow of Solids," Trans. Royal Soc. London, A 221: 163-168.

Griffith, A.A (1921), The Phenomenon of Rupture and Flow in Solids, *Philosophical Transactions of the Royal Physical Society, Vol. 221 PP. 163-198.*

Guimaraes, M.S., Valdes J.R, Palomino A.M, Santamaria J.C (2007), *Aggregate Production, Fines Generation during Rock Crushing, International Journal of Minerals Processing.* Vol.81, PP.237-247 http://www.thesustainablevillage.com/serlet/display/microenterprise/display/38.

Gupta, A. and Yan, D.S. (2006), Mineral Processing, Design and Operations: *An Introduction, Chapter 4: Jaw Crushers, Elsevier, Melbourne.*

Ham, C.W., Crane E.J and Rogers, W.L (1958), Mechanics of Machinery, *4th ed, Mc Graw-Hill Book, New York, NY.*

Henan Hongxing Mining Machinery Company Limited (2013), *Available at: www.hxjqchina.com/uploadfile/01.pdf* (accessed January 2013).

Holman, J.P. (1994). "Experimental Methods for Engineers" *McGraw-Hill, Inc;* New York.

Holte, J.E. and T.R. Chase, (1994). "A Force Transmission Index for Planar Linkage Mechanisms," *The Proceedings of the ASME Mechanisms Conference*, PP. 377-386.

Hudson, J. & Harrison, J. (1997), Engineering Rock Mechanics an Introduction to the Principles. *Oxford: Pergamon*, 444 p. ISBN 0-08-041912-7.

ILO- IPEC (2006), US Embassy Report Based in Uganda. *Report Based on the 2005-2006 Uganda Demographic and Health Survey.*

ILO-IPEC (2001), Child Labour in Uganda, *Report Based on the 2000-2001 Uganda Demographic and Health Survey.*

International Society for Rock Mechanism (1985). "Suggested Methods for Determining the Fracture Toughness of Rock" Int. J. Rock Mechs. Min. Sc. Geomech. Abtr; 25: 71-96.

Irwin, G.R (1957), Analysis of Stresses and Strains Near the Need of a Crack Traversing a Plate, *Journal of Applied Mechanics,* Vol. 24 PP. 361-364.

ISRM, (1988), Suggested Methods for Determining the Fracture Toughness of Rocks (Coordinator F. Outchterlony), *International Journal of Rock Mechanics and Geomechanics Abstracts,* Vol. 25, PP. 73-96.

ISRM, Commision (1979), The Complete ISRM Suggested Methods for Rock Characterization, Testing and Monitoring. *Edited by Urusay, R and Hudson*.

Jaeger, J. & Cook, N. (1979), Fundamentals of Rock Mechanics. 3rd ed, *London: Chapman,* 1979. 591 p. ISBN 0-412-22010-5.

Jambiya, G.K (1997), Poverty and the Environment. The Case of Informal Sand Mining, Quarrying and Lime-Making Activities in Dar-es-Salaam, Tanzania: *Research on Poverty Alleviation (REPOA).*

Kimbrell, J.T (1991), Kinetics Analysis and Synthesis *McGraw-Hill Incorporated*, New York, NY.

King, R.P. (2001), Modeling and Simulation of Mineral Processing Systems, *Butterworth -Heinemann, Boston.*

Korman. T., G. Bedekovic, T. Kujundzic and D. Kuhinec, (2015), Impact of Physical and Mechanical Properties of Rock on the Energy Consumption of a Jaw Crusher. *Physicochemical Problems of Mineral Processing*- Volume 51. Number 2, 2015, Paces 461 to 475.

Krought, S.R (1980), Determination of Crushing and Grinding Characteristics Based on Testing of Single Particles, *AIME Transactions*, Vol. 226, PP. 1957-1962.

Larson, R.E., Hosteler R.P and Edwards B.H (1994), *Calculus with Analytical Geometry, Chapter 4, D.C Health and Company.*

Legendre, Daniel and Ron Zevenhoven, (2014), Assessing the Energy Efficiency of a Jaw Crusher. *Energy Volume 74*, PP. 119 to 130.

Lin, C.C, and W-T. Chang, (2002), "*The Force Transmissivity Index of Planar Linkage Mechanisms," Mechanism and Machine Theory,* Vol.37, No. 12, PP. 1465-1485.

Lindqvist, Mala, (2008), Energy Considerations in Compressive and Impact Crushing of Rock, *Minerals Engineering*. Volume 21. Pp. 631 to 641.

Luo Zhonghua and Shehuan Li (2012). Optimization Design for Crushing Mechanism of Double Toggle Jaw Crusher. *Applied Mechanics and Materials Volumes 201-202, pp 312-316, 2016.*

Lytwynyshyn, G.R. (1990), Jaw Crusher Design, *MSc* Thesis-. *Northern University*, Evanston, August 1990.

Machine Roll, (2008), *http://www.machineroll.com/products.html*

Martin, G.H. (1982), Kinematics and Dynamics of Machines, *2nd ed., McGraw-Hill Incorporated*, New York, NY.

Mbandi Isabella, J. (2017), Assessment of the Environmental Effect of Quarrying in Kitengela Sub-County of Kajiado, Kenya. *MA Thesis, University of Nairobi*.

Metso Minerals (2003), "Norberg C series Jaw crusher", *Technical Publications*.

Metso Minerals, (2008), Nordberg C Series Jaw Crusher, *Technical Publication.*

Mular, A.L., Dong, N.H., Barrat, D.J (2002), Mineral Processing Plant Design, Practice and Control: *Proceeding, Vol 1, Society of Mining, Metallurgy and Exploration*.

Munyasi, D.M., Mutuli, S.M and Oduori, M.F (2013), "An Overview of the Small-Scale Stone Crushing Industry in Western Kenya" *Proceedings of the 20th Engineers International Conference*, Organized by the Institution of Engineers of Kenya, Tom Mboya Labour College, Kisumu, Kenya.

Murakami, Y. (1987). Stress Intensity Factors Handbook, Pergamon Press, New York.

Muskhelishvili, N.I (1963), Some Basic Problems of the Mathematical Theory of Elasticity, Fundamental Questions, Plane theory of Elasticity, Torsion and Bending, *Groningen P. Noordhoff.*

Naiper-Munn, T.J., Morell, S., Morrison, R.S., Kojovic, T. (1999), Mineral Communition Circuit- Their Operation and Optimization, *Julius Kruttschnitt Mineral Research Centre, Queensland.*

Nonkava, K., Monka, P., Hloch, S and Valicek, J (2001), "Kinematic Analysis of the Quick-Return mechanism in Three various Approaches" *Technical Gazette*, Vol. 18 No. 2, PP. 295-299.

Norton, R.I. (1992), Design of Machinery: An Introduction to the Synthesis and Analysis of Mechanisms and Machines, *McGraw-Hill.*

Oduori, M. F., D.M. Munyasi and S.M. Mutuli (2016), Analysis of the Single Toggle Jaw Crusher Force Transmission Characteristics. *Journal of Engineering, Volume 2016*, Article ID 1578142, 9 pp. 2016.

Oduori, M. F., S. M. Mutuli and D. M. Munyasi (2015), Analysis of the Single Toggle Jaw Crusher Kinematics. Journal of Engineering. *Design and Technology*, 13(2), pp 312-239.

Ottolini, Diego (2012), Unearthing the Invisible: Worst Forms of Child Labour in Nairobi and Nyanza Province (Kenya): *A Baseline Survey, Analytical Report, Sponsored by CESVI-Kenya.*

Peng. S. (1971), Stress Within an Elastic Circular Cylinder Loaded Uniaxially and Triaxially. *International Journal of Rock Mechanics and Mining Science* Vol. 8 PP. 399-423.

Pennsylvania Crusher Co-operation (2003), Crusher Selection, Handbook of Crushing *http://penscrusher,.com/1so113html*.

Pook L.P. (1972), Fatigue Crack Growth Data for Various Materials Deduced from the Fatigue Lives of Pre- cracked Plates: Stress Analysis and Growth Cracks, *A.S.T.M. PP. 106-124.*

Pritts, John (1984), A Manual of Geology for Civil Engineers, *Published by Word Scientific Publishing co. PLC Ltd, Singapore.*

Rooke, D.P and cartwright, D.J (1976), "Compendium of Stress Intensity factors" H.M.S.O London.

Rose H.E and English, J.E (1967), *Transactions of the IMM*, 76, C32.

Satyen Moray, Northan Throop, John Seryak, Chris Schemidt, Chris Fisher, mark D'Antonion (2005), "Energy Efficiency Opportunities in the Stone and Asphalt Industry," *Proceedings of the American Council for Energy Efficiency Economy*.

SBM, Mining and Construction Machinery (2013). "A Brochure", available at: www.sbmchina.com/pdf/jaw_crusher.pdf (accessed May 2013).

Schmidt, R.A and Rossmantihm, H.P (1983), Basics of Rock Fracture mechanics, Rock Fracture Mechanics ch 1. (Edited by H.P Rossmantihm), *Springer-Verlag. New York.*

Shigley, J.E and Vicker Jr. (1980), Theory of Machines and Mechanisms: *McGraw- Hill Book Company.*

Soong, R.C. and S. L. Wu, (2009), "Design of Variable Coupler Curve Four-bar Mechanisms", *Journal of the Chinese Society of Mechanical Engineers,* Vol. 30, No. 3, PP. 249-257.

Tada H., Paris P.C., and Irwin G.R (2000), The Stress Analysis of Cracks Handbook, *ASME Press New York.*

The Institute of Quarrying Australia (2013), "Technical Briefing Paper No.6: Crusher Selection III", available at: www.quarry.com.au/file/technical_papers/microsoft_word_technical_paper-no.6doc.pdf

Ugbogu O.C, Ohakwe J, Foltescu, V. (2000), Occurrence of Respiratory and Skin Problems Among Stone Quarrying Workers: *African Journal of Respiratory Medicine*

Vutukuri, V., Lama, R., Saluja, S. (1974), Handbook on Mechanical Properties of Rocks: Testing Techniques and Results, *Trans tech, 1974.*

Wang, Z. H. Yu, D. Tang, and J. Li, (2002), "Study on Rigid-body Guidance Synthesis of Planar Linkage," *Mechanism and Machine Theory*, vol. 37, No. 7, PP. 673-684.

Weiss, N.L. (1985), Jaw Crusher, SME Mineral Processing Handbook (Edited by N.L. Weiss), *Ch. 3B-4, SME/AIME, New York.*

Whittaker, B.N, Sign R.N. and Sun, G. (1992), Rock Fracture Mechanics- Principles, Design and Applications, *Elsevier, New York.*

Whitten, W.J. (1972), *Journal of the South African Institute of Mining and Metallurgy*, 73, 257.

Yashma, S, Morohasi, S. and Saito, F. (1979), Single Particle Crushing under Slow Rate of Loading, *Scientific Reports of the Research Institute*- Tohoku University Vol. 1, PP. 116-133.

Zhangfeng Zhao, Li Yanbiao, Li Wenhao, Zhan Xian, Zhu Xingliang and Zhong Jiang (20l5), Research on the Biaxial Compound Pendulum Jaw Crusher Based or Seven-Bar Mechanism. *Proceedings of the Institution of Mechanical Engineers Part C: Journal of Mechanical Engineering Science*, 0(0), pp 1-14.

Zhong, L., and K. Chen (2010), Study on Digital Platform for Jaw Crusher Design, *IEEE.*

Zuma, (1989), Stone Crushing in South Africa: *Proceeding of the 9th Symposium on Rock Mechanics,* Cape Town.

Appendix I: Standards for Uniaxial Compressive Strength (ISRM, ASTM)

Test Parameter	**ISHM**	**ASTM**
Minimum Specimen Diameter *D*, mm	50 to 54	50 to 54
Height lo diameter ratio, *H/D*	2 to 3	2.5 to3
Deviation from the right angle between the longitudinal axis and the ends (minutes)	3.5	3.5
End flatness (roughness), mm	0.01	0.01
End deviation from parallel, mm	3.5	3.5
Admissible roughness at sample sides, mm	OJ	0.3
Exactness of measurement *D*, mm	0.1	0.1
Exactness of measurement D_4mm	O.I	O.I
Contact platens diameter D_p mm	1 to 1.02	1 to 1.02
Thickness of the platens	$> D_p/3$	$> D_p/3$
Hardness of the platen contact surface, HRC	30	Unknown
Stiffness of me testing machine, MN/mm^2	0.2	Unknown
Minimum sample size	10	10
Loading rate $\sigma_1, MPa/s$	0.5 to 1	0.5 to 1